

Fall 2008

Dynamic responses of a 20-ton capacity feed buoy in an open ocean environment

Jonathan F. Horton

University of New Hampshire, Durham

Follow this and additional works at: <https://scholars.unh.edu/thesis>

Recommended Citation

Horton, Jonathan F., "Dynamic responses of a 20-ton capacity feed buoy in an open ocean environment" (2008). *Master's Theses and Capstones*. 382.

<https://scholars.unh.edu/thesis/382>

This Thesis is brought to you for free and open access by the Student Scholarship at University of New Hampshire Scholars' Repository. It has been accepted for inclusion in Master's Theses and Capstones by an authorized administrator of University of New Hampshire Scholars' Repository. For more information, please contact nicole.hentz@unh.edu.

DYNAMIC RESPONSES OF A 20-TON CAPACITY FEED BUOY
IN AN OPEN OCEAN ENVIRONMENT

BY

JONATHAN F. HORTON

B.S., University of Massachusetts Dartmouth, 2006

THESIS

Submitted to the University of New Hampshire

in Partial Fulfillment of

the Requirements for the Degree of

Master of Science

in

Ocean Engineering

September, 2008

UMI Number: 1459495

INFORMATION TO USERS

The quality of this reproduction is dependent upon the quality of the copy submitted. Broken or indistinct print, colored or poor quality illustrations and photographs, print bleed-through, substandard margins, and improper alignment can adversely affect reproduction.

In the unlikely event that the author did not send a complete manuscript and there are missing pages, these will be noted. Also, if unauthorized copyright material had to be removed, a note will indicate the deletion.

UMI[®]

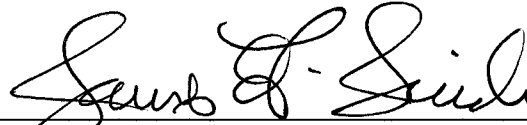
UMI Microform 1459495

Copyright 2008 by ProQuest LLC.

All rights reserved. This microform edition is protected against unauthorized copying under Title 17, United States Code.

ProQuest LLC
789 E. Eisenhower Parkway
PO Box 1346
Ann Arbor, MI 48106-1346

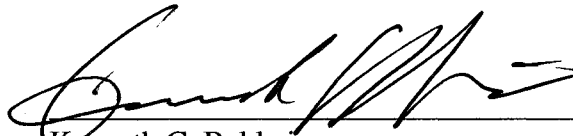
This thesis has been examined and approved.



James D. Irish
Thesis Director, Research Professor,
Ocean Engineering Program



M. Robinson Swift
Professor of Mechanical and Ocean Engineering



Kenneth C. Baldwin
Professor of Mechanical and Ocean Engineering

8/7/08

Date

*To my family and grandfather,
Francis A. Flynn*

ACKNOWLEDGEMENTS

I would like to thank all those who contributed to this work and helped me throughout my academic career at the University of New Hampshire. I would first like to thank two members of my thesis committee, Professors M. Robinson Swift and Kenneth C. Baldwin, for their involvement, support, and dedication to the thesis project. Special thanks go to my thesis advisor James D. Irish, whose guidance, patience, and time has been invaluable.

Thank you to Chad A. Turmelle for his previous work with the feed buoy and allowing me to use his data and figures. Thank you to Stanley J. Boduch and the crew of the R/V *Gulf Challenger* for their labors in the deployment and recovery of instrumentation at the demonstration site. Thank you to Judson C. DeCew for his efforts in the recovery operation at the demonstration site and his various help during the thesis writing process. Also, many thanks to all the Ocean Engineering graduate students and staff for their help and assistance throughout the project.

Lastly, I would like to thank my family – my mother Kathleen, my father Robert, and my brother James – for all their love and unwavering support throughout my thesis project and academic career. Special thanks to my grandfather Francis A. Flynn, who gave me the opportunity to go to school and always kept me on the path to success.

TABLE OF CONTENTS

ACKNOWLEDGEMENTS	iv
TABLE OF CONTENTS	v
LIST OF TABLES	vii
LIST OF FIGURES	viii
NOMENCLATURE	x
ABSTRACT	xi

CHAPTER	PAGE
I. INTRODUCTION	1
i. Background	1
ii. Previous Work	5
iii. Problem Definition	7
iv. Goals and Objectives	8
v. Approach	8
II. MATHEMATICAL BACKGROUND AND DATA ANALYSIS THEORY	11
i. Acceleration Theory	11
ii. Frequency Domain Analysis	12
iii. Linear Transfer Functions	14
iv. Wave Theory	15
v. Response Amplitude Operator	17
III. FIELD PROGRAM AND DATA PROCESSING	20
i. Overview	20
ii. Environmental Monitoring Mooring	20
iii. Motion Package	23
iv. Data Processing	26
v. Data Confidence	28

VI. FIELD DATA RESULTS	31
i. Results Overview	31
ii. Heave Results	42
iii. Surge Results	46
iv. Pitch Results	50
V. CONCLUSION	54
REFERENCES	58
APPENDIX A: Processed Field Program Data	60
APPENDIX B: MATLAB [®] Code	130

LIST OF TABLES

Table:	Description:	Page:
Table 4.1:	Wave Data from the Wave Rider Buoy	33
Table 4.2:	Additional Wave Data from the Wave Rider Buoy	34
Table 4.3:	Wave and Wind Data from GoMOOS Buoy B01	35

LIST OF FIGURES

Figure:	Description:	Page:
Figure 1.1:	Location of the Atlantic Marine Aquaculture Center's offshore demonstration site.	3
Figure 1.2:	A picture of the 20-ton capacity feed buoy at the demonstration site on March 11, 2008.	4
Figure 1.3:	Cross-section of 20-ton capacity buoy showing major buoy sections and major external components.	4
Figure 1.4:	General layout of the AMAC's submerged grid system at the offshore demonstration site.	5
Figure 1.5:	Diagram of the heave, surge, and pitch responses of the feed buoy.	9
Figure 3.1:	A picture of the environmental monitoring mooring at the demonstration site on March 11, 2008.	21
Figure 3.2:	An up close picture of the 20-ton capacity feed buoy at the demonstration site on March 11, 2008.	25
Figure 3.3:	The motion package at the bottom of the feed buoy's chine level on March 11, 2008.	25
Figure 3.4:	Plot of the 90% confidence limits for spectra.	30
Figure 4.1:	Plot of significant wave heights from the GoMOOS B01 buoy and the recovered wave rider data.	32
Figure 4.2:	Location of the GoMOOS B01 buoy compared to the environmental monitoring mooring and feed buoy.	33
Figure 4.3:	Surge, sway, and heave translations for the wave rider buoy on March 12, 2008 at 6 UTC.	35
Figure 4.4:	Surge, sway, and heave translations for the motion package inside the feed buoy on March 12, 2008 at 6 UTC.	36
Figure 4.5:	Roll, pitch, and yaw rotations for the motion package inside the feed buoy on March 12, 2008 at 6 UTC.	36
Figure 4.6:	Signal to noise ratio for wave elevation from the wave rider buoy.	38
Figure 4.7:	Signal to noise ratios for heave, surge, and pitch of the motion package.	39
Figure 4.8:	Comparison plot of heave, surge, and pitch RAOs, response spectra, and corresponding forcing spectra for March 12, 2008 at 6 UTC.	40
Figure 4.9:	Comparison plot of heave, surge, and pitch RAOs for March 12, 2008 at 6 UTC.	40
Figure 4.10:	Comparison of heave, surge, and pitch RAOs plotted against the physical and numerical model data.	41
Figure 4.11:	Experimental setup of the physical model testing in the UNH wave/tow tank.	41

Figure 4.12:	Heave RAO plotted against heave response of the feed buoy and wave elevation on March 12, 2008 at 6 UTC.	42
Figure 4.13:	Plot of the heave RAO with a 90% confidence interval.	43
Figure 4.14:	Comparison plot of heave RAO data to modeled data.	45
Figure 4.15:	Surge RAO plotted against surge response of the feed buoy and wave excursion on March 12, 2008 at 6 UTC.	47
Figure 4.16:	Plot of the surge RAO with a 90% confidence interval.	48
Figure 4.17:	Comparison plot of surge RAO data to modeled data.	49
Figure 4.18:	Scaled pitch RAO plotted against Pitch response of the feed buoy and wave slope on March 12, 2008 at 6 UTC.	50
Figure 4.19:	Plot of the pitch RAO with a 90% confidence interval.	51
Figure 4.20:	Comparison plot of pitch RAO data to modeled data.	53

NOMENCLATURE

Symbol:	Description:
\bar{a}	Average acceleration
Δt	Time interval
Δv	Velocity interval
a	Instantaneous acceleration
v	Velocity
x	Position
T	Record length
τ	Time Step
ω	Radian frequency
f	Frequency
t	Time
k	Wavenumber
g	Gravitational Constant
L	Wavelength
h	Water depth
z	Vertical position in the water column
A	Wave amplitude
ϕ	Velocity potential
η	Surface elevation
ζ	Wave excursion amplitude
θ	Wave slope amplitude
RAO	Response Amplitude Operator
V_D	Degrees of freedom (DOF)
δf	Frequency resolution

ABSTRACT

DYNAMIC RESPONSES OF A 20-TON CAPACITY FEED BUOY IN AN OPEN OCEAN ENVIROMENT

by

Jonathan F. Horton

University of New Hampshire, September, 2008

The 20-ton capacity feed buoy in operation at the Atlantic Marine Aquaculture Center's offshore demonstration site continues to serve as a leading model for marine aquaculture in the energetic ocean environment. Previous modeling and analysis proved survivability of the feed buoy in harsh storm driven seas, however, a field study was not performed at, or after, the time of deployment. This field program was conducted to find the dynamic responses of the buoy due to environmental forcing. Analysis of fair weather data shows small feed buoy responses in heave, surge, and pitch toward lower frequency waves commonly associated with storm events in the Gulf of Maine. Additionally, the study illustrated that higher frequency waves, which do not present any danger to the feed buoy or mooring, will excite the system. In general, feed buoy behavior is consistent with previous modeling, ensuring its survivability at the demonstration site.

CHAPTER I

INTRODUCTION

i. Background

Aquaculture is generally defined as the breeding, nurturing, and cultivation of sea products, such as finfish, algae, shellfish, or other marine organisms. Aquaculture is presently the fastest growing form of food production in the world and is becoming a significant source of food for many countries, including the United States. One area of aquaculture that is starting to get more attention and investigation is marine aquaculture. The marine aquaculture industry in the United States is relatively small when compared to overall United States and global aquaculture production. According to the National Oceanic and Atmospheric Administration (NOAA), world aquaculture production is about \$70 billion annually, with roughly \$1 billion belonging to the United States. Only about 20% of aquaculture in the United States deals with the production of marine species. Molluscan shellfish is about two-thirds of the marine aquaculture production in the United States; the remaining one third of total production consists of salmon (roughly 25%), shrimp (roughly 10%), and other species (NOAA, 2008). Present production of these marine species takes place mainly on land in tanks, in ponds, and in coastal waters under state jurisdiction. However, because of recent advances in offshore aquaculture technology, there has been a commercial drive to extend marine aquaculture operations to more exposed, energetic open ocean locations. With the present push to increase commercial marine aquaculture production in the offshore areas of the United States,

there come unforeseen issues and barriers. Some major barriers dealing with marine aquaculture are: (1) finding suitable sites in coastal and offshore areas, (2) clarifying regulatory and environmental requirements, (3) developing hatchery operations to provide fish for production systems, and (4) developing technologies and management practices for various ecosystems (NOAA, 2008). Developing technologies for marine aquaculture are of particular interest, because the engineered technology must be economically viable and meet certain design criteria for the energetic ocean environment.

To address these issues and barriers, the Open Ocean Aquaculture (OOA) Project was established in 1997, as a partnership between the University of New Hampshire (UNH) and NOAA. The project was created to provide research and development necessary to stimulate an environmentally sustainable offshore aquaculture industry in New England and the United States. This project has since evolved into the University of New Hampshire's Atlantic Marine Aquaculture Center (AMAC), where it works closely with commercial fishermen, coastal communities, private industry, and fellow marine research scientists to develop technology and knowledge to raise native, cold-water finfish and shellfish in exposed oceanic environments (AMAC, 2007). The center also has design projects and continuing research being conducted in various areas of offshore aquaculture.

The finfish aquaculture feed buoy is one such project being operated at AMAC's offshore demonstration site (seen in figure 1.1), which located south of the Isles of Shoals and approximately 12 km from the New Hampshire coast. This buoy as shown in figures 1.2 and 1.3, dubbed the "Aquamanna", was deployed at the site in the summer of 2007 after years of design and construction (Turmelle, 2007). The buoy is a remotely operable,

80-ton, automated fish feeding buoy that can hold up to 20 tons of food, and can feed four submerged net-pen fish cages at a time (layout shown in figure 1.4). It is currently used to feed crops of Atlantic cod (roughly 50,000 in a 3,000 m^3 Sea Station cage), but has been used to feed other species in the past, such as winter flounder and halibut (AMAC, 2007). As the buoy continues to serve as a platform for experimentation in offshore marine aquaculture, it endures tremendous environmental forcing due to frequent storm weather common to the Gulf of Maine in the winter and spring months. A study, including the implementation of model tests, was conducted during the design phase before deployment to address these environmental forcing concerns and to ensure buoy survival at the demonstration site.

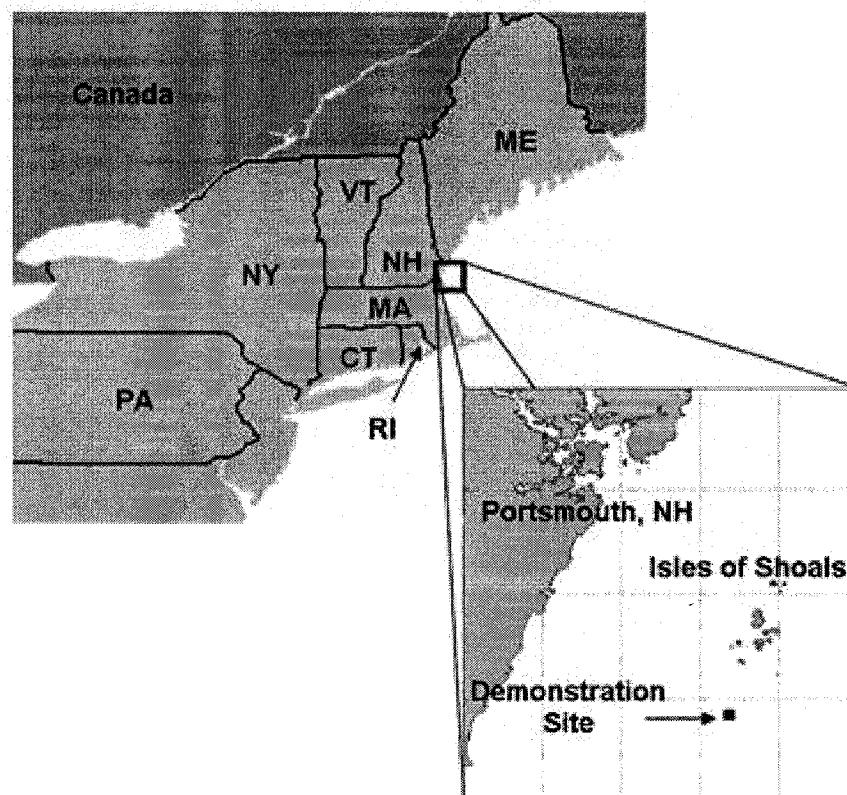


Figure 1.1: Location of the Atlantic Marine Aquaculture Center's offshore demonstration site off the coast of New Hampshire and south of the Isles of Shoals, USA (Turmelle, 2007).

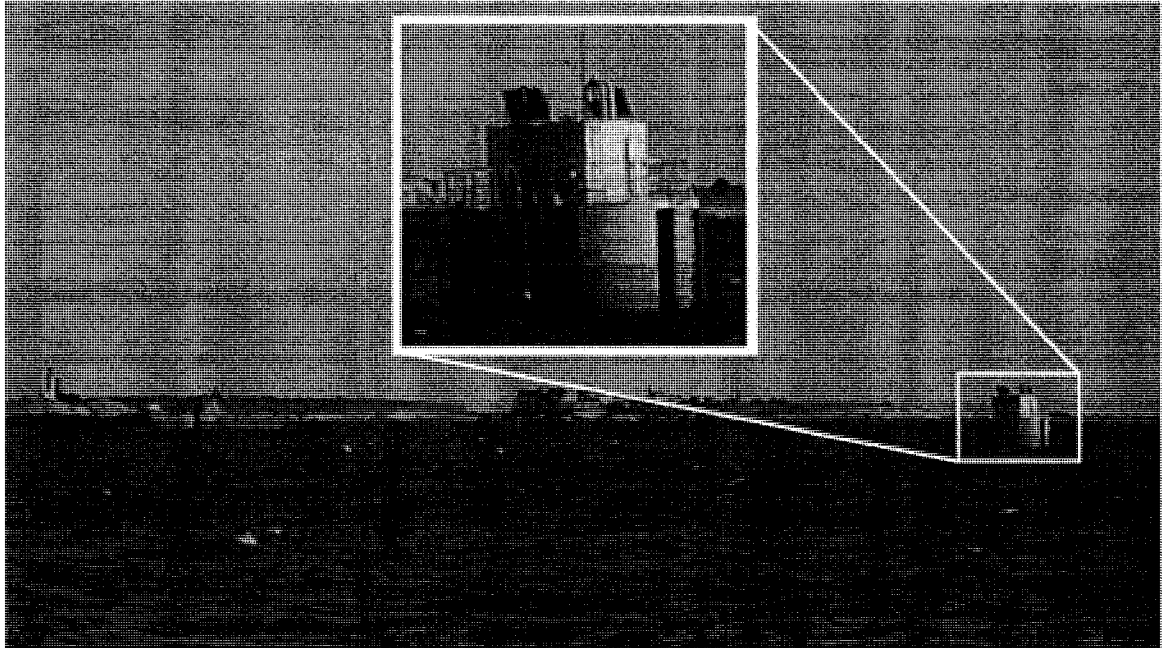


Figure 1.2: A picture of the 20-ton capacity feed buoy at the AMAC demonstration site on March 11, 2008. The Isles of Shoals can be seen in the background.

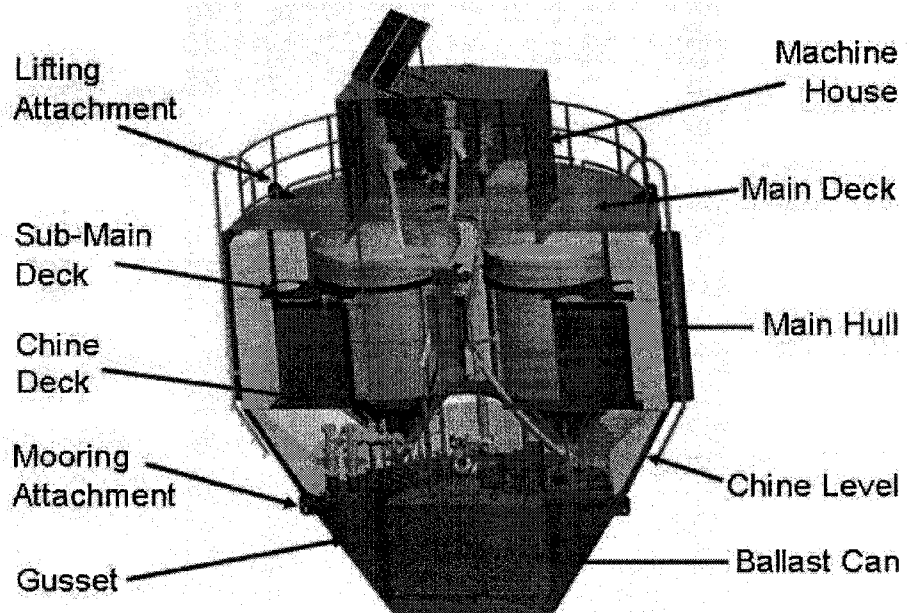


Figure 1.3: Cross-section of 20-ton capacity buoy showing major buoy sections and major external components at the AMAC's offshore demonstration site (Turmelle, 2007).

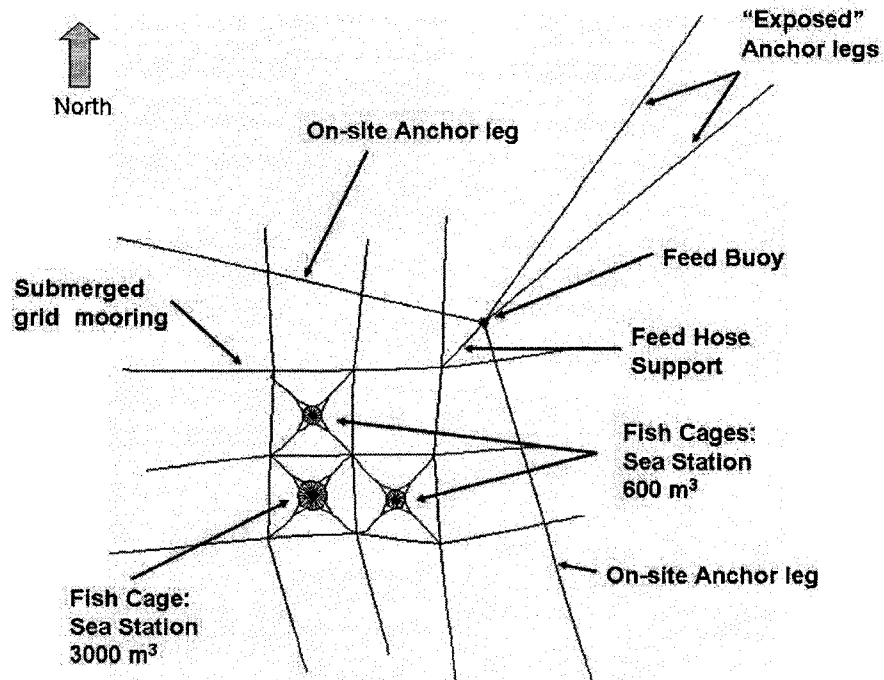


Figure 1.4: General layout of the AMAC's submerged grid system (as deployed) with the current design of the 20-ton feed buoy mooring at the offshore demonstration site (Turmelle, 2007).

ii. Previous Work

The comprehensive study of the 20-ton capacity feed buoy is described in Turmelle (2007). The thesis included the design, analysis, and construction of the buoy before its launch in the summer of 2007. More specifically, the thesis covered the topics of: buoy design criteria, construction, feed transfer system design, mooring system design, and both physical and numerical modeling. Hydrostatic analyses was conducted and included loading conditions for designing the buoy to withstand the harsh environmental conditions (e.g., large wave forcing from storm events) expected at the demonstration site in the south west corner of the Gulf of Maine. Loading conditions consisted of load (buoy full of fuel and feed), light (no feed or fuel in buoy), and ice (on the exterior surface of the buoy) conditions. The thesis concluded that all testing

conditions resulted in a positive metacentric height value, which indicated an acceptable, initial stability of the buoy (Turmelle, 2007).

To investigate the buoy's dynamic response in an open ocean environment the study included physical scale model and numerical model testing with regular sinusoidal, monochromatic waves. The physical scale model test incorporated the construction of a scale model of the buoy that was used in free-release and regular wave testing. The free release testing was conducted to determine the heave and pitch natural frequencies of the buoy; which provided insight into the buoy's motion in response to a variety of sea states as well as the overall stability of the buoy (Turmelle, 2007). The numerical model was generated using software package Marc.Mentat and was subjected to the same testing parameters of the physical scale model using Aqua-FE. The finite element modeling with Aqua-FE was consistent with the methods described in Tsukrov et al. (2003). Data from both tests were presented in the form of heave, surge, and pitch response amplitude operator (RAO) plots. With the exception of the surge RAO plots from both modeling methods, the curve shapes for the other RAO plot results were similar to each other; which meant that data obtained from using the numerical and physical models corroborated one another (Turmelle, 2007). Through both sets of testing, the study concluded that the buoy would be a wave follower with respect to vertical motion for large, long period waves that occur during severe weather storms. It also showed a heave resonance of the system at higher frequencies associated with small, fair-weather waves. It was predicted that the buoy would not have severe reactions (e.g., enough feed buoy response to put the deck under water or break away from the mooring lines) in response

to storm waves commonly observed at the buoy's location in the demonstration site (Turmelle, 2007).

iii. Problem Definition

The previous work done by Turmelle (2007) ensured feed buoy survivability in the open ocean by showing that the feed buoy would not be excited enough by large storm waves to put the deck under water. Because of this work, there was an opportunity to expand on earlier studies by incorporating a field program to collect environmental forcing and feed buoy system response data; which could be used for comparison to the physical and numerically modeled data. Assuming a linear system, the regular (sinusoidal, monochromatic) wave, physical scale and numerical modeling tests provided a sound engineering basis on how the buoy would respond in the open ocean (random sea) environment. A field program, however, would take this study a step further by showing actual feed buoy behavior at the demonstration site. It is also important to note that the feed buoy mooring system and components were simplified in the physical scale modeling in the UNH tow/wave tank. Because of this difference, a direct comparison to the modeled data cannot be made with a field program; however, having observational data to compare with trends presented in the modeled data would show if the feed buoy system is behaving as predicted. Overall, a field program would investigate feed buoy behavior in greater detail and provide researchers with the dynamic responses of the feed buoy system due to environmental forcing at the site.

Another minor and related problem with the feed buoy is its tendency to lose communication during storms with large waves. This problem is believed to stem from

the vertical rod communications antenna mounted on top of the feed buoy. This antenna was chosen for its strong radiation, or beam pattern, in the horizontal direction; however, the antenna has a beam pattern of plus and minus 30 degrees from the horizontal direction, so if the buoy rolls or pitches this amount, communication may be lost. If the roll or pitch of the buoy is less than 20 degrees, the antenna should work within parameters. Studying the roll or pitch response of the buoy to wave data may provide answers to which sea states will cause this communication problem.

iv. Goals and Objectives

The objectives of this research were to:

- Design and conduct a field program to collect environmental forcing (wave) and feed buoy system response data at the demonstration site.
- Design routines to process and interpret the collected observational data.
- Evaluate and explain the dynamic responses of feed buoy system.

v. Approach

To meet the goals and objectives of this study a method of approach was developed to find the feed buoy system responses to waves by deploying instrumentation at the demonstration site. The first step was the calibration and deployment of the environmental monitoring mooring (which is less formally called the “wave rider buoy”) to the southwest corner of the site. The wave rider buoy measured various environmental properties in the open ocean; however, for this study it measured the environmental forcing at the site by recording its own acceleration in the x-, y-, and z- directions (Irish

et al., 2001). The accelerations in the z-direction were processed into buoy heaves, which is the estimation of sea surface elevations at the site due to waves during the time of recording. At the same time, a motion package was mounted near the center of gravity inside the feed buoy, which was located in the northeast corner of the demonstration site, roughly 400 meters away from the wave rider buoy. The motion package, which was developed at Woods Hole Oceanographic Institution (WHOI), consists of various electronics, hardware, and a Systron Donner 6-axis motion sensor as the main sensing element (Irish et al., 2001). The sensing element measures the acceleration in the x-, y-, and z-directions and the rate of rotation around the three axes. These data were processed into the heave, surge, and pitch responses (shown in figure 1.5) of the feed buoy system.

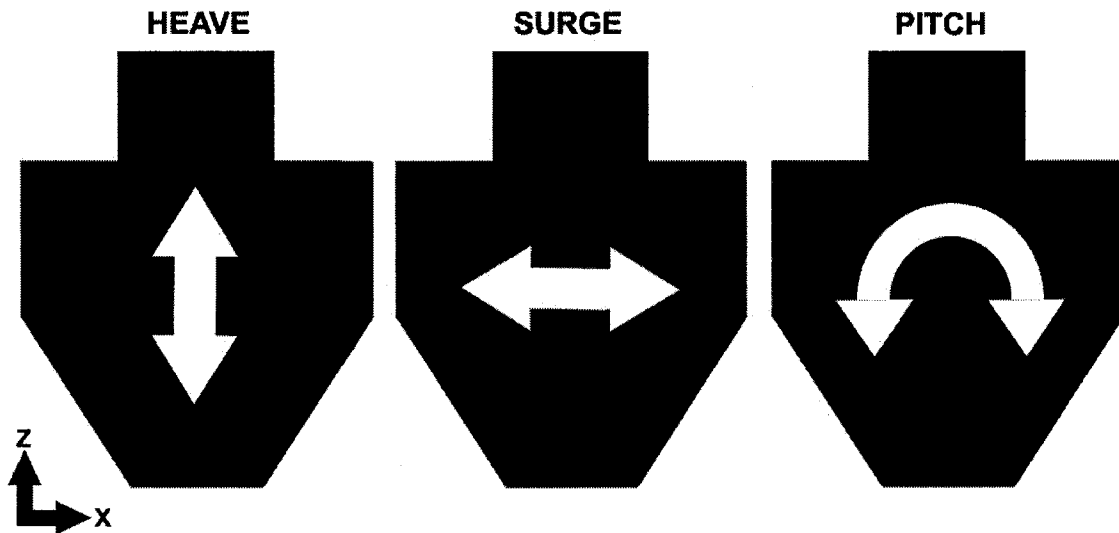


Figure 1.5: Diagram of the heave, surge, and pitch responses of the feed buoy. Heave is the linear vertical motion (z-axis), surge is the linear longitudinal motion (x-axis), and pitch is when the feed buoy rotates about the transverse (y-) axis.

Since lower frequency waves would have affect on the large feed buoy, data from both the motion package and wave rider buoy were collected over a month and a half

period starting in the spring of 2008. This large collection period provided a long enough duration to hopefully collect data from storm events (i.e., large wave forcing) that are common to the Gulf of Maine in the late winter and early spring time months. Once the observational data were collected, the motion package and wave rider buoy would be retrieved from the site and their corresponding data processed using MATLAB[®]. Wave rider data was processed into wave forcing spectra and the motion package data into heave, surge, and pitch response spectra. These spectra were used to calculate and plot the response amplitude operators (RAOs) for the feed buoy system. These results, the dynamic responses of the feed buoy system, were compared to the previous work by Turmelle (2007) as an attempt to substantiate the physical scale and numerical modeling. The resulting pitch, or roll, RAO data were examined further to determine which sea states may cause the feed buoy to pitch, or roll, in such a way that it would cause communication problems.

CHAPTER II

MATHEMATICAL BACKGROUND AND DATA ANALYSIS THEORY

i. Acceleration Theory

Acceleration is simply the rate at which an object's velocity changes with time. This quantity is expressed in units of length per time squared. Commonly, and throughout this thesis, it is expressed as units of meters per second squared or m/s^2 . For motion along any axis, the average acceleration (\bar{a}) over a time interval of Δt is

$$\bar{a} = \frac{v_2 - v_1}{t_2 - t_1} = \frac{\Delta v}{\Delta t}, \quad (2.1)$$

where the object initially had a velocity v_1 at time t_1 , and then a velocity v_2 at t_2 . The instantaneous acceleration (a), which is simply just referred to as acceleration, can be found by taking the derivate of the velocity with respect to time:

$$a = a(t) = \frac{dv}{dt}. \quad (2.2)$$

Since the acceleration of an object is time dependent, calculus methods can be used for motion analysis. The relationships between position, velocity, and acceleration can be expressed in terms of derivatives or integrals. Acceleration can be found from position (x) by using the formula

$$a = \frac{dv}{dt} = \frac{d^2x}{dt^2}, \quad (2.3)$$

where the acceleration of an object at any instant is the second derivative of its position $x(t)$ with respect to time.

Inversely, the position of an object can be found by integrating the acceleration twice with respect to time (Halliday et al., 2001). Many ocean observation devices and systems take advantage of these relationships. As in this study, both the wave rider buoy and feed buoy motion package used accelerometers to measure the acceleration in the x-, y-, and z- directions. From these recorded acceleration data, position (i.e., displacement) were computed through integration.

ii. Frequency Domain Analysis

Some of the fiercest and dominating forces on structures in the open oceans are the waves. Wave forces on offshore structures and systems are more complex due to their stochastic nature. Since it is difficult to obtain explicit mathematical expressions for these types of time series, a statistical approach is taken in this study to investigate the field results. Here the analysis is performed in the frequency domain using an assumed linear stochastic systems model. From this approach, relationships called linear transfer functions were developed between the system response and forcing mechanisms. This section, and the following, is organized in a similar manor used by Fredriksson (2001) and Fredriksson et al. (2003) to analyze the dynamics of a central spar fish cage and mooring system. In similar style, this theory is developed with continuous, infinite functions; however, the actual measured data was discrete and finite. Because of this, discrete versions of the formulas are used in computation. This includes using the fast Fourier transform (FFT) method on the actual measured data.

Typically, the auto-spectral density function is used to investigate system characteristics in the frequency domain (Ochi, 1998). This is developed from using the

auto-correlation function $R_{xx}(\tau)$, which is expressed as the ensemble average of the product of two time series measurements, $x(t)$, of the same time record shifted by a time step of τ ,

$$R_{xx}(\tau) = E[x(t) \cdot x(t + \tau)]. \quad (2.4)$$

These stochastic processes can also be described by different properties. If a process is stationary, then its joint probability distribution does not change when the origin of the time scale is shifted in time. If a process is ergodic, then all the statistics associated with the ensemble can be obtained from a single time series. If the stochastic process is both stationary and ergodic, the random process will not change its statistical properties with time, and the ensemble averages are equivalent to the time averages. With this, the auto-correlation can be evaluated by time averaging over the record length (T) according to

$$R_{xx}(\tau) = \lim_{T \rightarrow \infty} \frac{1}{T} \int_{-T/2}^{T/2} x(t) \cdot x(t + \tau) \cdot dt. \quad (2.5)$$

Ocean wave forcing and the system response are considered weak stationary and ergodic processes, this formula for the auto-correlation function can be used on wave records (Ochi, 1998). Since analysis of the data is to be done in the frequency domain, the continuous Fourier transform expressions are used to move the data between the time and frequency domains. Following similar notation from Oppenheim et al. (1997) and Ochi (1998), these expressions are defined as

$$X(\omega) = \int_{-\infty}^{\infty} x(t) \cdot e^{-j\omega t} \cdot dt \quad (2.6)$$

and

$$x(t) = \frac{1}{2\pi} \int_{-\infty}^{\infty} X(\omega) \cdot e^{j\omega t} \cdot dt. \quad (2.7)$$

Noting that

$$\omega = 2\pi \cdot f ,$$

where f is the frequency in Hertz. By taking the continuous Fourier transform of equation (2.5) with equation (2.6), a double sided, auto-spectral density function, $S_{DS}(\omega)$, can be obtained such that

$$S_{DS}(\omega) = \frac{1}{2\pi} \int_{-\infty}^{\infty} R_{xx}(\tau) \cdot e^{-j\omega\tau} \cdot d\tau . \quad (2.8)$$

This double sided auto-spectral density function is continuous for all frequencies between plus and minus infinity ($\pm\infty$) (Ochi, 1998). However, in practice and utilized by Fredriksson et al. (2003), a spectrum is usually represented between zero and positive infinity (∞) so that a one sided auto-spectral density function is used, where

$$S(\omega) = 2 \cdot S_{DS}(\omega) \text{ for } 0 \leq \omega \leq \infty . \quad (2.9)$$

iii. Linear Transfer Functions

Assuming a linear, time invariant system (also known as a LTI system), the relationship between the environmental forcing from waves, $x(t)$, and the output response of the feed buoy, $y(t)$, can be represented by an impulse response function $h(\tau)$. The relationship between input and output is described in the following expression:

$$y(t) = \int_0^{\infty} h(\tau) \cdot x(t-\tau) \cdot d\tau , \quad (2.10)$$

where $h(\tau) = 0$ for $\tau < 0$. Time averaging the product of $y(t) \cdot y(t+\tau)$ yields the following input and output auto-correlation relationship:

$$R_{yy}(\tau) = \int_0^{\infty} \int_0^{\infty} h(\alpha) \cdot h(\beta) \cdot R_{xx}(t+\beta-\alpha) \cdot d\alpha \cdot d\beta , \quad (2.11)$$

where α and β are separate time shift variables (Bendat and Peirsol, 2000). Taking the Fourier transform of equation (2.11), while applying the relationship described in equation (2.9), the linear transfer function relationship is obtained:

$$S_y(\omega) = |H(\omega)|^2 \cdot S_x(\omega), \quad (2.11)$$

where the linear transfer function is defined as the Fourier transform of $h(t)$,

$$H(\omega) = \frac{1}{2\pi} \int_0^{\infty} h(\tau) \cdot e^{-j\omega\tau} \cdot d\tau. \quad (2.12)$$

$H(\omega)$ is the frequency response function, which is a Fourier transform pair with the impulse response function. Only the gain portion (which is frequency dependent) of the linear transfer function in equation (2.11) is maintained, which reduces the complexity of the relationship between input forcing and output response. Also, the phase term associated with linear transfer function (equation 2.12) was not used in the study, only the magnitudes.

iv. Wave Theory

Wave characteristics in this study were derived using linear Airy wave theory as described by Dean and Dalrymple (1991). This theory is most accurate for low amplitude waves in deep water (i.e., when the depth of the water is much greater than the wavelength of waves) and is not mathematically intensive. This is the most practical theory to use because the feed buoy is situated in water roughly 52 meters deep, and the wave heights and lengths typically observed at the area are small compared to depth. It also keeps the mathematical computation and processing from becoming too intense and

complex. Using Airy wave theory, wave characteristics are described by the velocity potential (ϕ)

$$\phi = -A \frac{g}{2\pi \cdot f} \frac{\cosh(k(h+z))}{\cosh(k \cdot h)} \sin(kx - 2\pi \cdot f \cdot t), \quad (2.13)$$

Surface elevation (η)

$$\eta = A \cdot \cos(k \cdot x - 2\pi \cdot f \cdot t), \quad (2.14)$$

And dispersion relation

$$(2\pi \cdot f)^2 = g \cdot k \cdot \tanh(k \cdot h), \quad (2.15)$$

where A is the wave amplitude (half the wave height), f is the frequency, g is the gravitational constant (equal to 9.81 m/s^2), L is the wavelength, k is the wave number (equal to $2\pi/L$), h is the water depth (approximated to a depth of 52 meters for this study), z is vertical position in the water column, and x is the horizontal position along the surface (Dean and Dalrymple, 1991). Using a normal storm wave ($f \approx 9$ seconds, and $L \approx 126$ meters) typical to the area, $\tanh(k \cdot h)$ was computed to have a value of 0.99. Since $\tanh(k \cdot h)$ is nearly 1, the wave number (k) can be approximated by the formula:

$$k = \frac{(2\pi \cdot f)^2}{g}. \quad (2.16)$$

From these expressions, other wave characteristics such as wave excursion amplitude (ζ) and wave slope amplitude (θ) can be derived. The wave excursion amplitude is defined as the horizontal semi-axis of the ellipse formed by the water particle at the surface. It is found by taking the partial derivative of equation (2.13), with respect to x , to acquire the horizontal velocity component and then integrating the result

with respect to time (t) (Dean and Dalrymple, 1991). Finally, the oscillating term is dropped from the expression and it becomes:

$$\zeta = A \frac{\cosh(k \cdot h)}{\sinh(k \cdot h)}. \quad (2.17)$$

The wave slope amplitude is found in a similar way, where the partial derivative of equation (2.14) is taken with respect to x and the oscillating term is dropped (Dean and Dalrymple, 1991). The resulting expression for wave slope amplitude is:

$$\theta = k \cdot A. \quad (2.18)$$

v. Response Amplitude Operators

In sea keeping, response amplitude operators (RAOs) are linear transfer function magnitudes used to determine the effect that a sea state has upon the motion of a ship or structure in the water. These RAOs are found by dividing the amplitude of the response by the amplitude of the forcing for each wave frequency; thus making the expressions frequency dependent. From equation (2.11), the general the relationship between forcing and response for a linear system becomes:

$$S_r(\omega) = RAO^2 \cdot S_f(\omega), \quad (2.19)$$

where $S_r(\omega)$ is the response spectrum, $S_f(\omega)$ is the forcing spectrum, and the RAO is response amplitude operator magnitude. The heave, surge, and pitch RAOs are the results of interest in this study. The heave is the vertical motion of the structure, the surge is the horizontal motion of the structure in the direction of the waves, and the pitch is the rotation around the axis perpendicular to wave direction. The heave RAO is defined as the heave amplitude divided by wave elevation amplitude; the surge RAO is defined as

the surge amplitude divided by the wave excursion amplitude; and the pitch RAO is the pitch amplitude divided by the wave slope amplitude.

This study measured data in random sea environment and processed it in the frequency domain, the RAOs were calculated as a function of frequency using the auto-spectral method discussed earlier. The system forcing characteristics can be expressed in terms of energy density as the wave elevation auto-spectrum ($S_\eta(\omega)$), wave excursion auto-spectrum ($S_\zeta(\omega)$), and wave slope auto-spectrum ($S_\theta(\omega)$). The first two auto-spectra are expressed in meters squared per Hertz or m^2/Hz and the last auto-spectrum is expressed in radians squared per Hertz or rad^2/Hz . The wave elevation auto-spectrum was calculated from the measured wave height time series recorded by the wave rider buoy. The wave excursion and wave slope auto-spectra were then calculated from the wave elevation auto-spectrum using the following expressions,

$$S_\zeta(\omega) = S_\eta(\omega) \cdot [\tanh(k \cdot h)]^{-2} \quad (2.20)$$

and

$$S_\theta(\omega) = S_\eta(\omega) \cdot k^2, \quad (2.20)$$

respectively where wavenumber is a function of frequency according to the dispersion relation. Similarly, the auto-spectral motion response in heave ($S_h(\omega)$), surge ($S_s(\omega)$), and pitch ($S_p(\omega)$) are calculated using discrete forms of equations (2.8) and (2.9). Again, these auto-spectra are expressed in meters squared per Hertz (m^2/Hz) or radians squared per Hertz (rad^2/Hz). Based on the relationship between the forcing and response shown in equation (2.11), the auto-spectral techniques were used to find the linear transfer functions (i.e., RAOs) for these responses:

$$|H_h(\omega)| = \left[\frac{S_h(\omega)}{S_\eta(\omega)} \right]^{1/2}, \quad (2.22)$$

$$|H_s(\omega)| = \left[\frac{S_s(\omega)}{S_\zeta(\omega)} \right]^{1/2}, \quad (2.23)$$

and

$$|H_p(\omega)| = \left[\frac{S_p(\omega)}{S_\theta(\omega)} \right]^{1/2}, \quad (2.24)$$

where $H_h(\omega)$ is the heave transfer function, $H_s(\omega)$ is the surge transfer function, and $H_p(\omega)$ is the pitch transfer function.

CHAPTER III

FIELD PROGRAM AND DATA PROCESSING

i. Overview

The field measurement program in this study was comprised of two parts: data collection from a motion package mounted in the feed buoy, and data collection from the wave rider buoy deployed near the feed buoy at the demonstration site. The wave rider was used to collect wave forcing records, and the data collected from the motion package was used to measure the system response of feed buoy. Both of these systems were deployed to the demonstration site (with a water depth of roughly 52 meters) in the spring of 2008, from March 11th to April 31st. This time period was chosen because of the likelihood that storm events would occur and cause low-frequency, high-energy storm waves. In turn, these waves would provide large responses in the feed buoy system. Descriptions of the instruments parameters and setup, along with the data processing routines, will be discussed in the following sections.

ii. Environmental Monitoring Mooring

The environmental monitoring mooring, or wave rider buoy, was available at the Center for Ocean Engineering at UNH for this study to collect environmental forcing data by following the waves at the site (shown in figure 3.1). It was deployed in the morning of March 11, 2008 at a position of 42° 56.4574' North latitude and 70° 38.0819' West longitude in the south west portion of the demonstration site (about 400 meters away

from the feed buoy's northeast corner of the AMAC site). The wave rider buoy was taken to the site aboard the R/V *Gulf Challenger*, which is a 50-foot aluminum research vessel for the UNH Marine Program, and put into position by the crew. The position of buoy is roughly 3 kilometers south of the Isle of Shoals, and about 12 kilometers from the New Hampshire coastline. A telemetry link with the buoy was established on deployment to make sure the buoy was working and operating normally.

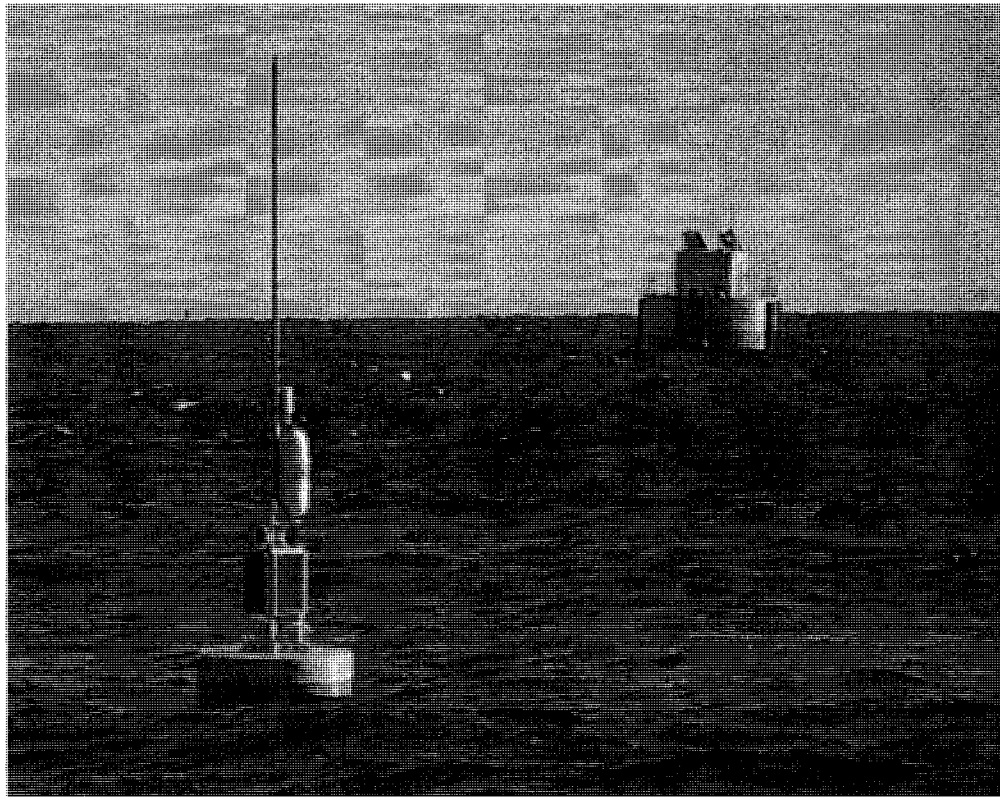


Figure 3.1: A picture of the environmental monitoring mooring (i.e., wave rider buoy) in the foreground deployed at the open ocean aquaculture site on March 11, 2008. The 20-ton capacity feed buoy can be seen in the background.

For this study, the instruments on the buoy were set to burst sample at the beginning of every hour starting at 00:00:00 coordinated universal time (UTC). UTC is sometimes used interchangeably with Greenwich Mean Time (GMT), however, the main difference is that UTC is an atomic time and GMT is an astronomical time. Each burst

sampled heave (z-direction) acceleration of the buoy for a duration of 20 minutes at rate of 5 Hz. The accelerations (with a range of ± 1.5 g) were measured by a Summit Instrument 3-axis accelerometer (model 34103A) installed on the electronics/signal conditioning board in the dry well of the buoy. The accelerometers themselves are force-balance systems which consist of a highly magnetic mass hung from a bearing; which is in a null position and counterbalanced by a magnetic (torque) coil located at the axis of rotation of the mass (Muramatsu, 2000). In general, when acceleration is applied to the sensor, a force is exerted on the mass which attempts to move away from the null position. When the sensor detects motion, the coil current is increased by means of an amplifier or electronics to maintain the null position. The current through the coil is proportional to the acceleration of the sensor (Muramatsu, 2000). In the case of the Summit Instrument 3-axis accelerometer, the outputs are voltages and the output for each axis is directly proportional to the acceleration along that axis. Each record from the wave rider buoy consisted of 6,000 data points, and was stored internally on a flash card in the dry well of the buoy. Saving it internally also eliminated the need of transmitting and receiving the data, which usually experiences communication problems in stormy seas. A more detailed report on the workings of the environmental monitoring mooring can be found in Irish et al. (2001), and Irish and Fredriksson (2003). The buoy was recovered from the demonstration site by the R/V *Gulf Challenger* and crew on April 31, 2008.

iii. Motion Package

The Center for Ocean Engineering at UNH also provided the motion package to measure the motion responses of the feed buoy (shown in figure 3.2) to wave forcing. It was deployed during the same trip to deploy the wave rider buoy, and was mounted inside the feed buoy. The motion package consists of Systron Donner motion sensors and hardware measuring the acceleration (measured in g's per volt) and rotation rates (measured in degrees per second) around the x-, y-, and z- axis. The main electronics of the motion package consisted of a Systron Donner 6-axis motion sensor element (i.e., BEI MotionPak), a filter/signal condition card, and a PC-104 based data recording system (including a hard drive), which were all housed in a watertight aluminum canister. More specifically, the BEI MotionPak uses three orthogonally mounted quartz angular rate sensors and three high performance linear servo accelerometers to measure rotations and motions, respectively. As described in Madni et al. (1996), the quartz rate sensor (QRS) consists of a micro-miniature, double-ended, piezoelectric quartz tuning fork and a supporting structure. Using the Coriolis Effect, a rotational motion about the tuning fork's longitudinal axis produces a DC voltage proportional to the rate of rotation. The linear servo accelerometers in the motion package were force-balance systems as well; and have the same general theory as the wave rider accelerometers described in the previous section. Nonetheless, a more detailed report on the motion package and all the specific components used can be found in Irish et al. (2001). For the field program, the canister was band-strapped to a silo support beam and set on top of the concrete ballast inside the feed buoy (shown in figure 3.3). The position of the motion package was at the bottom of the chine level. This is the lowest serviceable area of the feed buoy and near

the estimated depth of the center of gravity. However, not directly on the center axis (roughly 1.65 meters off center) since there was nowhere to band-strap the motion package down and it would have inhibited operator movement about the chine level.

Before deployment, the motion package was calibrated against local gravity in the laboratory and programmed to burst sample at the beginning of every two hours starting at 00:00:00 coordinated universal time (UTC). Each burst sampled the directional acceleration and rotation of the buoy for the duration of 18.2 minutes at rate of 10 Hz. Each record consisted of 10920 data points, and was stored internally on a hard drive in the canister. The motion package was oriented in such a way that the x-direction axis, corresponding to surge, was in the southwest to northeast direction; and the y-directional axis, corresponding to sway, was in the northwest-southeast direction. The z-directional axis still corresponded to heave. The pitch and roll is the rotation around y- and x- axis, respectively. Like the wave rider buoy, the motion package was also recovered by the R/V *Gulf Challenger* and crew on April 31, 2008.

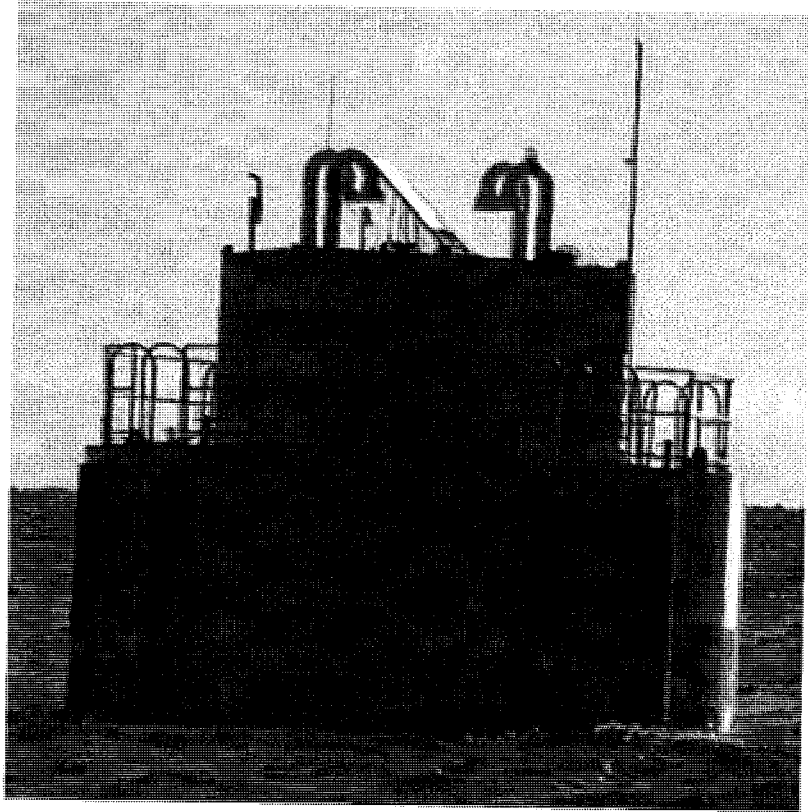


Figure 3.2: An up close picture of the 20-ton capacity feed buoy at the open ocean aquaculture site on March 11, 2008.



Figure 3.3: The motion package being strapped down, at the bottom of the feed buoy's chine level, by Stanley Boduch (Open Ocean Aquaculture Research Engineer) on March 11, 2008.

iv. Data Processing

The data processing techniques discussed here are similar with procedures set forth by the National Oceanic and Atmosphere Administration's (NOAA) National Data Buoy Center (NDBC). The NDBC is part of the National Weather Service (NWS) and is in charge of the development and operation of a network of data collecting buoys and coastal stations around the United States and the world (www.ndbc.noaa.gov). The data processing techniques are not exactly the same as the NDBC's methods because NDBC motion packages have damped gimbaled accelerometers. More information on the NDBC's procedures for non-directional and directional wave data analysis can be found in Earle (1996). Since the time series data recorded from sensors in the wave rider buoy and the motion package was discretely sampled, discrete versions of the formulas discussed in chapter two were used in the MATLAB[®] data processing. MATLAB[®] is a numerical computing environment and programming language which allows easy manipulation of data, implementation of algorithms, and data plotting. The discrete nature of the data allowed for Fast Fourier Transforms (FFT) methods to be used in transforming the raw data into the frequency domain. Once the data was transformed and Butterworth filtered, the response amplitude operators (RAOs) were processed and plotted.

The processing of the observational data to responses had two parts: motion package data were processed first, then the corresponding wave rider data. The data from the motion package was read as an acceleration (measured in g's per volt) time series array or rotation rate time series array, which has instrumentation calibration taken into account (these calibration values can be seen in the MATLAB[®] functions in appendix

B). The raw acceleration time series data then passed to a function which converted the data from g's to meters per second squared; then the mean and linear trend were removed; then it was filtered through a fourth-order, high-pass, Butterworth filter with a 0.0333 Hz cutoff frequency; and finally, it was integrated twice (using the trapezoidal rule) to a displacement time series. The filter was needed due to the tendency of accelerometers to introduce spurious energy (i.e., noise) into acceleration spectra, particularly at low frequencies (Earle et al., 1984). This low frequency noise problem is common to the accelerometers installed in the motion package and waver rider buoy, which showed up in the recovered data. Examining the signal to noise ratio for the data over the entire frequency range allowed for appropriate cutoff frequencies to be used in plotting; so that the plots were representative of recorded signal than instrument noise. The 0.0333 Hz cutoff frequency corresponds to 30 second waves, so waves or feed buoy motions of greater periods will be filtered out. This seems reasonable because storm waves of interest in this region were typically in the range of 6 to 12 seconds; with the larger storms usually producing waves in the 8 to 11 second range in the Gulf of Maine. In another function, the rotational time series data is computed similarly to the displacement data; however, it is only integrated (using the trapezoidal rule) once to a degree time series. This is because the motion package records rotational data as a rotation rate (degrees per second) not acceleration. The degree time series data also has an additional step of being converted to radian time series data, which is more commonly used for RAO plots dealing with rotations. Once the displacement and rotational time series are both computed, the data were converted to frequency domain spectra using an FFT method. The FFT method used 1024 data point blocks (non-overlapping), which

smoothes the spectra and normalizes them to units of spectral density. Once all the response and forcing spectra were found, the heave, surge, and pitch RAOs were computed using the same procedure as shown equations (2.22), (2.23), and (2.24). The data for the wave rider is processed similar to the motion package, besides the fact it does not have any rotational time series data to be processed and used 512 data point blocks. For a more detailed understanding of the processing routines, please refer to the MATLAB[®] code in appendix B.

v. Data Confidence

Uncertainty in results from data with random statistics is always a problem for studies involving the open ocean environment. To obtain confidence in the data, the 90% confidence intervals were computed for the RAO data. The confidence interval of an estimate is the range where the true value is most likely to be. In other terms, a given confidence level represents the probability that a random sample falls within that interval 90% of the time. Confidence intervals are calculated so that a certain percentage of the intervals include the unknown value. The interval used in this study was the 90% confidence interval, meaning 10% of the values might not fall in this range. These confidence intervals are bounded by upper and boundaries called confidence limits. The closer these limits are to each other, the narrower the interval range becomes and the more precise the estimate is. In terms of spectral confidence limits, the process being sampled is assumed to be a Gaussian random process in time, where the spectrum values are distributed with V_D degrees of freedom (DOF) as expressed in equation 3.1. This can also be expressed as twice the number of blocks averaged together:

$$V_D = 2 \cdot T \cdot \delta f, \quad (3.1)$$

where T is the length of the record and δf is the desired final frequency resolution. However, as the degrees of freedom are increased (i.e., confidence increased) for a fixed record length, δf increases hence there is a decrease in frequency resolution. In general, the more data averaged together, the more the results will represent the statistics of the environment, thus giving more confidence in the data. Since data point blocks were used in the FFTs, the spectra from the wave rider and motion package were averaged with 11 blocks (22 DOF) and 10 blocks (20 DOF), respectively. These gave frequency resolution of ~ 0.0092 Hz for both the wave rider and motion package spectra. These resolutions correspond to ~ 109 second waves, which is far below the 10 to 12 second maximum period waves seen in the Gulf of Maine. Using a table of 90% confidence levels adapted from table A9.6 in Koopmans (1974), the upper and lower spectral limits for the corresponding number of degrees of freedom were interpolated as 1.795 and 0.647 for the wave rider spectra and 1.843 and 0.637 for the motion package spectra. The values adapted from table A9.6 are plotted in figure 4.20 for clarity. Multiplying the corresponding wave rider and motion package spectra with the limits allowed for the confidence intervals to be computed. Once computed, the upper and lower limit spectra were processed separately in the same manor as shown in equations (2.22), (2.23), and (2.24) for the RAOs. However, the upper RAO confidence limit was found by taking the square root of the upper limit spectra of the response divided by the lower limit spectra of the forcing; and vice versa for the lower RAO confidence limit. This way of computing the two limits is a first order estimate, which provided the broadest interval making it a slightly conservative estimate.

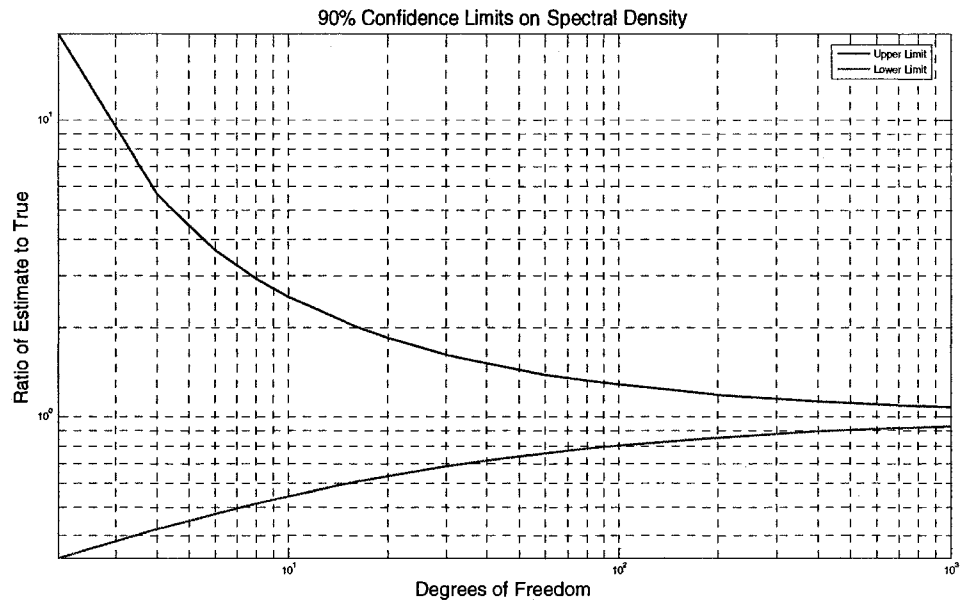


Figure 3.4: Plot of the 90% confidence limits for spectra, adapted from table A9.6 in Koopmans (1974).

CHAPTER IV

FIELD DATA RESULTS

i. Results Overview

Data storage devices with the recorded observational data from both the wave rider buoy and feed buoy motion package were taken to the laboratory to be processed after their recovery on April 31, 2008. Upon a brief inspection of the recovered data, the motion package only recorded data from 16 UTC on March 11th to 12 UTC on March 13th. Since the motion package only sampled every 2 hours over this 2 day period, only 23 sets of data were recorded to the hard drive. After further investigation, it was determined that the motion package failed because of a bad battery pack. The wave rider buoy, however, collected data for the entire deployment from March 11th to April 31st; yet only a small fraction of this collected data can be used because of the failure in the motion package.

Significant wave height values were computed from the recovered wave rider buoy data and are plotted in figure 4.1 (and listed in table 4.1). The significant wave height is simply the average height (trough to crest) of the top one-third (largest) waves recorded; it is approximately equal to four times the standard deviation of the displacement from the mean sea level (Dean and Dalrymple, 1991). Additional wave data from the wave rider buoy is listed in table 4.2. For good measure, the wave rider data is compared to data from the GoMOOS B01 (Western Maine Shelf) buoy, which is a part of the Gulf of Maine Ocean Observing System (GoMOOS). The GoMOOS B01 buoy is to

the north-northeast of the open aquaculture site as shown in figure 4.2. The significant wave heights from the GoMOOS B01 buoy for the corresponding time period are also displayed in figure 4.1. Additional data downloaded from the GoMOOS website (<http://www.gomoos.org/>) for this time period is shown in table 4.3.

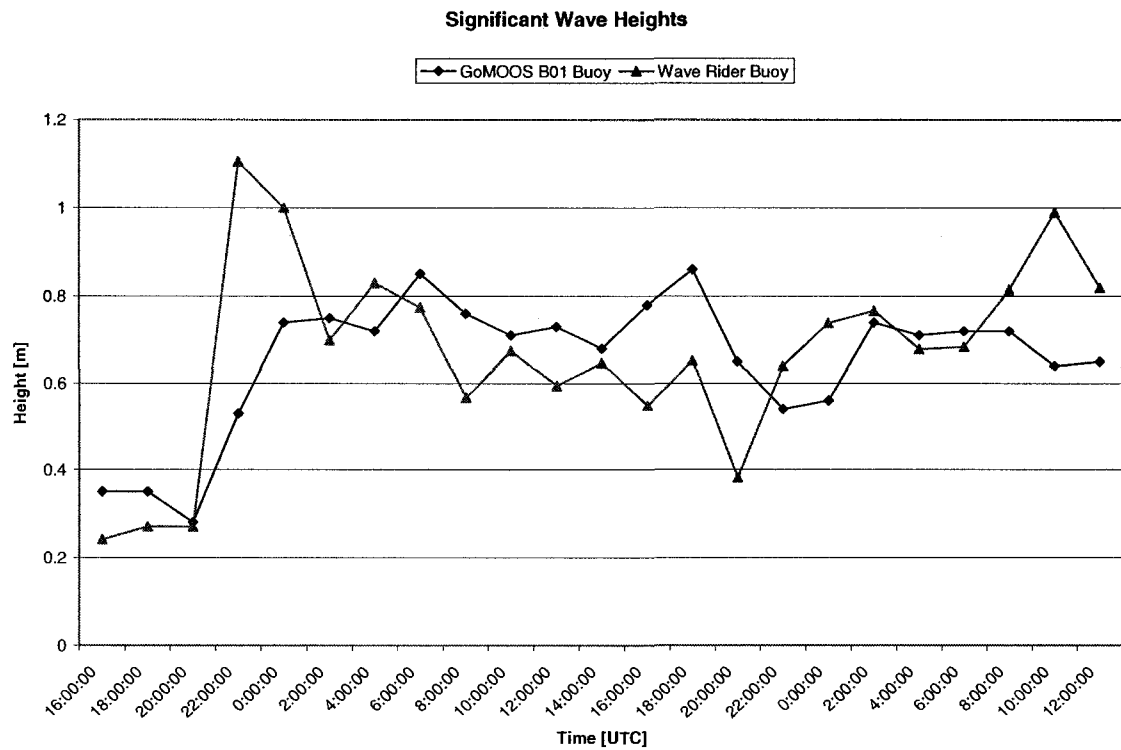


Figure 4.1: Plot of significant wave heights in the southwest area of the Gulf of Maine from the recovered wave rider data (shown in red) at the demonstration site and the GoMOOS B01 buoy (shown in blue) between March 11th and 13th. Data for the GoMOOS B01 (Western Maine Shelf) buoy was downloaded from the GoMOOS website (<http://www.gomoos.org/>).

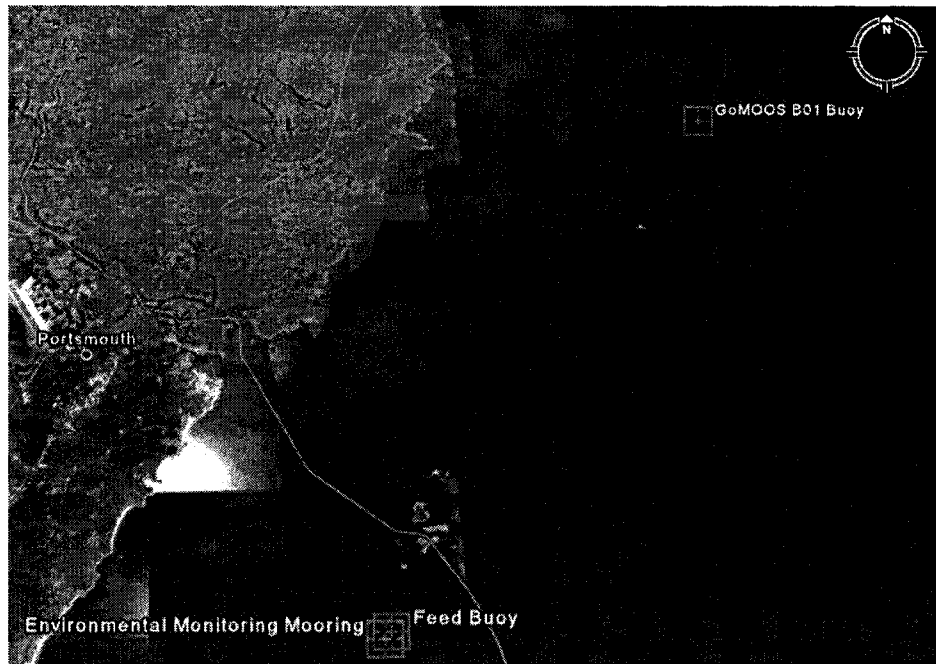


Figure 4.2: Location of the GoMOOS B01 buoy compared to the environmental monitoring mooring (i.e., wave rider buoy) and the feed buoy. The GoMOOS B01 buoy is roughly 31.5 km to the northeast of the environmental monitoring mooring. This figure was constructed using Google Earth.

Table 4.1: Wave Data from the Wave Rider Buoy

Date	Time [UTC]	Sig. Wave Height [m]	Dominate Wave Period [s]
3/11/2008	16:00:00	0.2411	7.9
3/11/2008	18:00:00	0.2706	9.3
3/11/2008	20:00:00	0.27	2.7
3/11/2008	22:00:00	1.1044	3.1
3/12/2008	0:00:00	0.9999	3.5
3/12/2008	2:00:00	0.6995	3.9
3/12/2008	4:00:00	0.8293	3.7
3/12/2008	6:00:00	0.7745	4.5
3/12/2008	8:00:00	0.5669	5.1
3/12/2008	10:00:00	0.6747	4.9
3/12/2008	12:00:00	0.594	4.1
3/12/2008	14:00:00	0.6469	4.7
3/12/2008	16:00:00	0.5487	4.5
3/12/2008	18:00:00	0.6525	4.7
3/12/2008	20:00:00	0.381	4.3
3/12/2008	22:00:00	0.64	4.1
3/13/2008	0:00:00	0.7383	2.9
3/13/2008	2:00:00	0.7668	3.1
3/13/2008	4:00:00	0.6788	2.8
3/13/2008	6:00:00	0.684	3.1
3/13/2008	8:00:00	0.814	2.8
3/13/2008	10:00:00	0.9894	3
3/13/2008	12:00:00	0.8188	4.7

Table 4.2: Additional Wave Data from the Wave Rider Buoy

Date	Time [UTC]	Max. Wave Height [m]	Min. Wave Height [m]	Mean Wave Height [m]	Standard Deviation [m]
3/11/2008	16:00:00	0.4944	0.0741	0.1536	0.0764
3/11/2008	18:00:00	0.6605	0.0564	0.1685	0.0934
3/11/2008	20:00:00	0.5724	0.057	0.1694	0.0904
3/11/2008	22:00:00	19.3861*	0.071	1.2505	0.4691
3/12/2008	0:00:00	2.1029	0.0974	0.5114	0.4169
3/12/2008	2:00:00	1.7959	0.0609	0.3688	0.2863
3/12/2008	4:00:00	1.5742	0.1373	0.4353	0.33
3/12/2008	6:00:00	2.2332	0.0891	0.4093	0.3152
3/12/2008	8:00:00	1.1861	9.21E-04	0.2911	0.2389
3/12/2008	10:00:00	1.4296	0.1283	0.3598	0.2671
3/12/2008	12:00:00	1.2418	0.1801	0.3414	0.2203
3/12/2008	14:00:00	1.4753	0.1594	0.3492	0.2638
3/12/2008	16:00:00	1.5767	0.1191	0.3131	0.207
3/12/2008	18:00:00	1.108	0.2004	0.3869	0.2214
3/12/2008	20:00:00	0.7276	0.022	0.2244	0.1386
3/12/2008	22:00:00	1.5901	0.3641	0.4573	0.1842
3/13/2008	0:00:00	1.7935	0.1183	0.4492	0.2662
3/13/2008	2:00:00	1.3499	0.3776	0.5193	0.2117
3/13/2008	4:00:00	1.2353	0.4891	0.5524	0.1406
3/13/2008	6:00:00	1.6003	0.0185	0.3865	0.2715
3/13/2008	8:00:00	1.7231	0.0417	0.4487	0.3219
3/13/2008	10:00:00	2.1876	0.0482	0.497	0.4329
3/13/2008	12:00:00	1.568	0.0453	0.4205	0.3343

* Large wave height is due to instrumentation error in the record.

As it is shown in figure 4.1 and tables 4.1 and 4.2, there were no large storm waves recorded by the field program. However, there were two times where the wave forcing approached one meter in significant wave height for both buoys: March 12, 2008 at 6 UTC and March 12, 2008 at 18 UTC. The data set on March 12, 2008 at 6 UTC also has the wind direction along the x-axis of the motion package orientation, and pitch being the rotation around y-axis of the motion package. Since this data set has one of the top wave heights and appropriate average wind (and therefore wave) direction, it is the example data set for the results section. The rest of the data sets, with similar trends, can be found at the end of the thesis in appendix A. The corresponding wave rider translations, motion package translations, and motion package rotations for March 12, 2008 at 6 UTC can be seen in figures 4.3, 4.4, and 4.5, respectively.

Table 4.3: Wave and Wind Data from GoMOOS Buoy B01

Date:	Time [UTC]:	Sig. Wave Height [m]	Dominate Wave Period [s]	Wind Speed [m/s]	Avg. Wind Direction
3/11/2008	16:00:00	0.35	8	2.7	S
3/11/2008	18:00:00	0.35	10.7	5.5	SSE
3/11/2008	20:00:00	0.28	2.5	5	SW
3/11/2008	22:00:00	0.53	2.9	6.6	S
3/12/2008	0:00:00	0.74	3.6	6.9	S
3/12/2008	2:00:00	0.75	4	7.5	S
3/12/2008	4:00:00	0.72	4	7.6	SSW
3/12/2008	6:00:00	0.85	4	8.3	SW
3/12/2008	8:00:00	0.76	4.6	7	SSW
3/12/2008	10:00:00	0.71	4.6	6.4	SSW
3/12/2008	12:00:00	0.73	4.6	6.4	SSW
3/12/2008	14:00:00	0.68	4	5.5	SSW
3/12/2008	16:00:00	0.78	4.6	3.1	WNW
3/12/2008	18:00:00	0.86	5.3	3.9	NW
3/12/2008	20:00:00	0.65	5.3	2	NNW
3/12/2008	22:00:00	0.54	5.3	2.6	NNW
3/13/2008	0:00:00	0.56	2.9	7.6	NNW
3/13/2008	2:00:00	0.74	3.2	9.5	NW
3/13/2008	4:00:00	0.71	2.9	8.7	WNW
3/13/2008	6:00:00	0.72	2.9	8.7	NW
3/13/2008	8:00:00	0.72	2.9	8.9	NW
3/13/2008	10:00:00	0.64	2.9	7.7	NW
3/13/2008	12:00:00	0.65	2.9	7.6	NNW

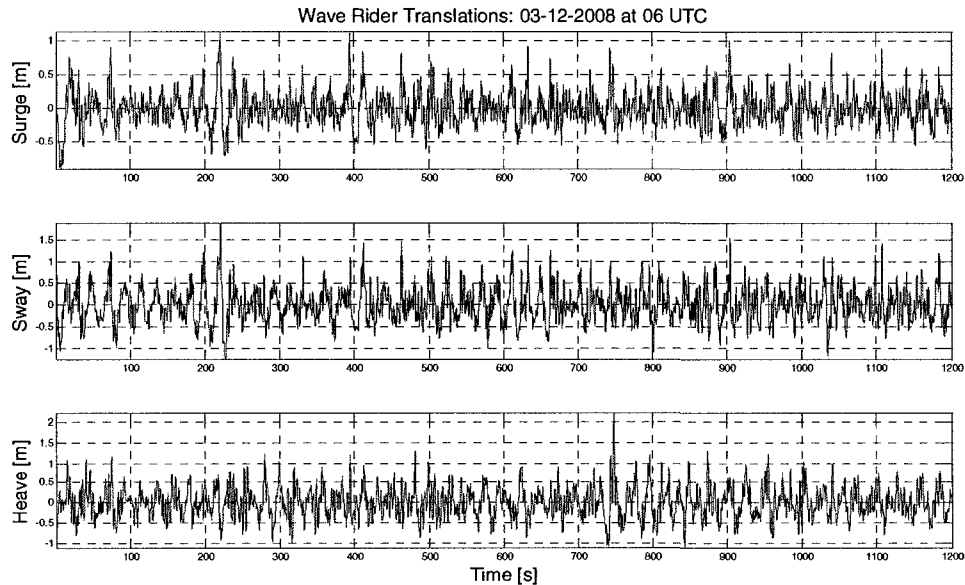


Figure 4.3: Surge, sway, and heave translations measured in meters for the wave rider buoy on March 12, 2008 at 6 UTC.

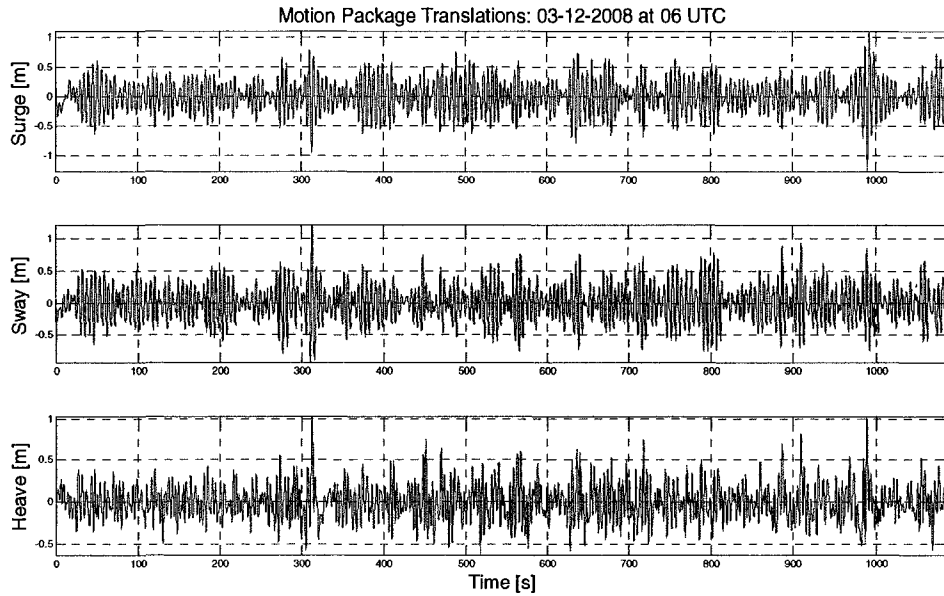


Figure 4.4: Surge, sway, and heave translations measured in meters for the motion package inside the feed buoy on March 12, 2008 at 6 UTC.

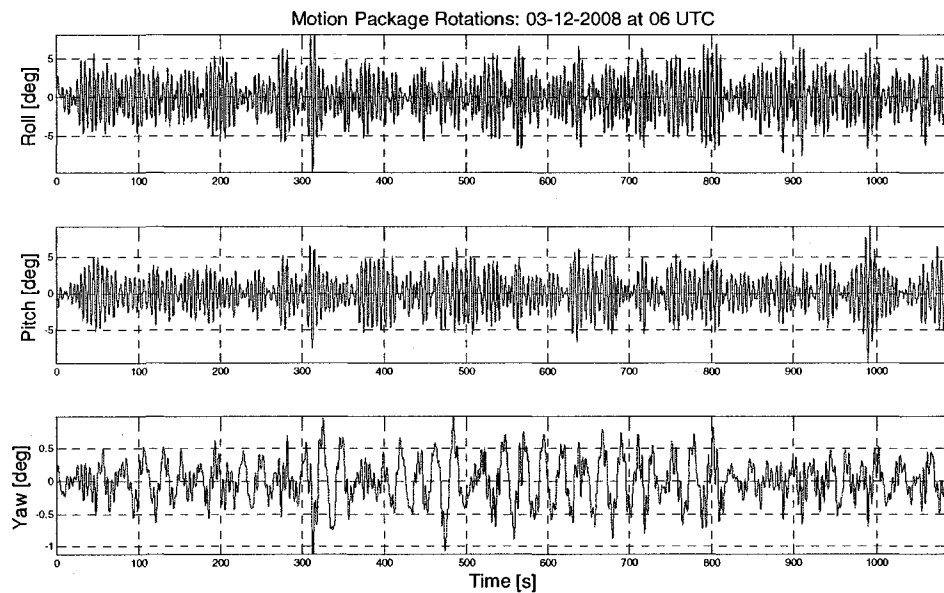


Figure 4.5: Roll, pitch, and yaw rotations measured in degrees for the motion package inside the feed buoy on March 12, 2008 at 6 UTC.

Visually from figure 4.3, the heave of the wave rider is in the .05 to 1 meter range, similar to the wave data from the GoMOOS B01 buoy. The pitch (and roll) of the motion package (figure 4.5) is in the plus and minus 5 degree range, which seems

reasonable for the fair-weather sea state. The roll seems slightly higher than the pitch, which is probably due to directional spreading in random seas. The mooring of the feed buoy may add to this effect because it is fortified (i.e., additional mooring lines) in a northeast bearing (which is along the x-axis of the motion package). That direction is typical of storm events in the Gulf of Maine during the winter-spring months. Also, the feed hoses which exit the feed buoy in the southwest direction, may provide some additional retarding effects on the response. Effects of the mooring lines and feed hoses on the feed buoy is evident when examining the buoy's yaw in figure 4.5, where the data shows much longer periods than in the roll and pitch; which is most likely due to the slow twisting of the feed buoy about the mooring. And because the pitch, and roll, never exceeded 9° degrees in all the data sets, no conclusions can be made on the communication problem from feed buoy tilting as mentioned in chapter 1. This problem would have to be addressed in an additional study.

To obtain the instrument noise levels for comparison with the measured data sets on March 12, 2008 at 6 UTC, the motion package and wave rider were left running in a fixed position (i.e., no movement) for a regular sampling interval before their deployment on March 11, 2008. These “noise” data sets were processed in the same manner as the field data sets. Once computed, the measured field and noise data was used to obtain the signal to noise ratios (SNR) for wave elevation from the wave rider buoy and heave, surge, and pitch from the motion package. The signal to noise ratio was not computed for wave excursion and slope since they are derived from the wave elevation. The signal to noise ratio is simply defined as the ratio of a signal power to the noise power corrupting the signal. In this study, the signal to noise ratios are expressed in decibels as:

$$SNR(f) = 10 \cdot \log_{10} \left(\frac{S_{Signal}(f)}{S_{Noise}(f)} \right) \quad (4.1)$$

where $S_{Signal}(f)$ and $S_{Noise}(f)$ are the respective spectral densities. The larger the SNR, the less corrupted the signal is. As it can be seen in figures 4.6 and 4.7, there are large signal to noise ratios for all the signals in the range 0.1 Hz to 0.4 Hz, which corresponds to the range of waves of interest in the field program. The wave elevation SNR decreases significantly below 0.2 Hz; while the heave, surge, and pitch SNRs decrease significantly below 0.17 Hz. A lower cutoff frequency of 0.17 Hz for all the data in the study was chosen because the wave elevation SNR only decreased by ~10 dB from the maximum value in figure 4.6; and the signal to noise ratios for the feed buoy responses, in figure 4.7, were at their maximums above 0.17 Hz. Because of this, all the spectra and RAO plots are shown over a frequency range of 0.17 Hz to 0.4 Hz.

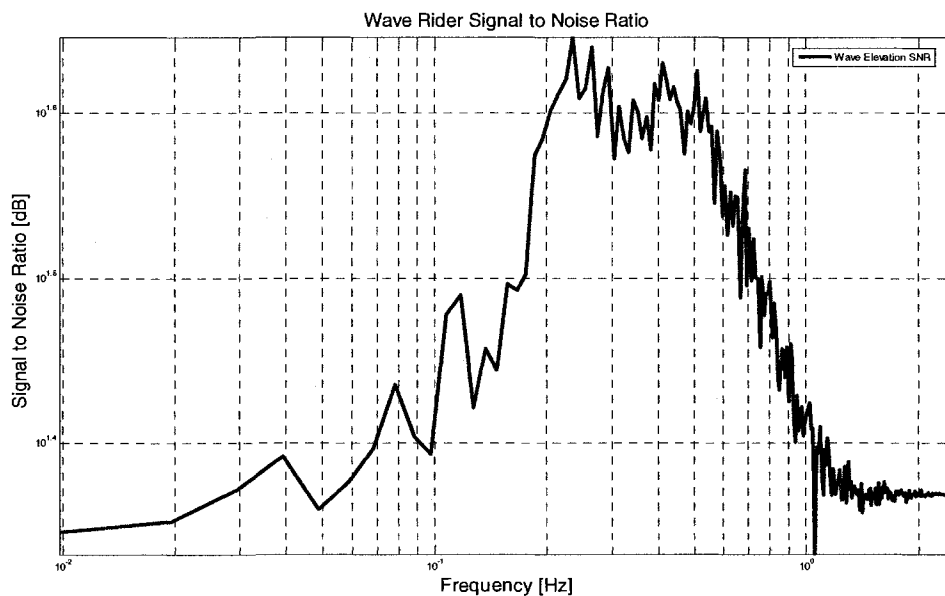


Figure 4.6: Signal to noise ratio for wave elevation from the wave rider buoy plotted in decibels versus frequency. The maximum SNR value shown is ~44 dB.

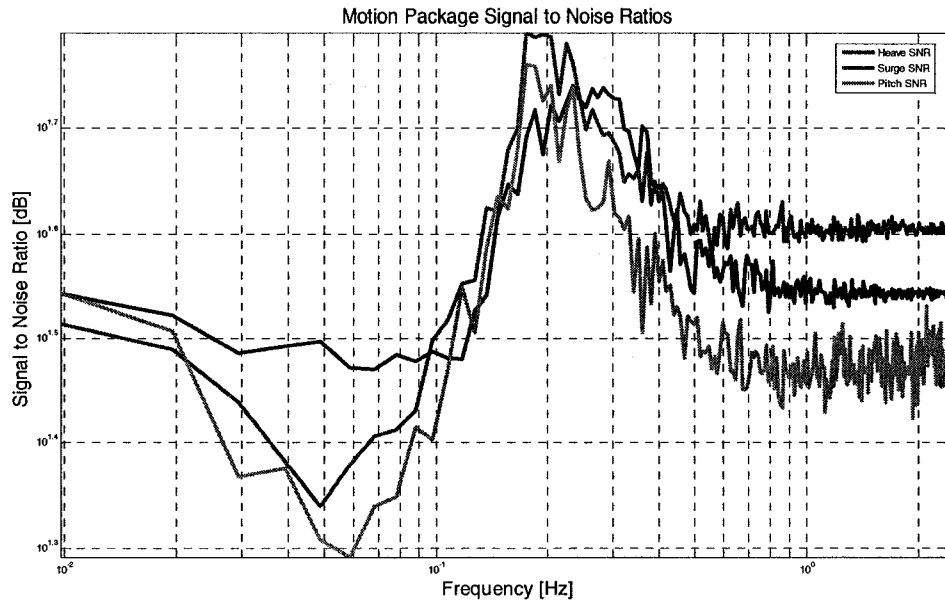


Figure 4.7: Signal to noise ratios for heave (shown in blue), surge (shown in red), and pitch (shown in green) of the motion package plotted in decibels versus frequency. The maximum SNR values shown for heave, surge, and pitch are ~55 dB, ~61 dB, and ~58 dB, respectively.

After some processing of the recorded data, feed buoy response (heave, surge, and pitch), forcing, and RAO data were plotted. A comparison of heave, surge, and pitch response spectra to the forcing spectra can be seen in figure 4.8; and a comparison of heave, surge, and pitch RAOs can be seen in figure 4.9. The heave, surge, and pitch RAOs are plotted against the physical and numerical model data from Turmelle (2007) in figure 4.10. The experimental setup of the physical model testing in the UNH wave/tow tank from Turmelle (2007) is shown in figure 4.11. Figures 4.8 through 4.10 correspond to only the data recorded on March 12, 2008 at 6 UTC, however, these trends can be seen in all the other recorded data sets which are presented in appendix A. The results and figures for March 12, 2008 at 6 UTC are discussed thoroughly in the following heave, surge, and pitch result sections.

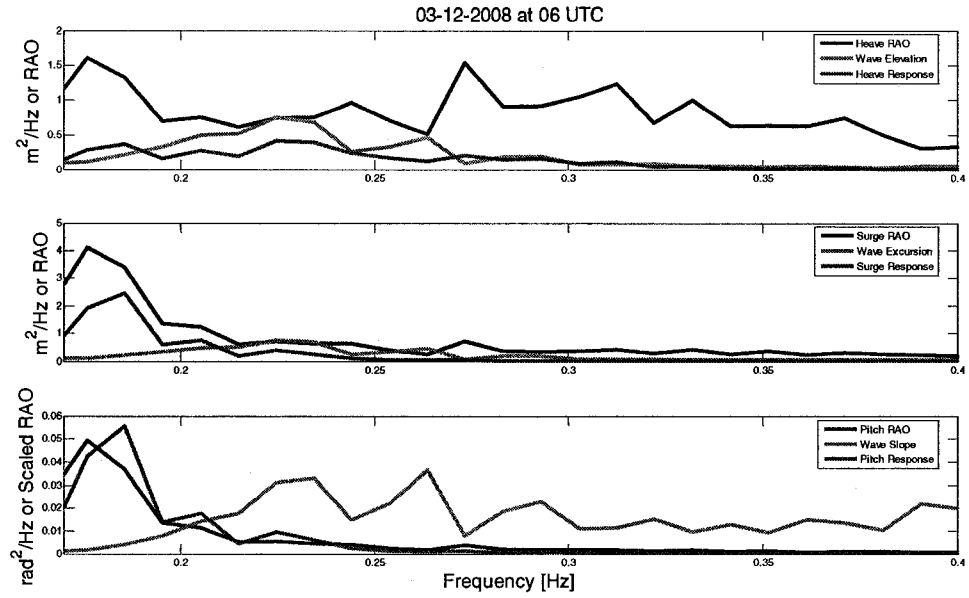


Figure 4.8: Comparison plot of heave, surge, and pitch RAOs (shown in blue), response spectra (shown in red), and corresponding forcing spectra (shown in green) for March 12, 2008 at 6 UTC. The pitch RAO was scaled down by a factor of 100 to make the plot more viewable.

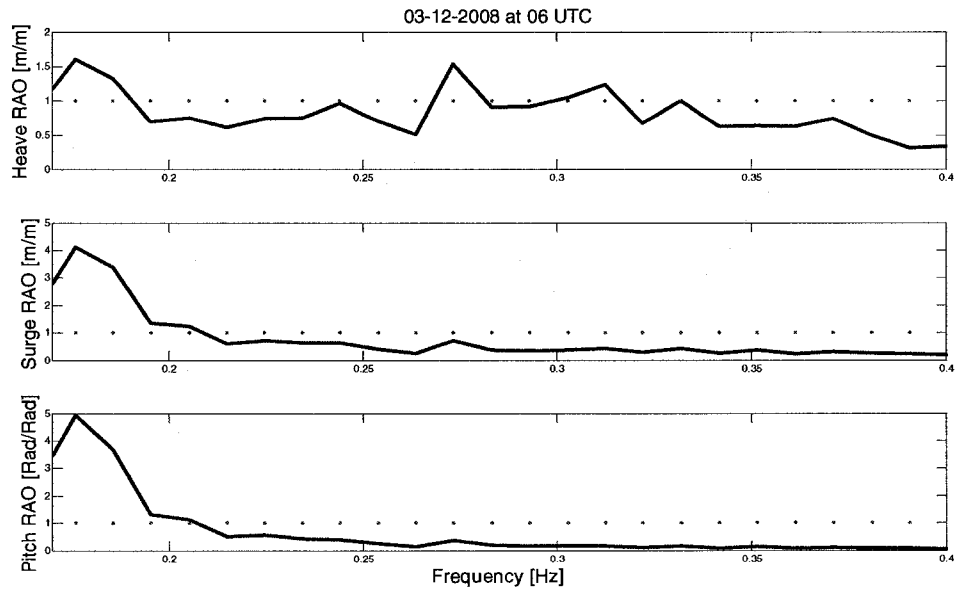


Figure 4.9: Comparison plot of heave, surge, and pitch RAOs (shown in blue) for March 12, 2008 at 6 UTC.

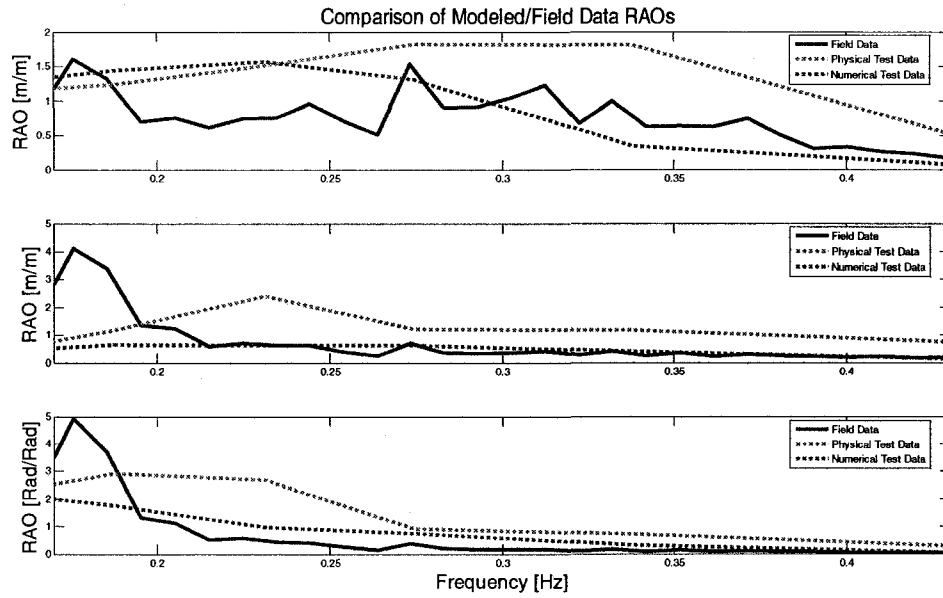


Figure 4.10: Comparison of heave, surge, and pitch RAOs plotted against the (regular wave, load case) physical and numerical model data from Turmelle (2007).

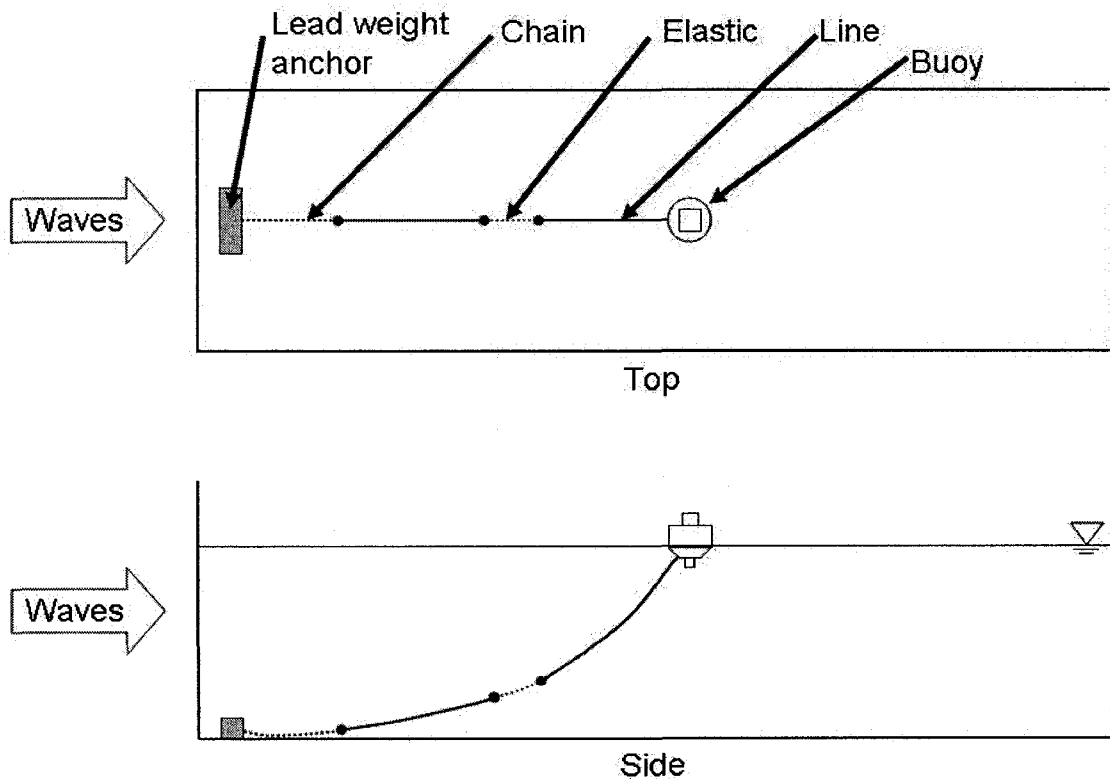


Figure 4.11: Experimental setup of the physical model testing in the UNH wave/tow tank (Turmelle, 2007).

ii. Heave Results

Using the techniques described in chapter 2, the heave response of the feed buoy due to wave forcing on March 12, 2008 at 6 UTC was processed and plotted. A plot of displacement for the feed buoy and wave elevation, along with the heave RAO (i.e., transfer function), can be seen in figure 4.12; and a plot of the corresponding heave RAO by itself with a 90% confidence interval can be seen in figure 4.13.

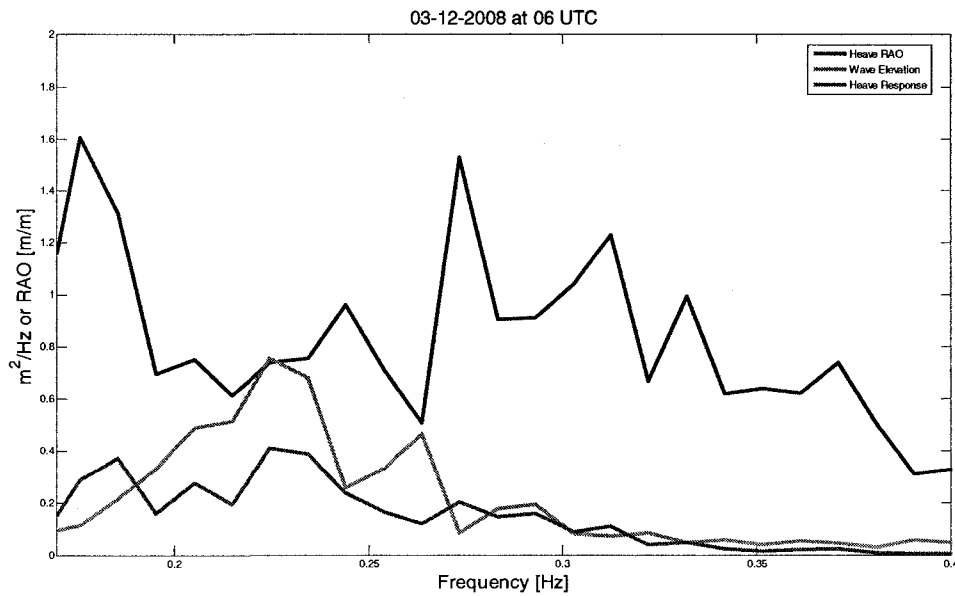


Figure 4.12: Heave RAO plotted against heave response of the feed buoy and wave elevation (forcing) on March 12, 2008 at 6 UTC.

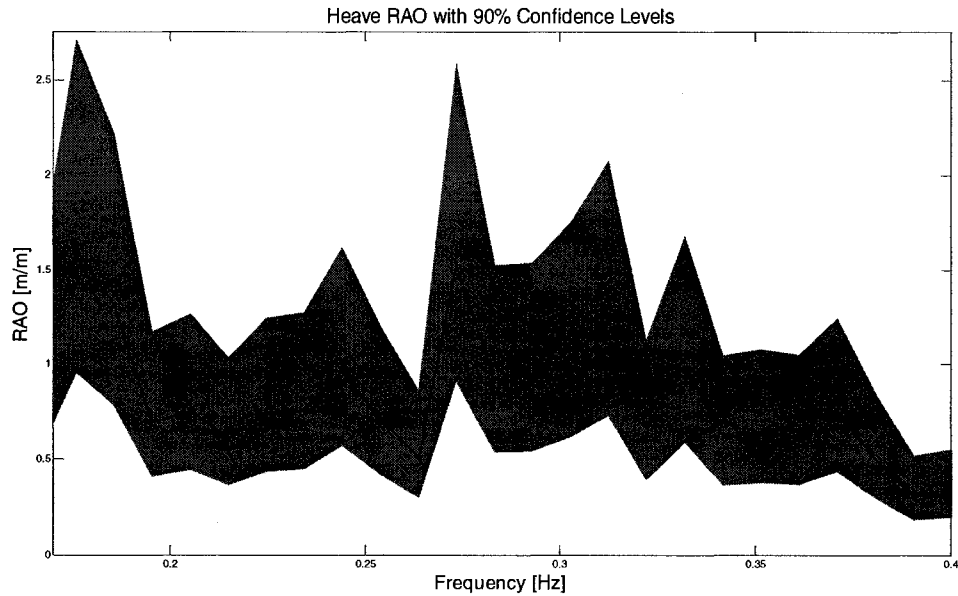


Figure 4.13: Heave RAO, with a 90% confidence interval, for the feed buoy on March 12, 2008 at 6 UTC. The maximum difference between heave RAO and the 90% confidence interval was +1.104. The differences in the lower frequency range, where larger storm waves would be present, were about 10 times smaller than the maximum. However, the computed interval shows relative confidence in the RAO data, especially for the lower frequencies which are of most importance for the feed buoy in the random sea environment.

As it is shown in figure 4.12, the wave energy (i.e., forcing) is focused around 0.225 Hz (corresponding to a dominate wave period of ~4.5 seconds) in roughly a ± 0.1 Hz range. There is feed buoy response in the 0.35 to 0.17 Hz range, corresponding to ~2.9 to ~5.9 second waves, which are typical to the demonstration site in fair weather and is a range of interest in this study. Again, storm waves would have had long dominate wave periods between 6 and 10 seconds; since none were present during recording, feed buoy response diminishes towards the lower frequencies. Figure 4.13, which plots the heave RAO curve from figure 4.12 with a 90% confidence interval, shows resonance for wave frequencies in the 0.34 to 0.17 Hz range (corresponding roughly to ~2 to ~6 second waves); and the RAO values diminish towards the higher frequencies past 0.34 Hz. The

distributed response may be caused by the vertical restraint of the feed buoy to the mooring lines and the feed hoses. There is also a large resonance peak (RAO value of ~ 1.6) around 0.18Hz (corresponding to ~ 5.5 second waves) in this resonance range. As it shown in the following result sections, this resonance peak is attributed to the motion package not being positioned exactly at the center of the feed buoy; where the buoy's rolling or pitching back and forth may trick the vertical accelerometer in interpreting the slow tilting as heave. In general though, the feed buoy system was designed to handle resonances from higher frequency, fair-weather waves, so no problems should arise in the system because of them. The slight choppiness in all the plots could be due to the low wave forcing and response magnitude when the data was recorded. These low values are more susceptible to random instrument and system noise. However the choppiness of the data does not appear to be significant when the 90% confidence interval is examined in figure 4.13.

Not shown in the plots because of the noise problem, the curve diminishes to very low values of RAO below 0.17 Hz; and below 0.1 Hz, the RAO curve starts to increase towards positive infinity, which is due to low frequency noise and negligible wave energy in the denominator of the RAO expression (i.e., "dividing by zero" situation). Again, the RAO values drop off as frequency increases positively out of the resonance range, which is typical of a heave RAO plot (i.e., the high frequency magnitudes drop off due to inertia of the system). The magnitude values approaches unity towards the lower frequencies (outside the resonance frequency range) are typical of a heave RAO plot. These results show system response diminishing towards lower frequencies and that the feed buoy may follow storm type waves. Since there was no strong wave forcing in the lower

frequencies the heave results are limited. However, it still allows for the prediction that the feed buoy system would endure storm events without any complications. This was the same prediction in Turmelle (2007), where numerical and physically modeling was used. Even though a direct comparison cannot be made from the model tests since the field mooring system, shown previously in figure 1.4, was not modeled exactly (as shown in figure 4.11). The physical model test in the UNH wave tank was modeled with only one mooring line. However, a comparison can be made to show similar trends in the data. This comparison is shown in figure 4.14 where the physical and numerical heave RAO data (for the loaded case) is plotted against the heave RAO from this study.

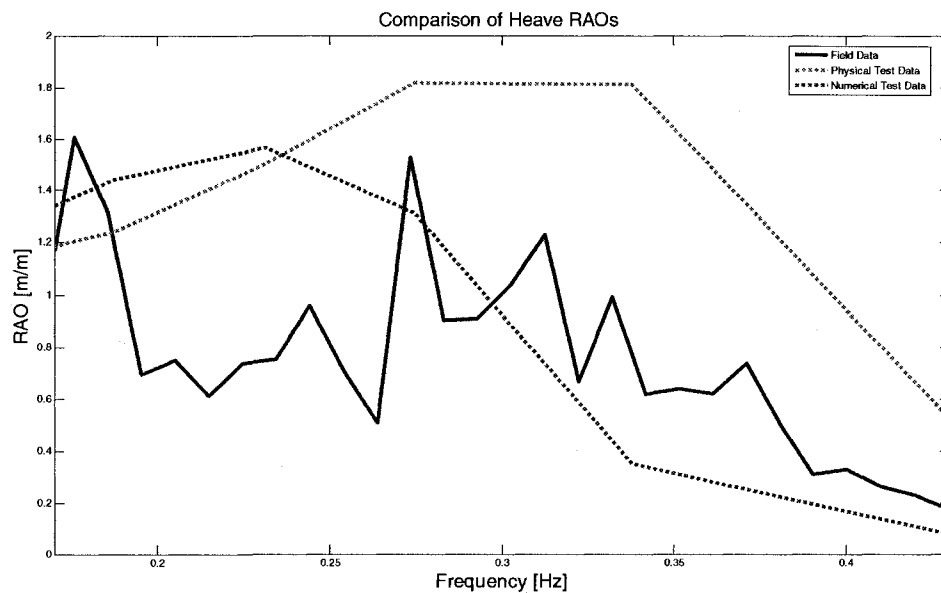


Figure 4.14: Comparison plot of heave RAO data. The (regular wave, load case) physical and numerical models from Turmelle (2007) are shown in green and red, respectively. The modeled data plotted against the heave RAO for the (random sea) field data set on March 12, 2008 at 6 UTC (shown in blue). The loaded case for the physical and numerical model data was used because the feed buoy was never empty of food and fuel during the field study.

As it can be seen in figure 4.14, the field data shows similar behavior to the modeled data. The numerical model data, which were computed in Aqua-FE, is shown as

a red dotted curve. The physical model data acquired from tank testing is shown as a green dotted curve. It should be noted that numerical model data were found by tweaking the Aqua-FE program to match the physical model data results. As they are not independent of each other, the physical model data is of interest for comparison, not the numerical model data. However, both are plotted for clarity and completeness. The expected natural frequency from the tank tests (free release and single mooring) is about 0.28 Hz. Again, the field data results show a more distributed response mostly at lower frequencies, where the damping is mostly due to the mooring lines and feed hoses. Overall, the field data mimics the trends in the modeled data, where it similar resonance towards the higher frequencies and smaller feed buoy excitation towards the lower frequencies.

iii. Surge Results

Using the techniques described in chapter 2, the surge response of the feed buoy due to wave excursion forcing on March 12, 2008 at 6 UTC was processed and plotted. A plot of horizontal displacement for the feed buoy and wave excursion, along with the surge RAO, can be seen in figure 4.15; and a plot of the corresponding surge RAO by itself with a 90% confidence interval can be seen in figure 4.16. As it is shown in figure 4.15 (and similar to figure 4.12), wave excursion energy was focused around 0.225 Hz (corresponding to a dominate wave period of ~4.5 seconds) in roughly a ± 0.1 Hz range. Again, the slight choppiness of the data could be due to the low wave excursion forcing magnitude when the data were recorded, making the low values more susceptible to

random instrument and system noise. However the choppiness of the data does not appear to be significant when the 90% confidence interval is examined in figure 4.16.

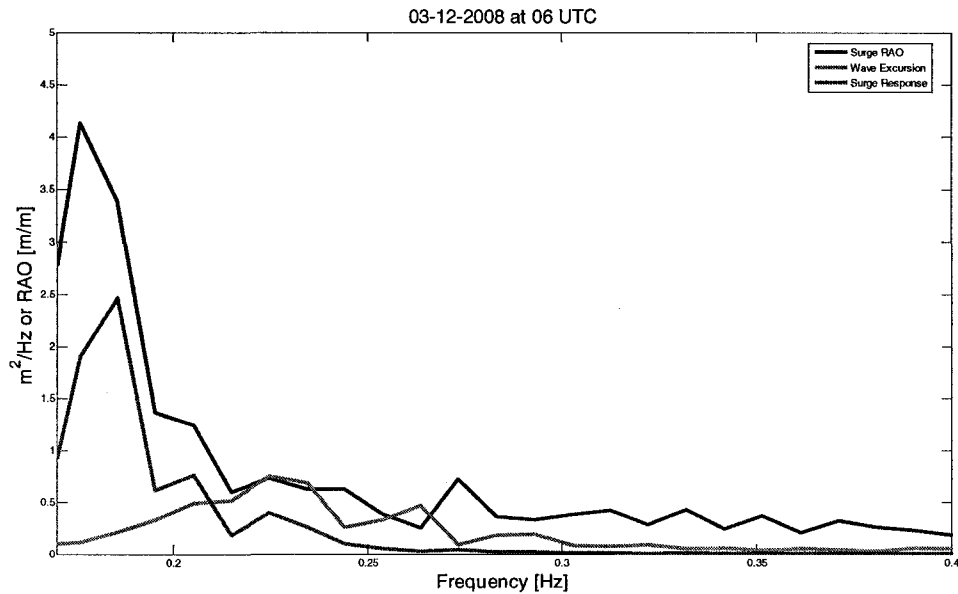


Figure 4.15: Surge RAO plotted against surge response of the feed buoy and wave excursion (forcing) on March 12, 2008 at 6 UTC.

In general though, the surge RAO of the feed buoy is below or close to unity in magnitude as expected, except for a large response (RAO value of ~ 4.1) around 0.18 Hz. This resonance peak around 0.18 Hz is most likely the source for the same peak seen in the heave RAO plot (figure 4.12). The resonance peak may correspond to the horizontal movement of the feed buoy against the mooring and attached feed hoses; and as feed buoy yaws, the buoy will turn until the mooring lines are taut, leading to more buoy surge and pitch. Also, the additional attachments connected to the feed buoy appear to be slowing the response down. However, the surge RAO values, excluding the large resonance peak, are below or approaching unity for the entire plot. This behavior is typical of an over-damped system and shares similar trends to typical surge RAO plots.

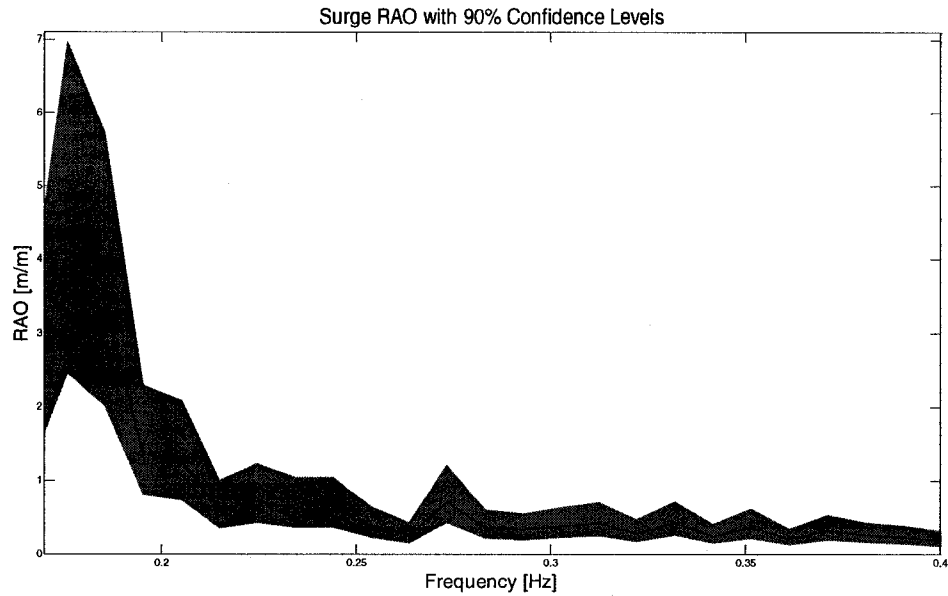


Figure 4.16: Surge RAO, with a 90% confidence interval, for the feed buoy on March 12, 2008 at 6 UTC. The maximum difference between surge RAO and the 90% confidence interval was +2.810. The differences in the lower frequency range, where larger storm waves would be present, were about 10 times smaller than the maximum. However, the computed interval shows relative confidence in the RAO data, especially for the lower frequencies which are of most importance for the feed buoy in the random sea environment.

This behavior was also similar to the prediction in Turmelle (2007), where numerical and physically modeling was used. Again, a direct comparison cannot be made from the model tests since the field mooring system was not modeled exactly. However, a comparison can be made to show similar trends in the data, which is shown in figure 4.17. The figure shows the physical and numerical surge RAO data (for the loaded case) plotted against the surge RAO from this study.

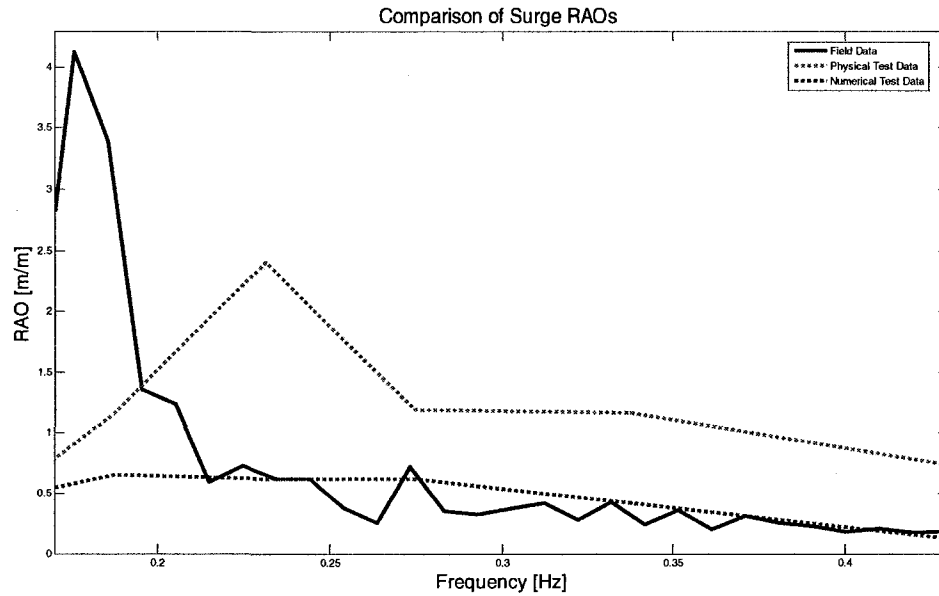


Figure 4.17: Comparison plot of surge RAO data. The (regular wave, load case) physical and numerical models from Turmelle (2007) are shown in green and red, respectively. The modeled data plotted against the surge RAO for the (random sea) field data set on March 12, 2008 at 6 UTC (shown in blue). The loaded case for the physical and numerical model data was used because the feed buoy was never empty of food and fuel during the field study.

As it can be seen in figure 4.17, the field data shows similar trends to the modeled data. The numerical model data, which were computed in Aqua-FE, is shown as a red dotted curve. The physical model data acquired from tank testing is shown as a green dotted curve. Again, the physical model data were of interest for comparison, not the numerical model data; but both are plotted for completeness. The physical model tank tests indicated that the resonance should occur at a slightly higher frequency (around ~0.23 Hz) than the large response in the field data (around 0.18 Hz). The magnitude of the field data resonance peak was larger than the modeled peak as well; which again may be due to the heave and surge coupling. Overall though, the field data mimics the behavior in the modeled data; where there is a resonance peak towards the higher, fair-weather wave frequencies, but close or below unity in the typical wave range.

iv. Pitch Results

Again using the techniques described in chapter 2, the pitch response of the feed buoy due to wave slope forcing on March 12, 2008 at 6 UTC was processed and graphed. A plot of pitch for the feed buoy and wave slope, along with the pitch RAO, can be seen in figure 4.18; and a plot of the corresponding pitch RAO by itself with a 90% confidence interval can be seen in figure 4.19. As it is shown in figure 4.18, wave slope energy is focused towards the higher frequencies above 0.17 Hz; this occurs because smaller wind driven waves are steeper and provide higher wave slope. Again, the slight choppiness of the data could be due to the low wave slope forcing magnitude when the data were recorded, making the low values more susceptible to random instrument and system noise. However the choppiness of the data does not appear to be significant when the 90% confidence interval is examined in figure 4.19.

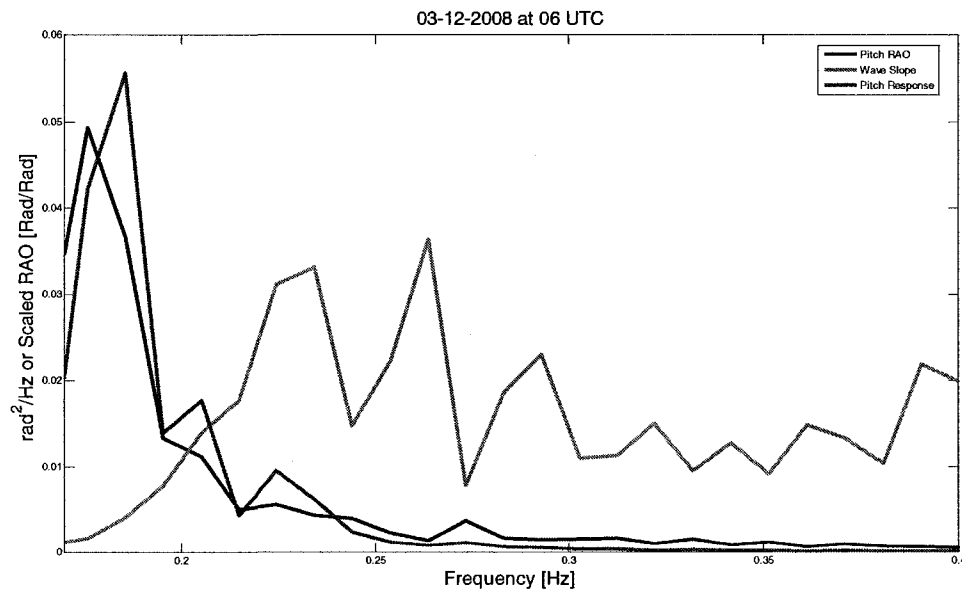


Figure 4.18: Scaled pitch RAO plotted against Pitch response of the feed buoy and wave slope (forcing) on March 12, 2008 at 6 UTC. The pitch RAO was scaled down by a factor of 100 to make the plot more viewable.

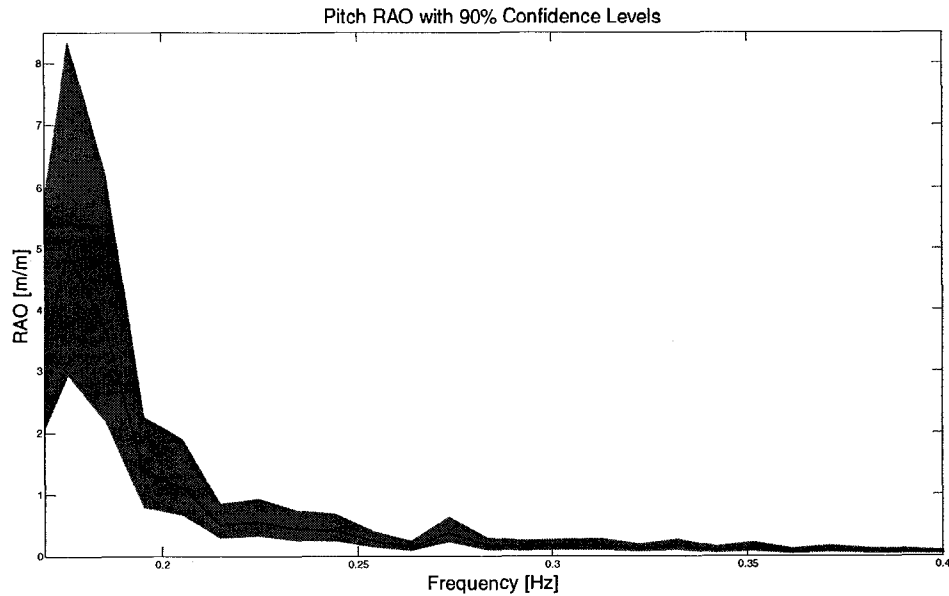


Figure 4.19: Pitch RAO, with a 90% confidence interval, for the feed buoy on March 12, 2008 at 6 UTC. The maximum difference between pitch RAO and the 90% confidence interval was +3.395. The differences in the lower frequency range, where larger storm waves would be present, were about 10 times smaller than the maximum. However, the computed interval shows relative confidence in the RAO data, especially for the lower frequencies which are of most importance for the feed buoy in the random sea environment.

In general though, the pitch RAO of the feed buoy was below or approaching unity in magnitude in the 0.35 Hz to 0.17 Hz range, except for the large peak (RAO value of ~4.9) around 0.18 Hz. This slightly larger peak around 0.18 Hz is similar to the resonance peak seen in the surge RAO plot (figure 4.16). The peak is probably due at least in part to a nonlinear coupling with the surge response peak. The coupling could be due to the horizontal motion of the feed buoy, which may be generating moments about the mooring attachment point(s). Not shown in figure 4.19 because of the noise problem, the curve diminishes to very low values of RAO below 0.17 Hz; and below 0.1 Hz, the data start to blow up because the response spectrum is divided by very small values of wave slope as frequency decreases (i.e., “dividing by zero” situation).

Excluding the large peak around 0.18Hz, the pitch RAO values were approaching 1 for low frequencies. There is a resonance towards the higher, fair-weather wave frequencies and the pitch RAO values eventually dies off as frequency increases out of the typical wave period range. All these items make the plot (figure 4.19) similar to a typical pitch RAO plot. These behaviors in the pitch RAO field data were similar to the predictions in Turmelle (2007), where numerical and physical modeling was used. Again, a direct comparison cannot be made from the model tests since the field mooring system was not modeled exactly. However, a comparison can be made to show similar trends in the data. This comparison is shown in figure 4.20 where the physical and numerical pitch RAO data (for the loaded case) is plotted against the pitch RAO from the study. As it can be seen from the rest of figure 4.20, the field data show similar behavior to the modeled data.

The numerical model data, which was computed in Aqua-FE, is shown as a red dotted curve. The physical model data acquired from tank testing is shown as a green dotted curve. Again, the physical model data is of interest for comparison, not the numerical model data; but both are plotted for completeness and clarity. There are no extremely large resonance peaks present in the physical and numerical model tests as seen in the field data pitch RAO. Again, this is probably due in part to how the mooring system was modeled in the UNH wave/tow tank. The resonance peak from the field data is roughly twice the predicted values from the physical modeling. Also, in the physical model tank tests the pitch natural frequency was close to, and may be associated with, the peak around 0.18 Hz in the field data (shown in figure 4.20). Overall, the field data closely mimics the trends in the physical model data where the pitch RAO has resonance

towards the higher, fair-weather wave frequencies and dies off as wave frequency increases.

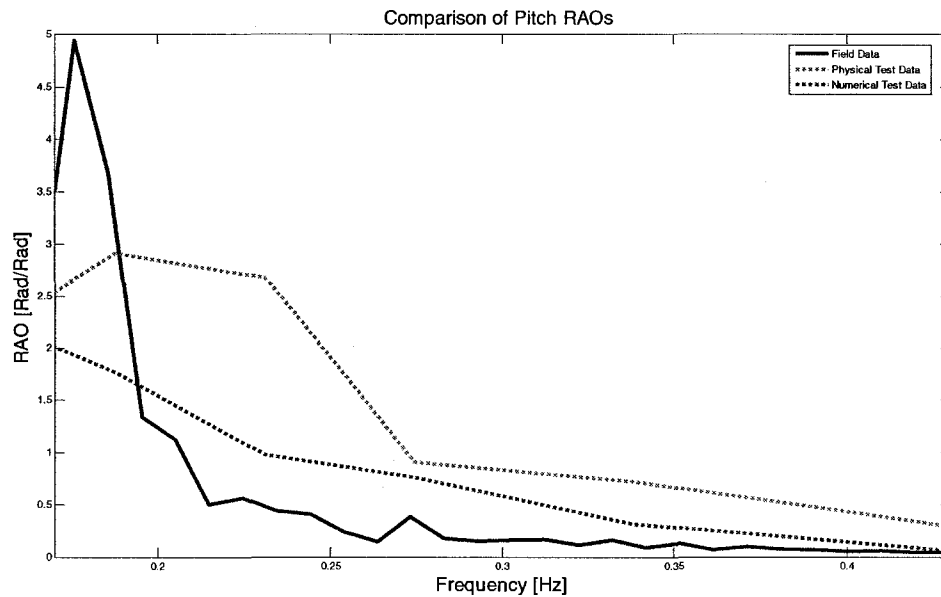


Figure 4.20: Comparison plot of pitch RAO data. The (regular wave, load case) physical and numerical models from Turmelle (2007) are shown in green and red, respectively. The modeled data plotted against the pitch RAO for the (random sea) field data set on March 12, 2008 at 6 UTC (shown in blue). The loaded case for the physical and numerical model data was used because the feed buoy was never empty of food and fuel during the field study.

CHAPTER V

CONCLUSION

The 20-ton capacity feed buoy at the Atlantic Marine Aquaculture Center's test site continues to serve as an important project, where it verifies and demonstrates that aquaculture can be done offshore in the open ocean environment. With its success in feeding finfish crops, it is a feasible paradigm for anyone interested or involved in this newer area of aquaculture. Before researchers or investors might consider setting up a similar site in the open ocean, they would need to know how the feed buoy performs in energetic, stormy seas. During the design phase of the feed, physical model tank testing and numerical modeling was performed to provide answers on how the buoy would respond when it encountered waves due to severe weather. These tests presented good insight into the dynamic responses of the feed buoy system and proved survivability; but did not provide definitive answers. In response, this field program was implemented to measure the dynamic responses of the feed buoy due to actual environmental forcing at the test site. Instruments were deployed on March 11th and retrieved on April 31st in the spring of 2008. The field equipment obtained the data by recording environmental (wave) forcing from a monitoring mooring; and by collecting the feed buoy's displacement and rotational responses from a motion package mounted inside the buoy. Once the data was retrieved from the instruments, it was processed using MATLAB[®] routines.

Due to an instrumentation failure inside the motion package, only 24 sets of data were recorded over a two day period. Because of this failure, the results came from fair-weather seas where no extreme forcing due to storms or strong winds was recorded. Storm waves were desired since they would have given stronger forcing, and therefore larger responses, to compare with survivability limits. However, the recovered data still provided first order results and provided reasonable insight into the feed buoy's behavior due to typical waves seen at the site.

All the RAO results showed trends approaching unity for low values of wave frequency. The heave RAO result illustrates a typical heave RAO plot; however, had a more distributed response over lower frequencies and resonance in the 2 to 6 second wave period range. This range corresponds to waves that the feed buoy, and mooring system, can handle without difficulties. The dampening of the heave response, seen in the field data, may be attributed to the restraint from the mooring lines and the feed hoses. Also, the heave RAO values died off as frequency increased, which was expected and was attributed to the smaller period waves having no affect on the buoy. An unpredicted peak (RAO of ~ 1.6), around 0.18 Hz, was present in the field results, which subsequent analysis attributed to the surge resonance.

The surge RAO results also modeled a typical surge RAO plot with the exception of a strong resonance (RAO of ~ 4.1) around 0.18 Hz; which was attributed to feed buoy movement against the mooring. The RAO values were mostly below and approached unity as frequency decreased. Again, additional mooring lines and hoses appear to be slowing the response down. The pitch RAO results modeled a typical pitch RAO plot

with the exception of a large peak (RAO of ~4.9) around 0.18 Hz, which was due in part to a nonlinear coupling with the surge response peak. This coupling may be contributed to the horizontal motion of the feed buoy generating moments about the mooring attachment point(s). The 0.18 Hz peak may also incorporate the pitch natural frequency; which was found from previous physical model tank testing.

In general, the field program obtained first order results and conclusions essential to understanding the feed buoy's actual dynamic responses. However, as aforementioned, the program did not encounter any extreme environmental forcing. Analysis of nominal wave data indicated that the RAOs for all three responses show values approaching unity for very low frequency waves; and the resonance of the RAOs plots (predominantly shown in the heave plots) were towards the higher frequency waves. This indicates that when there are large storms present at the AMAC site, the feed buoy will show little response or excitation due to the larger waves associated with storms. Additionally, with the resonance being towards the higher frequencies, the feed buoy will be excited by smaller waves which do not present any danger to the feed buoy or mooring system. The study also showed that in fair-weather waves the buoy would not roll and pitch to a degree that would limit communications. However, the large resonance in the pitch RAO could potentially cause problems with feed buoy operations, and the comfort of any operators onboard, during an energetic sea state. Overall, the feed buoy is behaving in the manor it was modeled and designed, ensuring its survivability at the AMAC demonstration site.

The RAO results from the field data had similar trends to the RAO plots created from past physical and numerical modeling. However, the surge and pitch RAOs from field data showed higher and sharper resonances than the results from modeling. Nonetheless, these tests showed that tow/wave tank and Aqua-FE modeling are excellent design tools for trending the responses of large, moored structures in the open ocean environment. They not only produce reasonable results, but are cost effective and time saving as well. These methods provide alternatives to conducting large, lengthy, and expensive field programs when structure survivability is only of interest. However field data is required when there is a desire for absolute certainty in the modeling techniques.

Since the field program did not record severe weather data during its deployment, another field program should be created to continue the work done in this study. Data from storm events and larger period waves could provide answers to the communication problem and give greater confidence to the RAO results. With large forcing at low frequencies, it also may be possible to resolve the RAO curves below 0.17 Hz. The analysis could also be expanded to include additional tank and numerical modeling to make better comparisons into why some of the discovered trends and peaks exist in the RAO results. With this additional study, and possibly more modeling, a complete model of the feed buoy response to environmental forcing could be obtained. A more realistic feed buoy model would provide greater confidence to new investors or researchers entering this growing area of marine aquaculture.

REFERENCES

Atlantic Marine Aquaculture Center. (2007) *About the Atlantic Marine Aquaculture Center*. Retrieved June 2, 2008, from: <http://ooa.unh.edu/about/about.html>.

Ahern, John. (2002). Validation of Wave Measurement Buoy. Master's Degree Thesis submitted in partial requirement for the Ocean Engineering degree program. University of New Hampshire, Durham, NH. 101 p.

Bendat, J.S., Peirsol, A.G. (2000). Random Data: Analysis and Measurement Procedures, Third Edition. Wiley, John & Sons Inc., New York, NY. 624 p.

Dean, R.G., Dalrymple, R.A. (1991). Water Wave Mechanics for Engineers and Scientists. World Scientific Publishing, River Edge, NJ. 353 p.

Earle, M.D. (1996). *Nondirectional and Directional Wave Data Analysis Procedures*. NDBC technical document 96-01. Stennis Space Center, MS. 37 p.

Earle, M.D., Steele, K.E., Yuan-Huang L.H. (1984). *Wave Spectra Corrections for Measurements with Hull-Fixed Accelerometers*. IEEE Journal of Oceanic Engineering.

Fredriksson, D.W., Swift, M.R., Irish, J.D., Tsukrov, I.I., Celikkol, B. (2003). *Fish Cage and Mooring System Dynamics using Physical and Numerical Models with Field Measurements*. *Aquacultural Engineering* 27, pp. 117-146.

Fredriksson, D.W. (2001). Open Ocean Fish Cage and Mooring System Dynamics. Ph.D. Dissertation submitted to the University of New Hampshire in partial fulfillment of the Engineering Systems Design Program. Durham, NH, September 2001.

Halliday, D., Resnick, R., & Walker, J. (2001). Fundamentals of Physics, Sixth Edition. John Wiley, & Sons, Inc, New York, NY. 1184 p.

Irish, J.D., Carroll, M., Singer, R., Newhall, A., Paul, W., Johnson, C., Witzell, W., Rice, G. (2001). *Instrumentation for Open Ocean Aquaculture Monitoring*. Woods Hole Oceanographic Institution Technical Report WHOI-2001-15. 95 p.

Irish, J. D., Fredriksson, D.W. (2003). *Telemetering Environmental Monitoring Buoy and Mooring*. OCEANS 2003 proceedings, Vol. 5, pp. 2589-2595.

Irish, J.D., Fredriksson, D.W., Boduch, S. (2004) *Environmental Monitoring Buoy and Mooring with Telemetry*. *Sea Technology*, pp. 14-19.

Koopmans, L.H. (1974). The Spectral Analysis of Time Series. Academic Press, Inc., New York, NY. 366 p.

Madni, A.M., Wan, L.A., Hammons, S. (1996). *A Microelectrical Quartz Rotational Rate Sensor for Inertial Applications*. Aerospace Applications Conference proceedings, Vol. 2, pp. 315-332.

Muramatsu, B., Eibeck, P.A. (2000). *Types of Accelerometers*. Retrieved July 20, 2008, from: http://bits.me.berkeley.edu/beam/acc_2b.html.

National Oceanic and Atmospheric Administration. (2008). *Aquaculture in the United States*. Retrieved June 2, 2008, from: <http://aquaculture.noaa.gov/us/welcome.html>.

Ochi, M.K. (1998). *Ocean Waves: the Stochastic Approach*. Cambridge University Press, New York, NY. 331 p.

Oppenheim, A.V., Willsky, A.S., Nawab, S.H. (1997). *Signals and Systems, Second Edition*. Pearson Education, Upper Saddle River, NJ. 957p.

Tsukrov, I., Eroshkin, O., Fredriksson, D. W., Swift, M.R. and Celikkol, B. (2003). *Finite Element Modeling of Net Panels Using Consistent Net Element*. *Ocean Engineering*, 30, pp. 251-270.

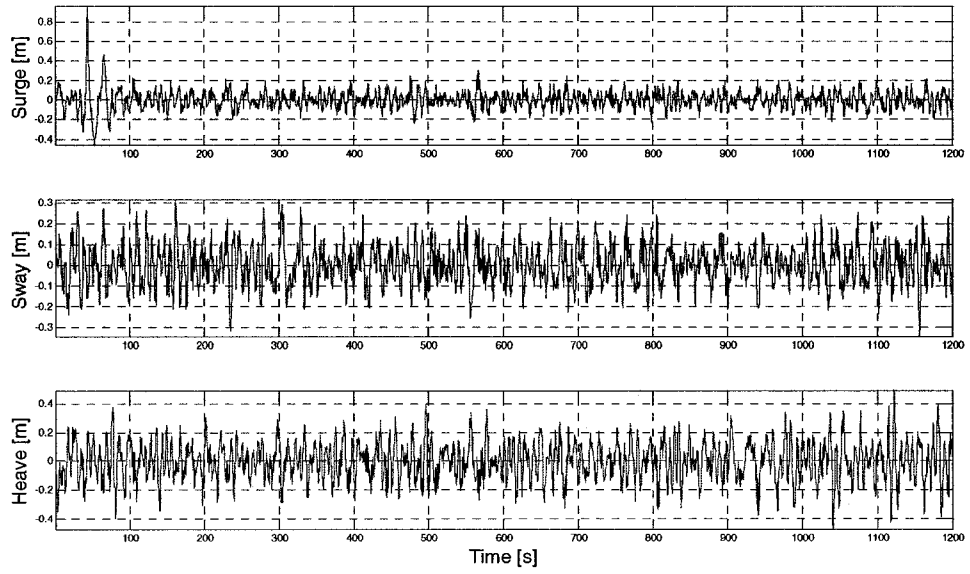
Turmelle, Chad A. (2007). *Development of a 20-Ton Capacity Open Ocean Aquaculture Feed Buoy*. Master's Degree Thesis submitted in partial requirement for the Ocean Engineering degree program. University of New Hampshire, Durham, NH. May 2007. 122 p.

APPENDIX A

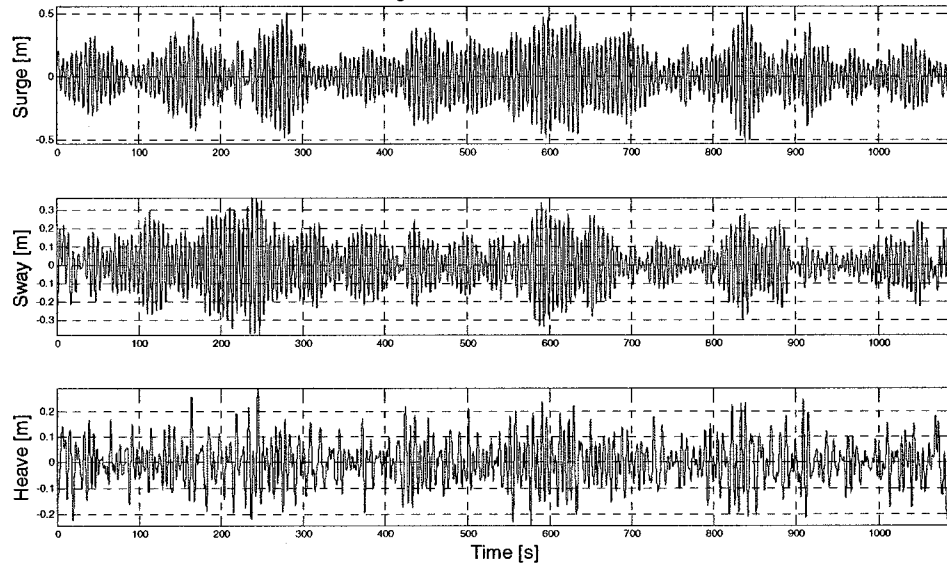
PROCESSED FIELD PROGRAM DATA FROM MARCH 11th TO MARCH 13th

3/11/2008 at 16:00:00 UTC

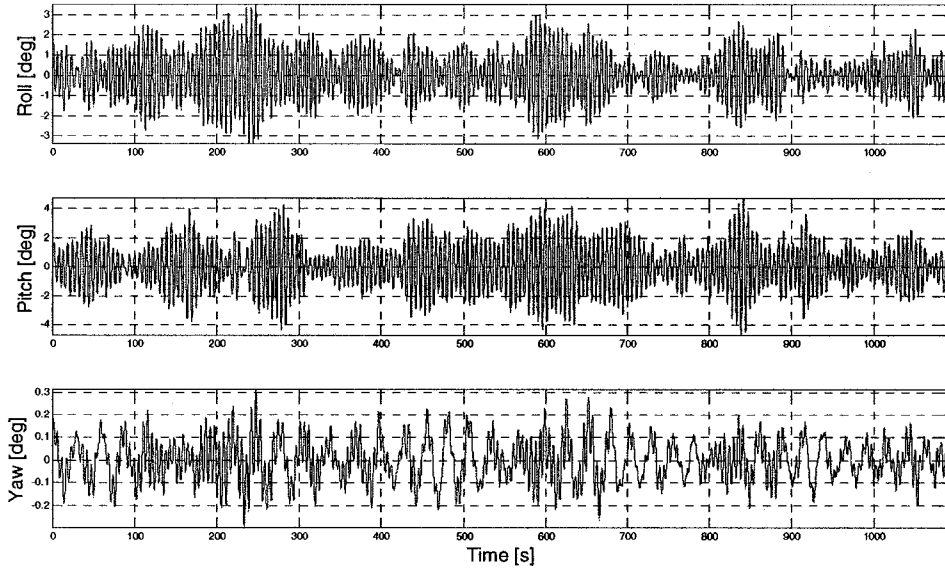
Wave Rider Translations: 03-11-2008 at 16 UTC



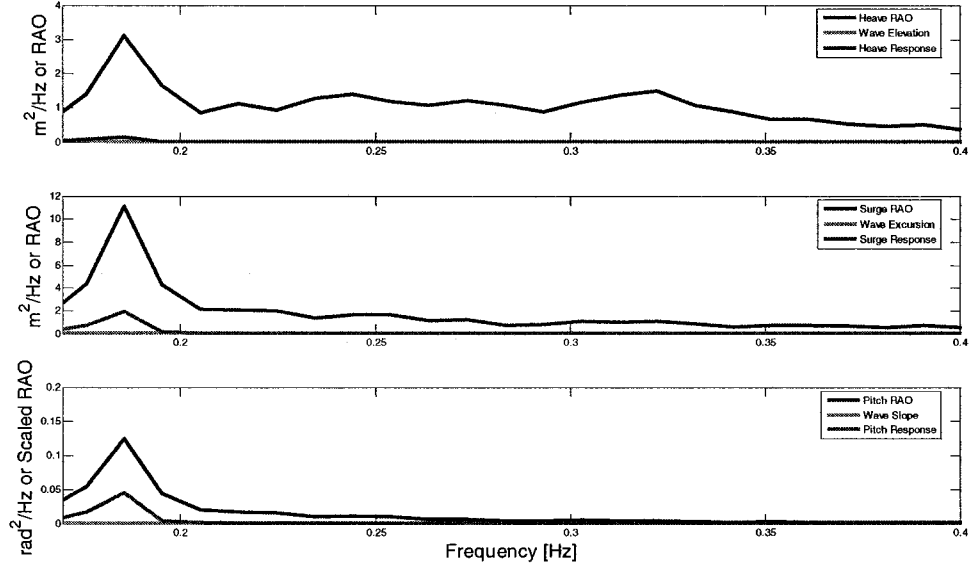
Motion Package Translations: 03-11-2008 at 16 UTC



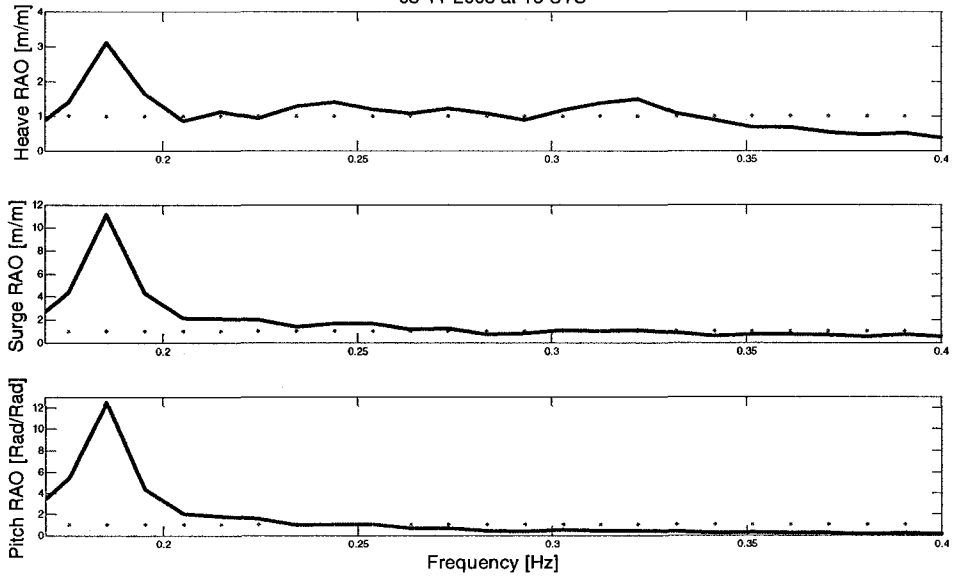
Motion Package Rotations: 03-11-2008 at 16 UTC



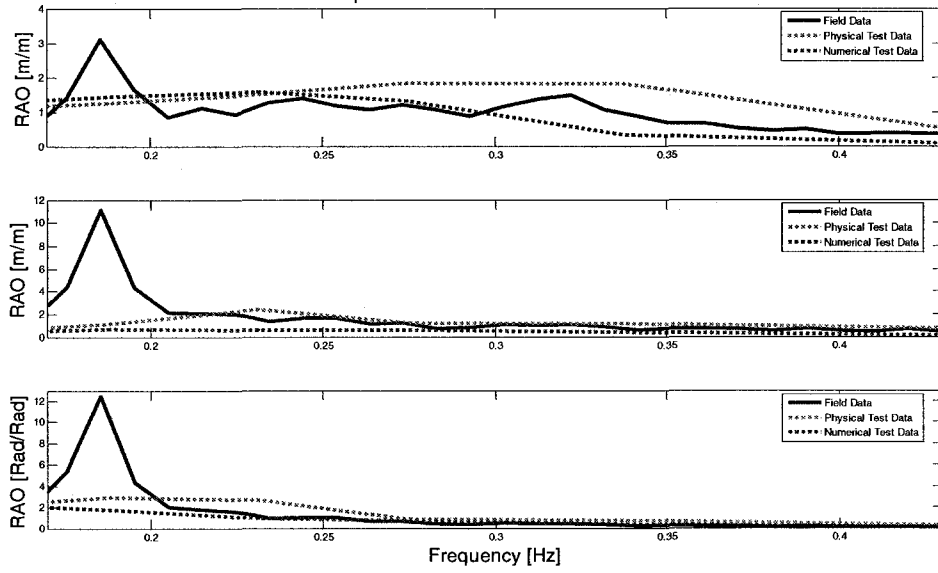
03-11-2008 at 16 UTC



03-11-2008 at 16 UTC

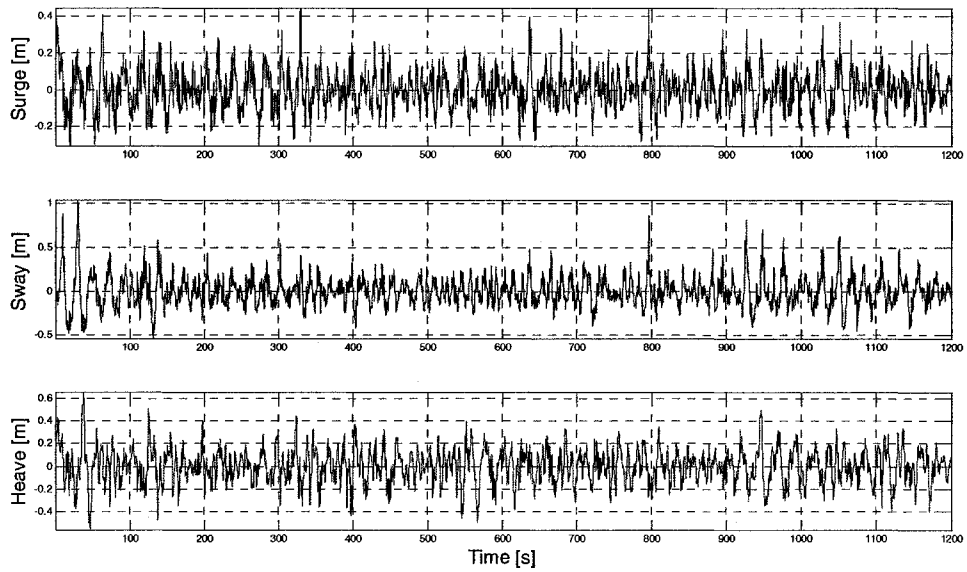


Comparison of Modeled/Field Data RAOs

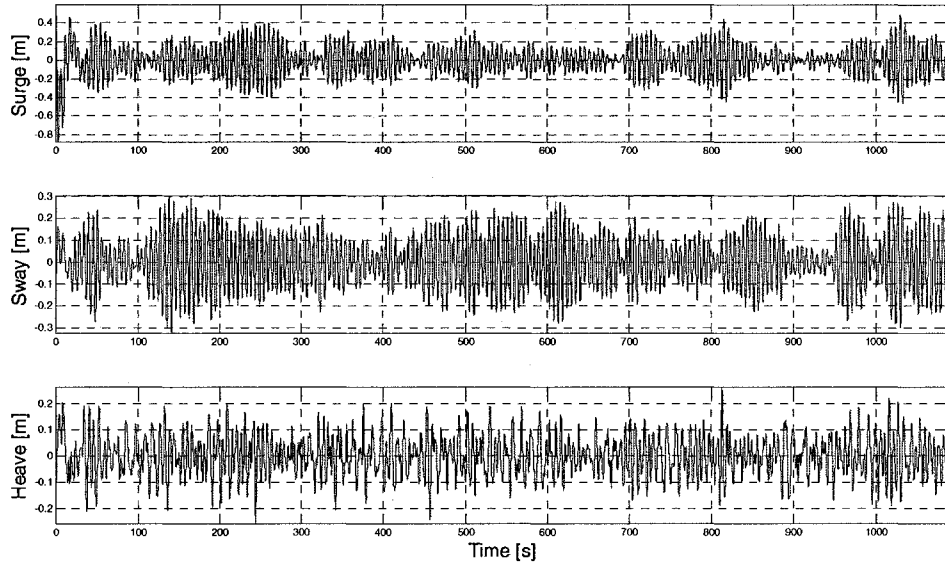


3/11/2008 at 18:00:00 UTC

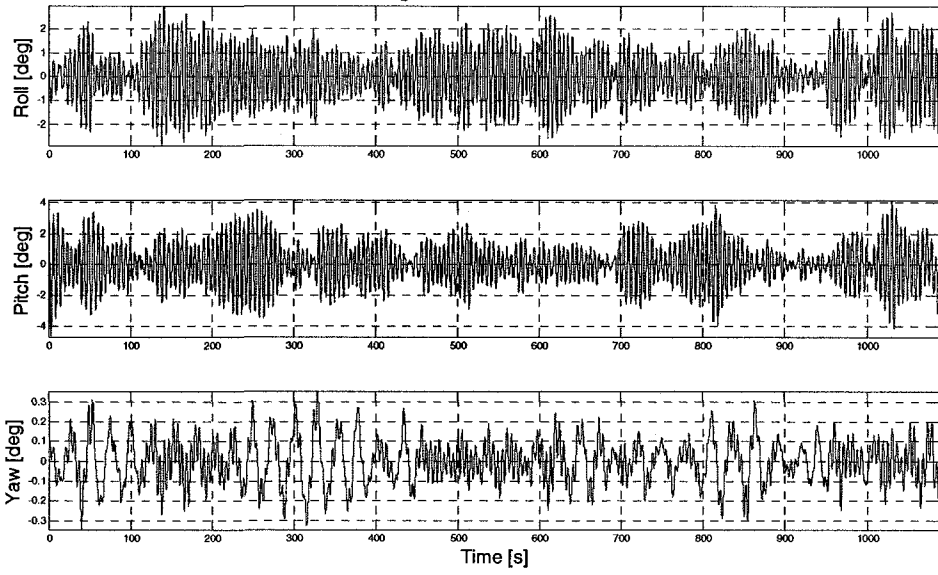
Wave Rider Translations: 03-11-2008 at 18 UTC



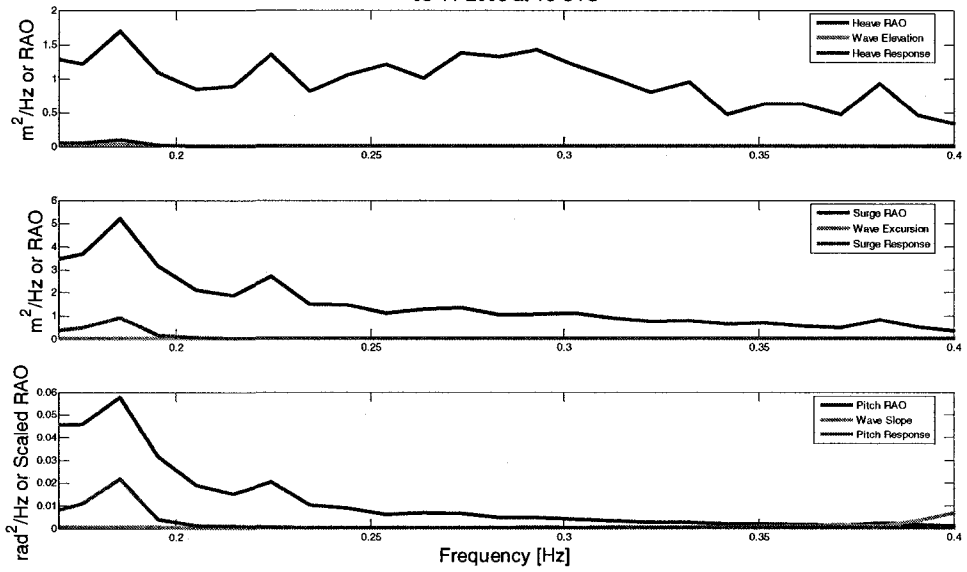
Motion Package Translations: 03-11-2008 at 18 UTC

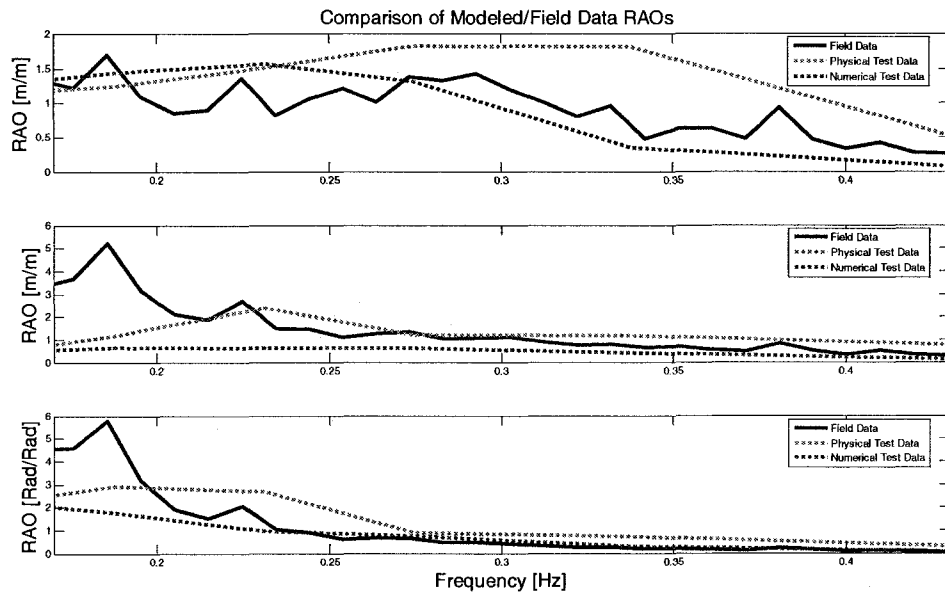
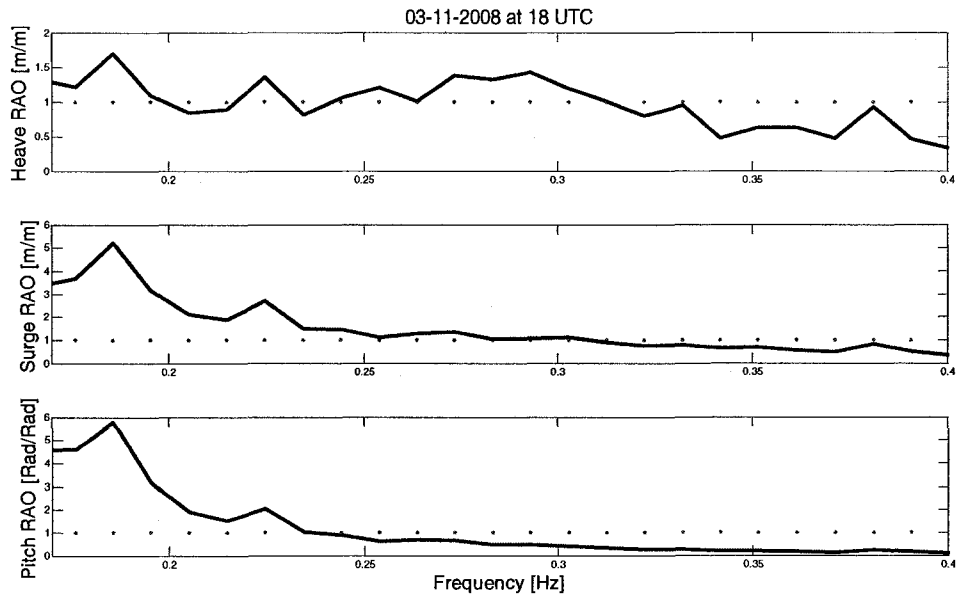


Motion Package Rotations: 03-11-2008 at 18 UTC

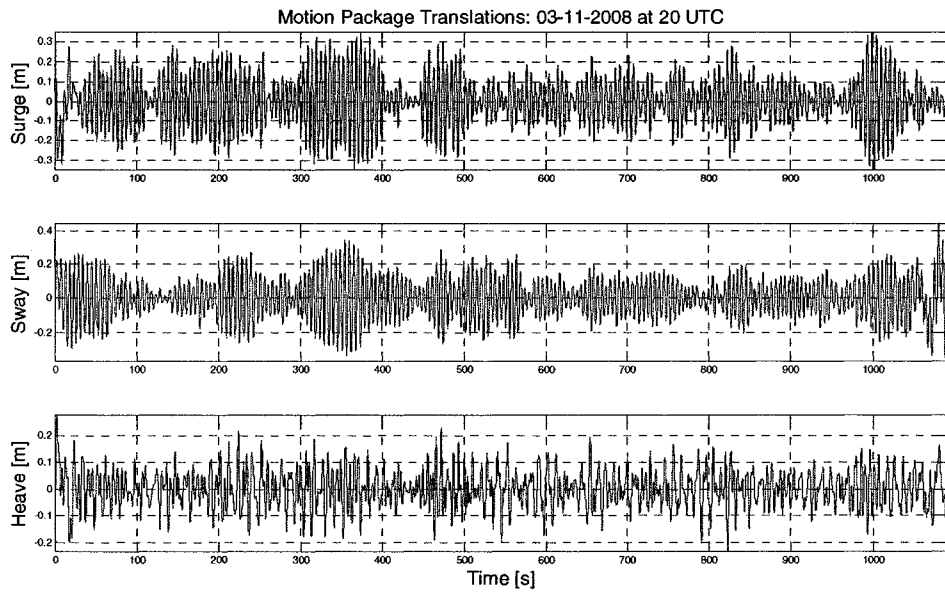
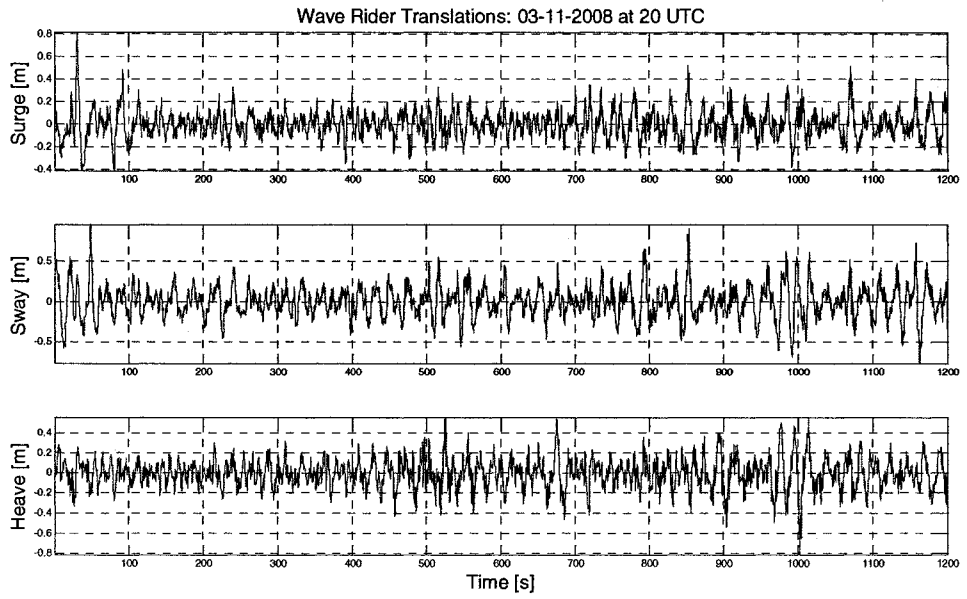


03-11-2008 at 18 UTC

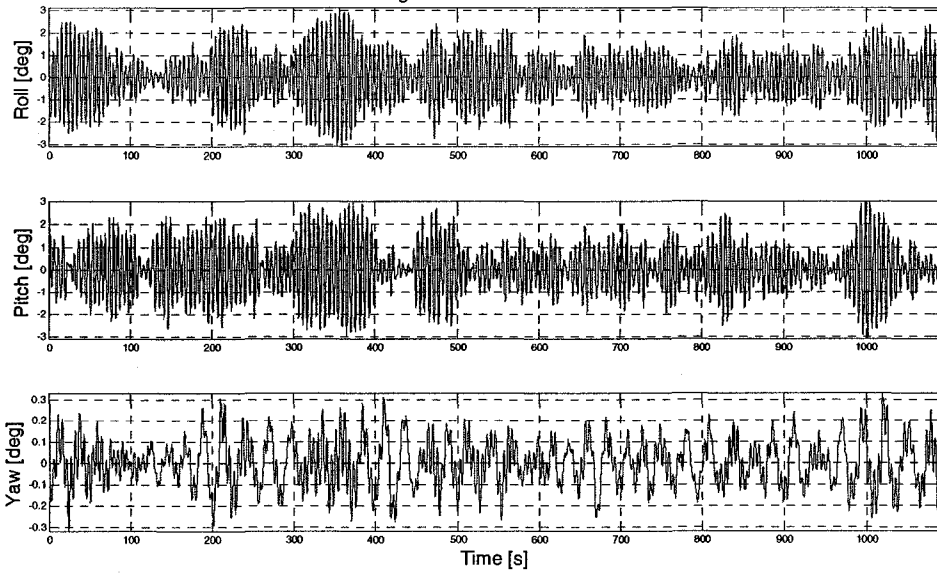




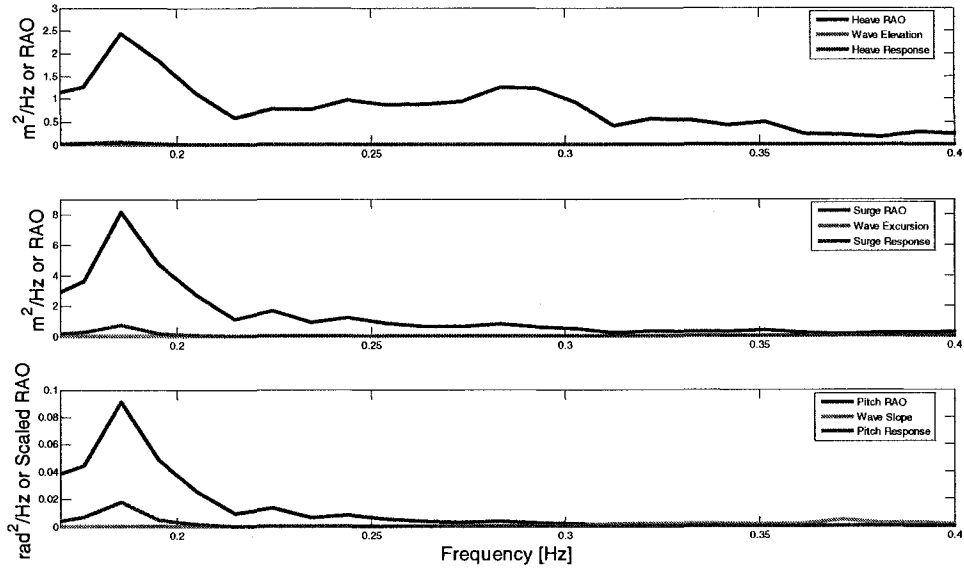
3/11/2008 at 20:00:00 UTC

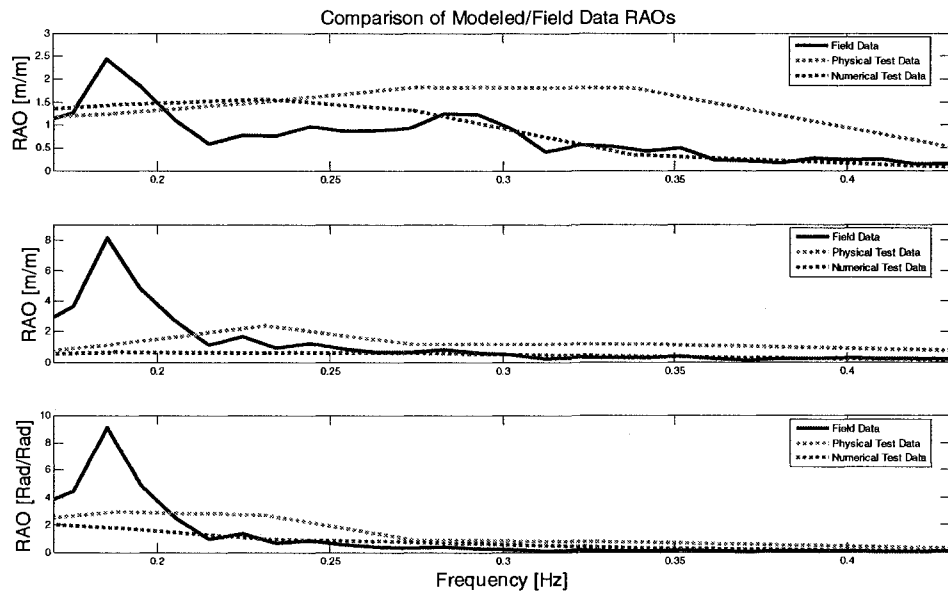
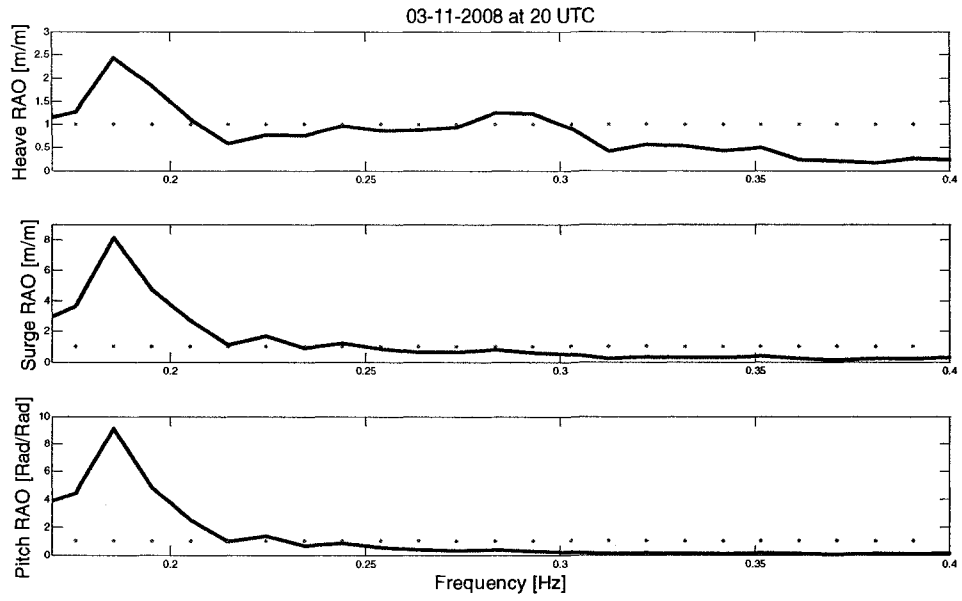


Motion Package Rotations: 03-11-2008 at 20 UTC



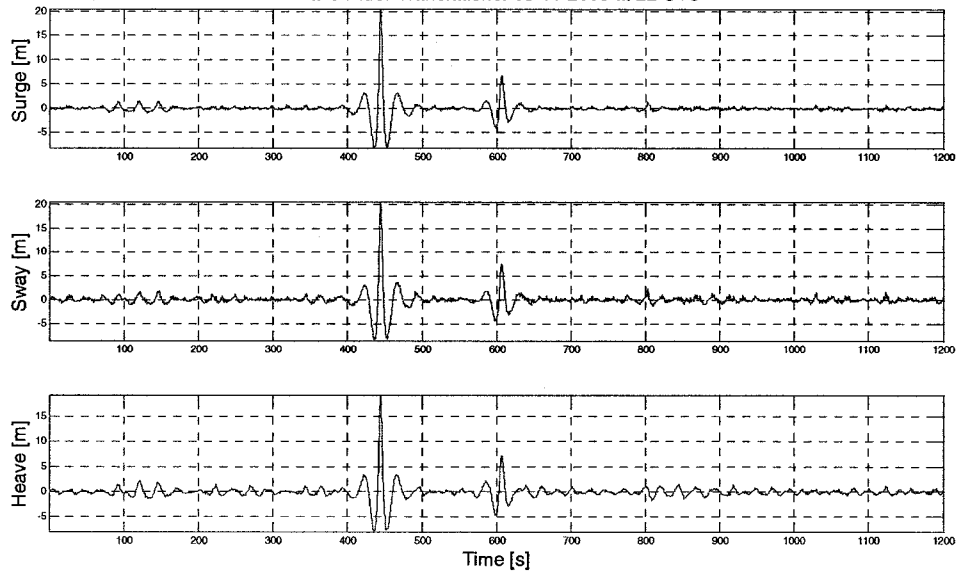
03-11-2008 at 20 UTC



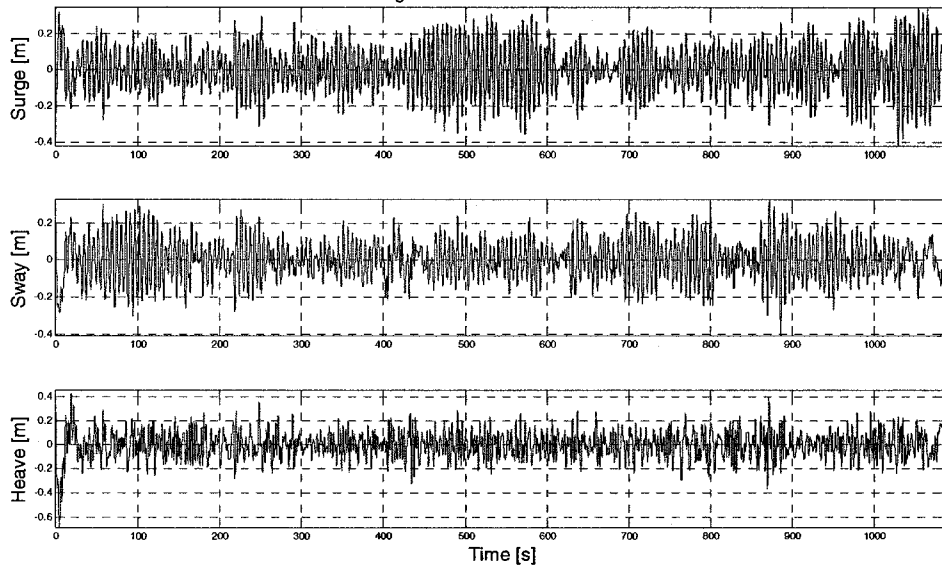


3/11/2008 at 22:00:00 UTC

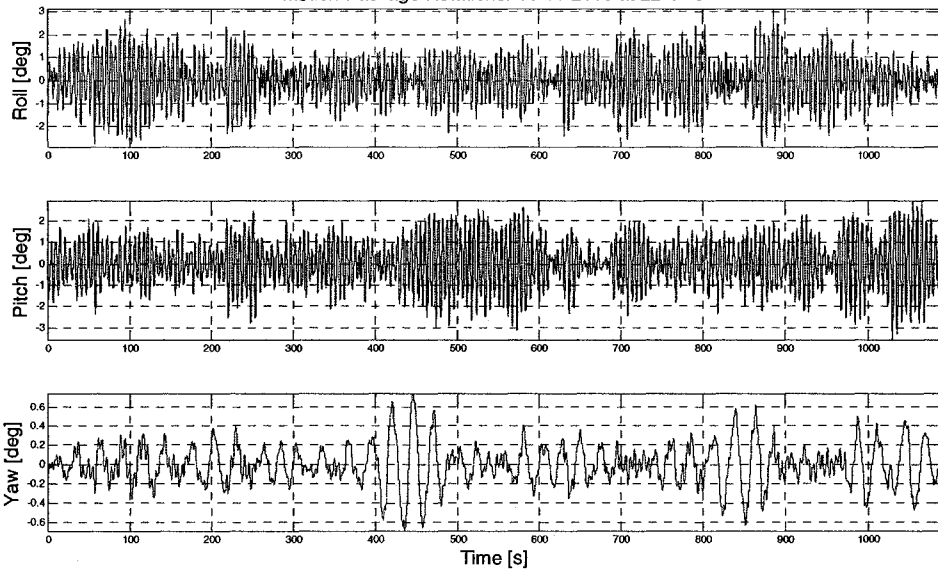
Wave Rider Translations: 03-11-2008 at 22 UTC



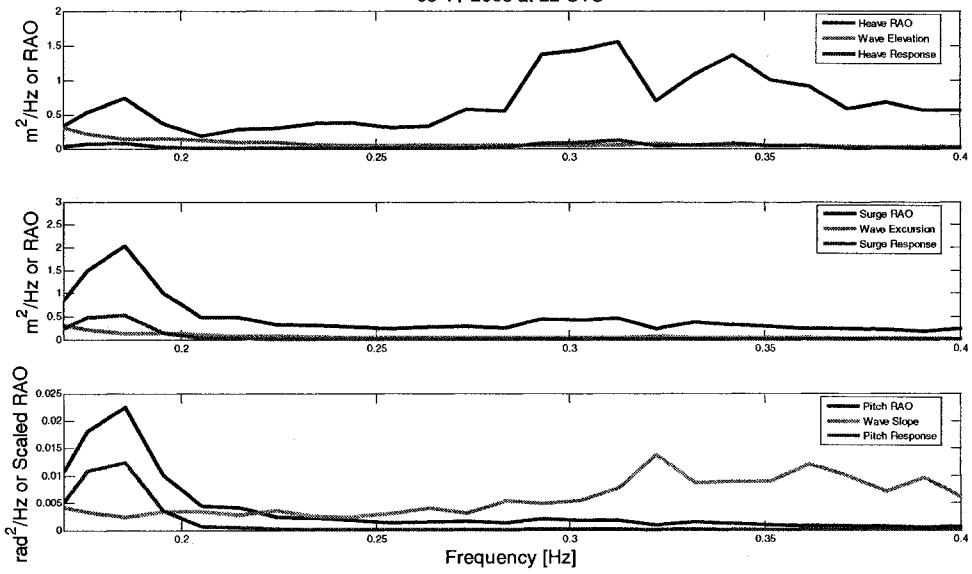
Motion Package Translations: 03-11-2008 at 22 UTC

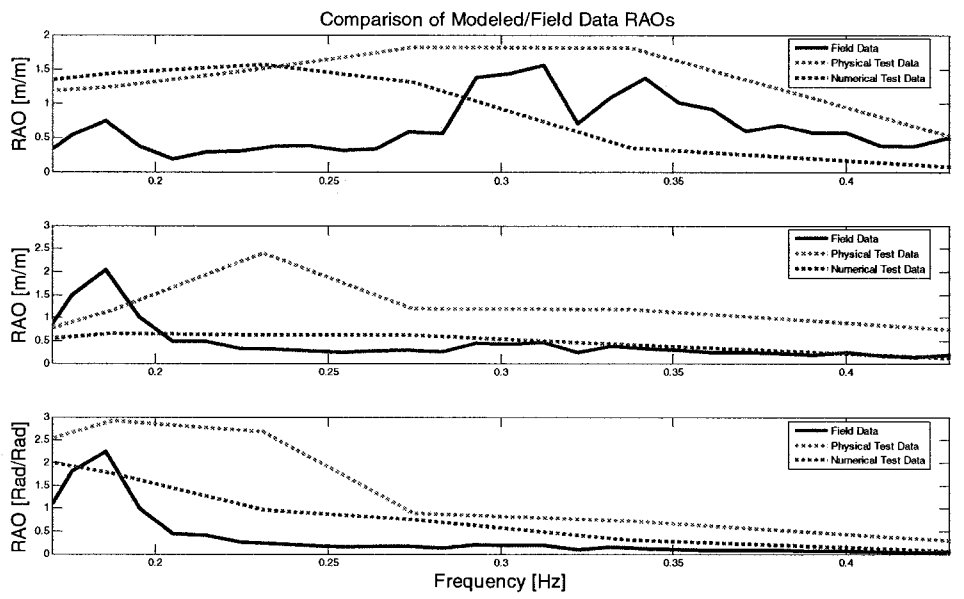
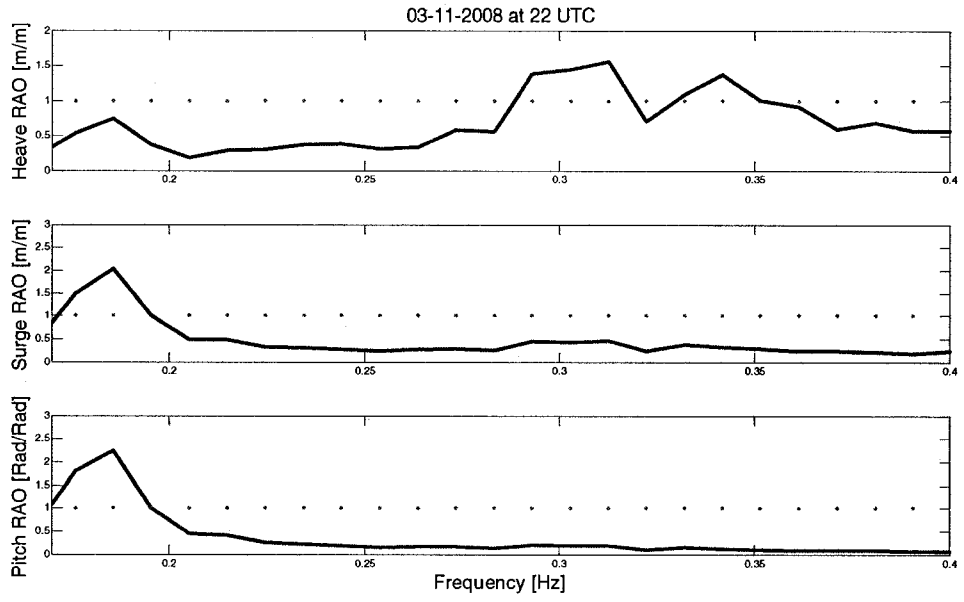


Motion Package Rotations: 03-11-2008 at 22 UTC



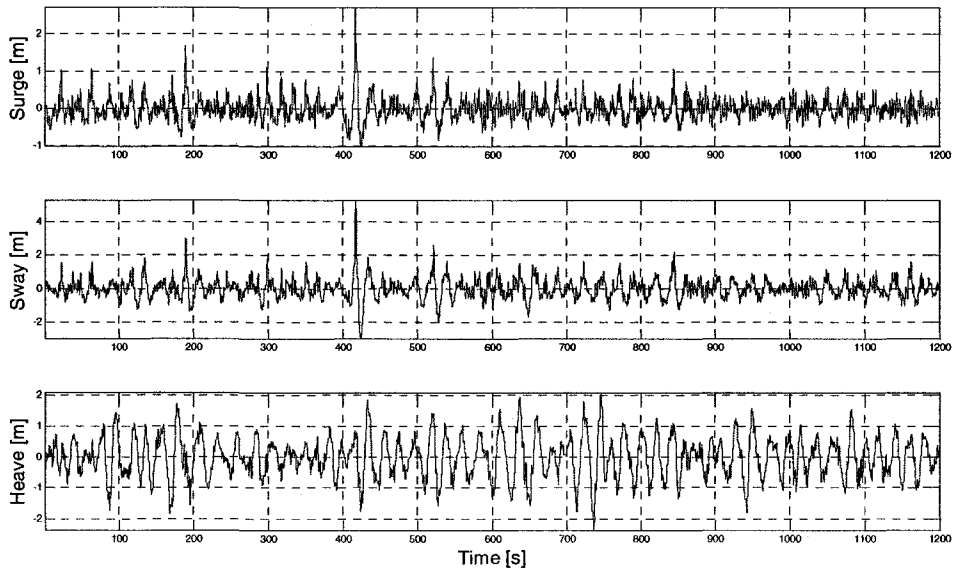
03-11-2008 at 22 UTC



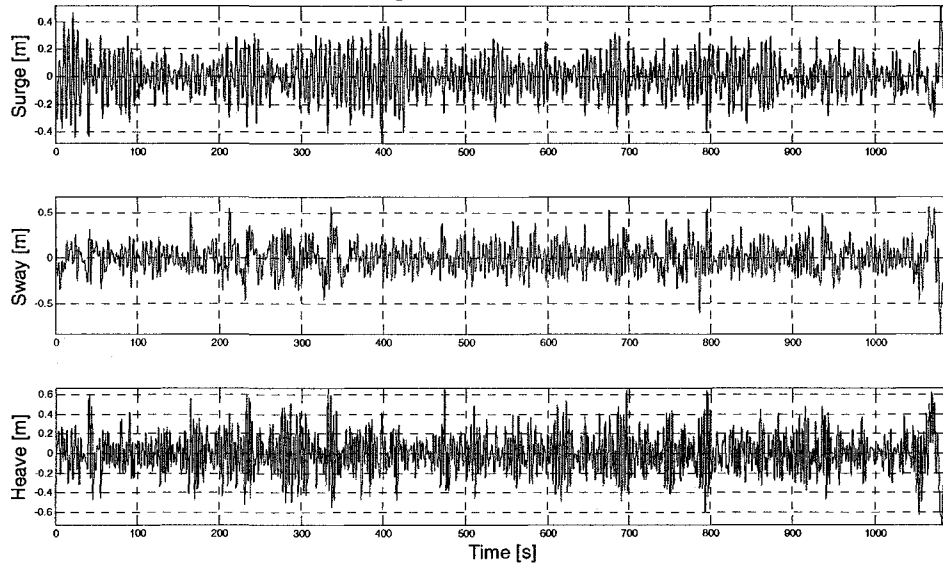


3/12/2008 at 0:00:00 UTC

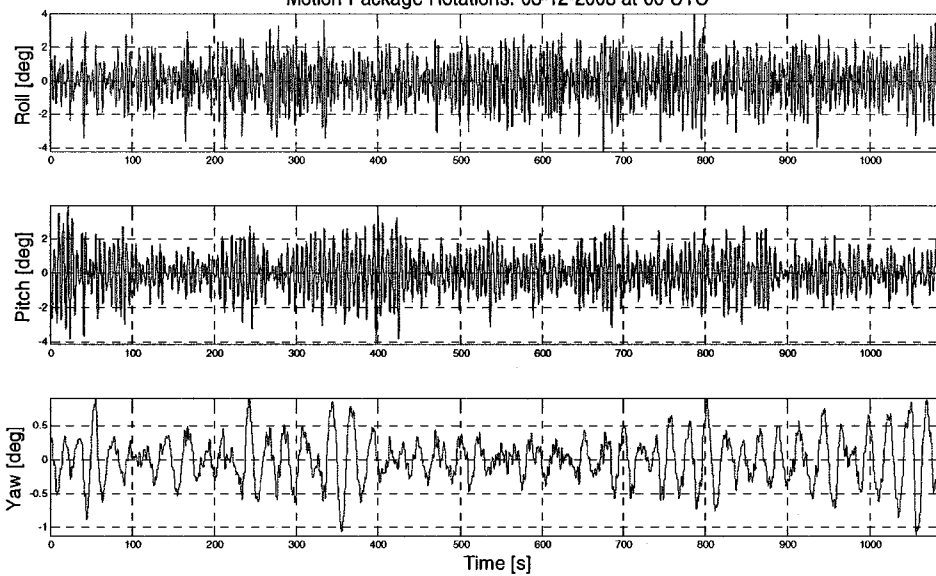
Wave Rider Translations: 03-12-2008 at 00 UTC



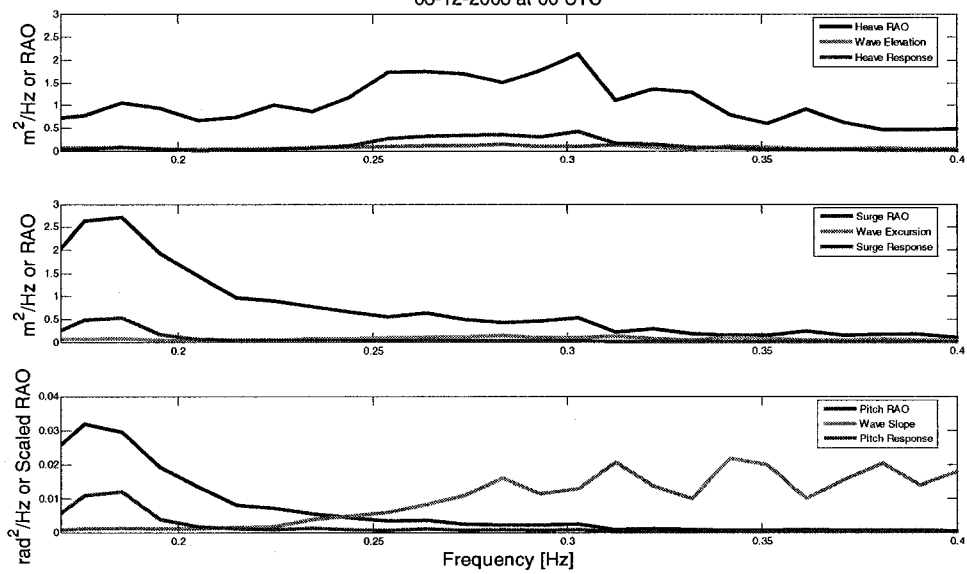
Motion Package Translations: 03-12-2008 at 00 UTC

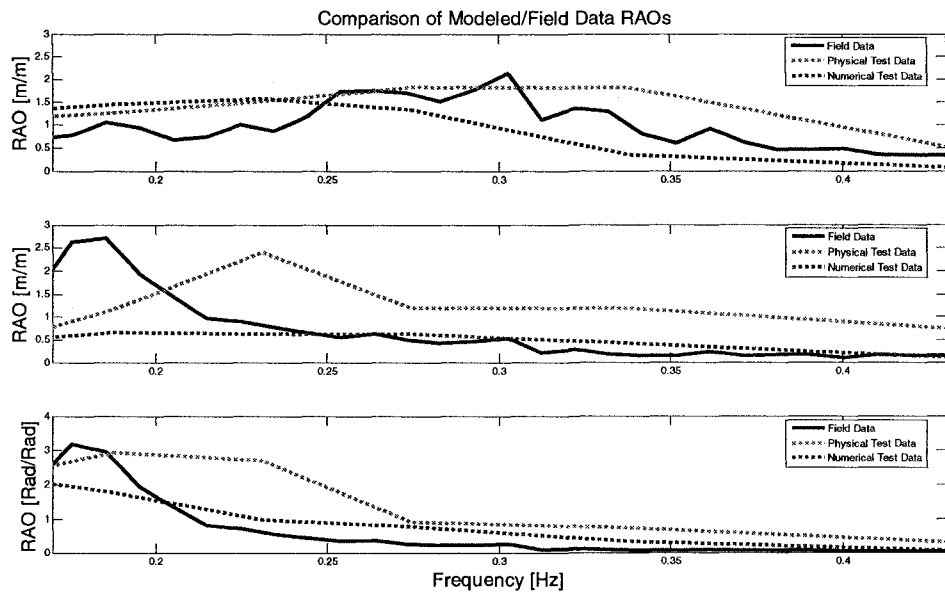
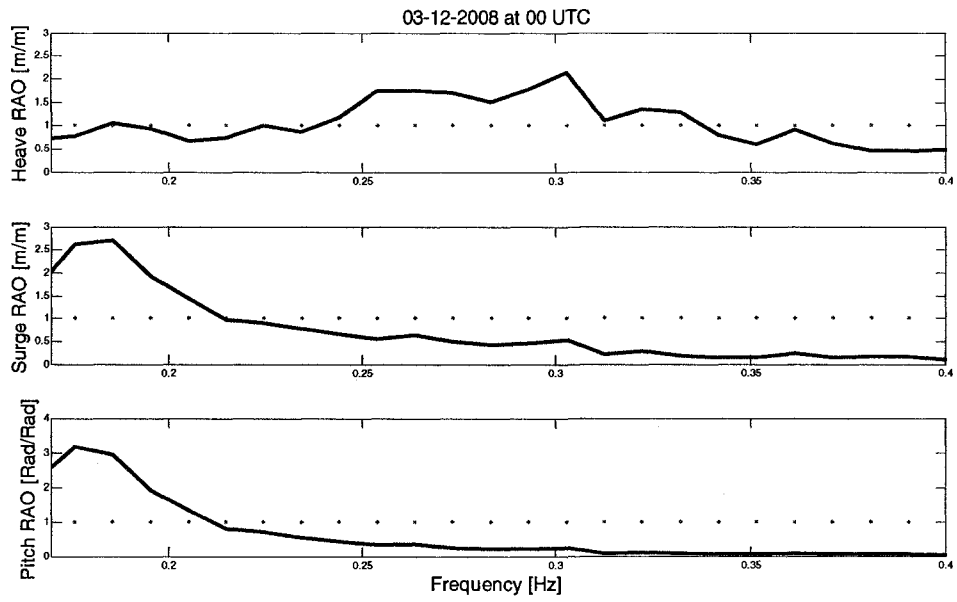


Motion Package Rotations: 03-12-2008 at 00 UTC



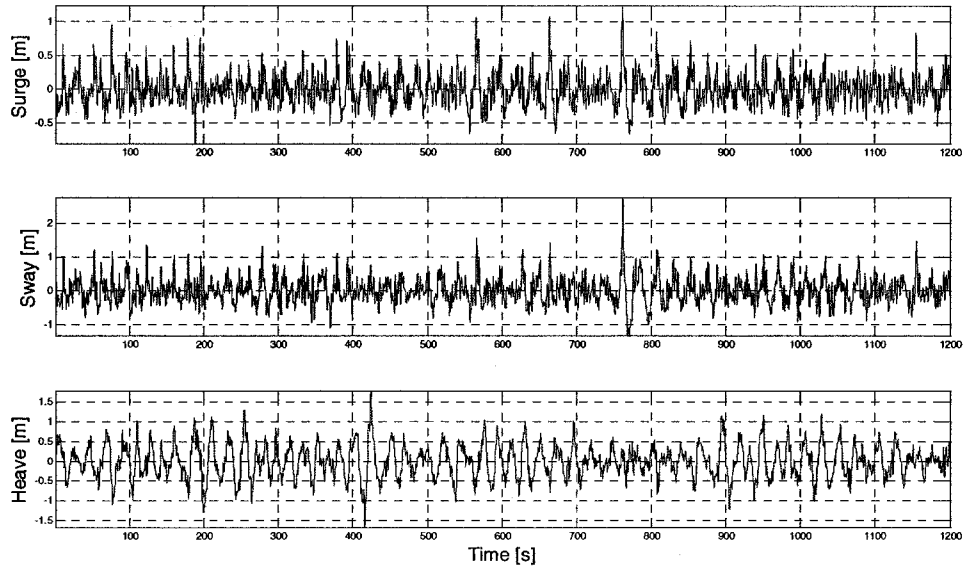
03-12-2008 at 00 UTC



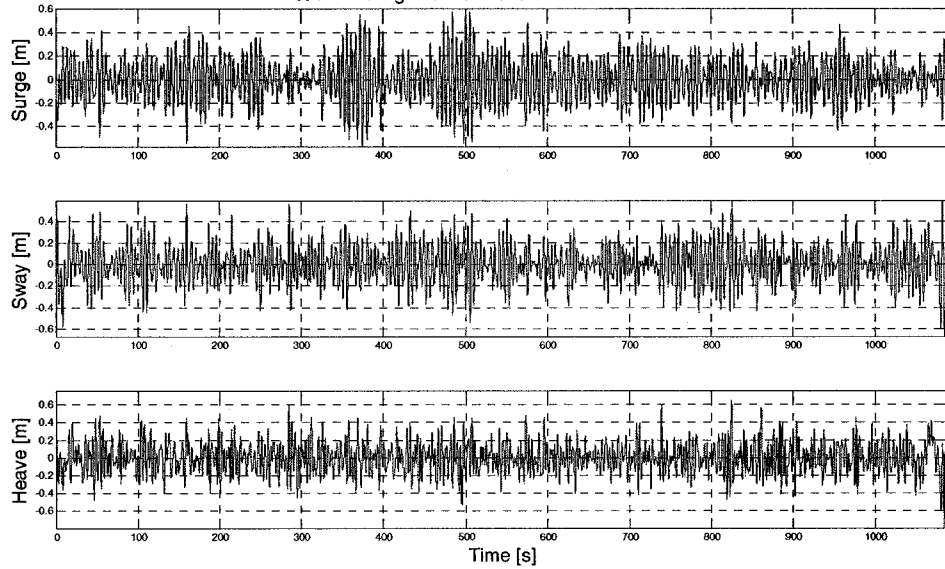


3/12/2008 at 2:00:00 UTC

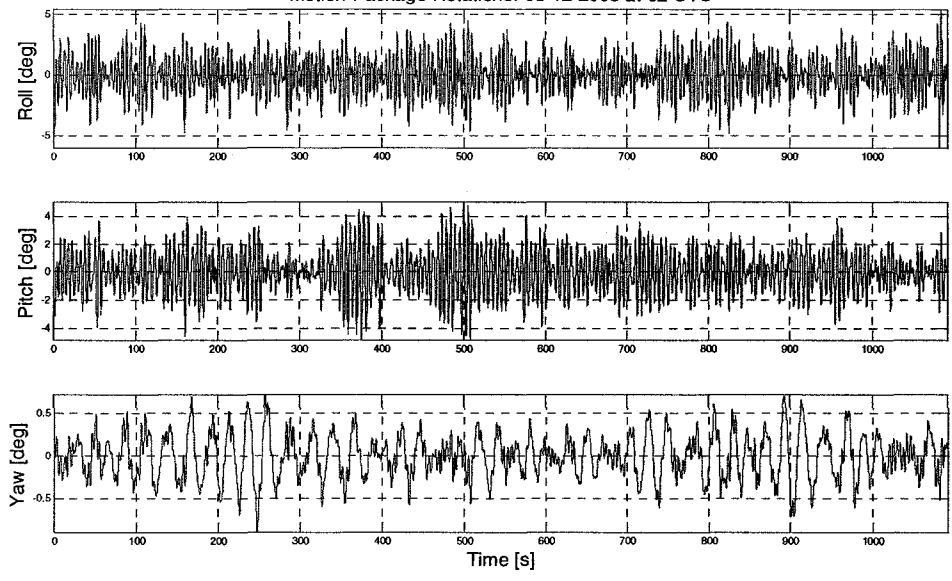
Wave Rider Translations: 03-12-2008 at 02 UTC



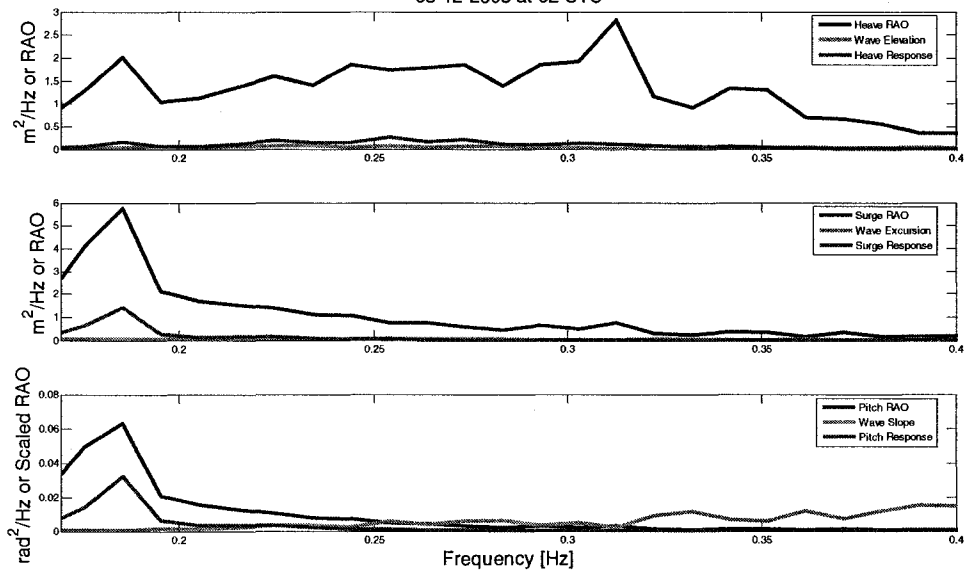
Motion Package Translations: 03-12-2008 at 02 UTC

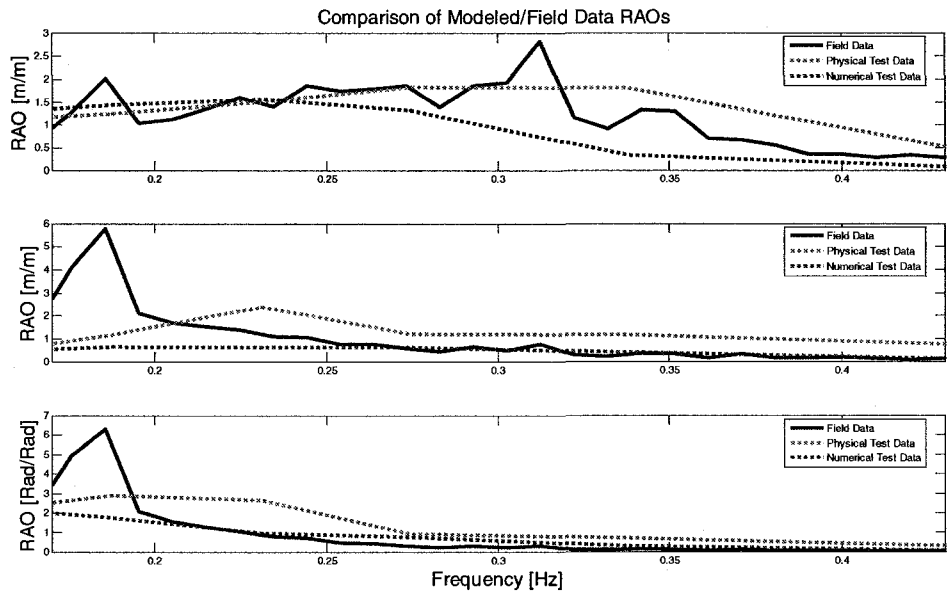
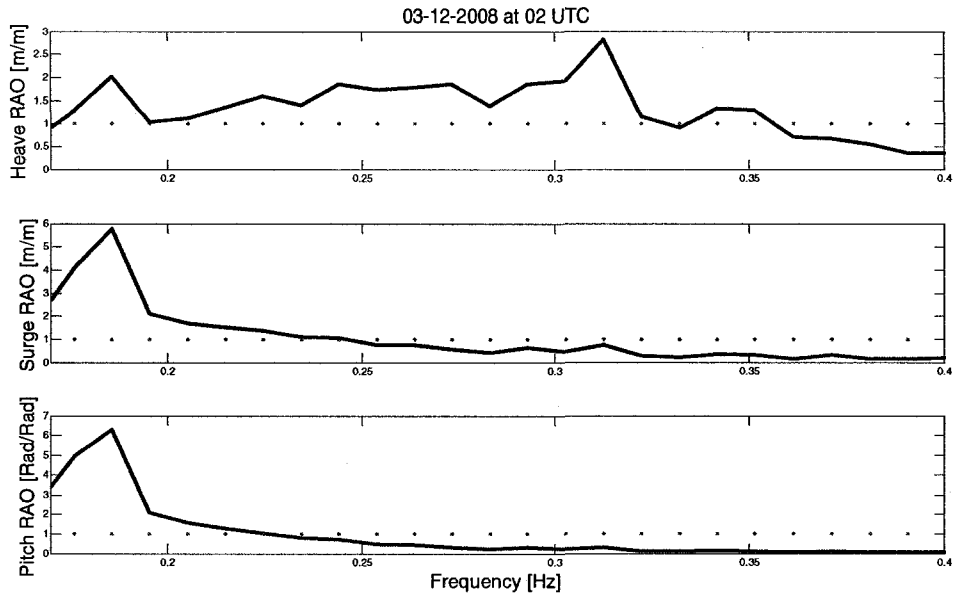


Motion Package Rotations: 03-12-2008 at 02 UTC



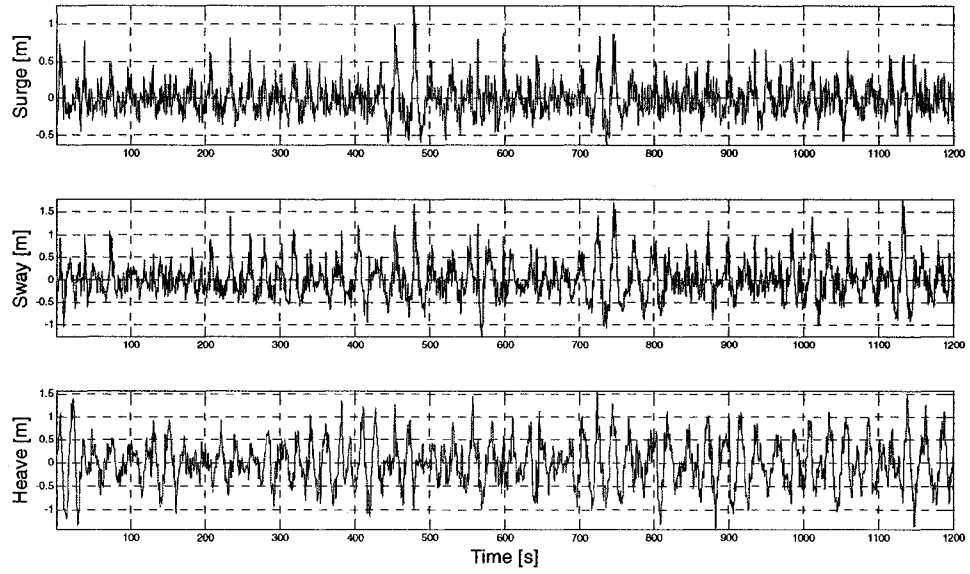
03-12-2008 at 02 UTC



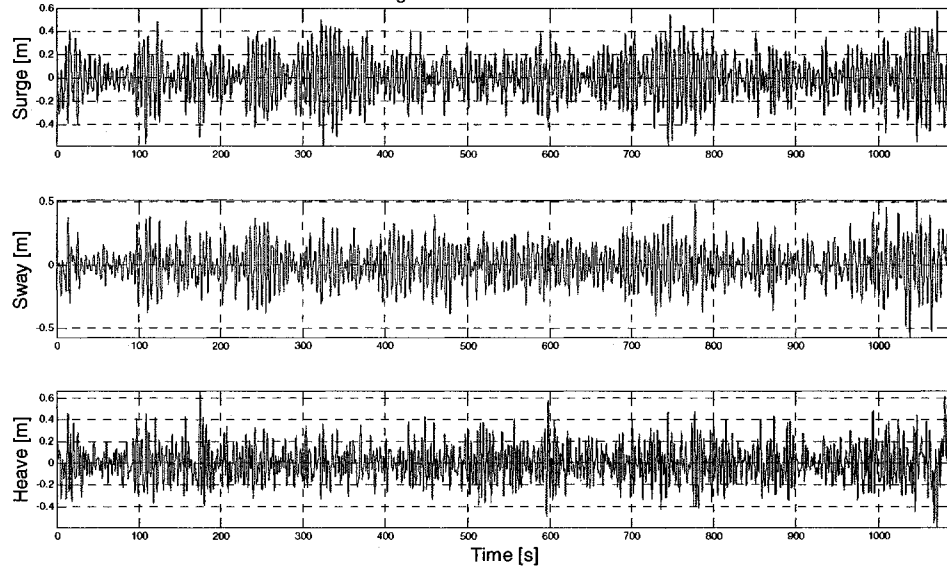


3/12/2008 at 4:00:00 UTC

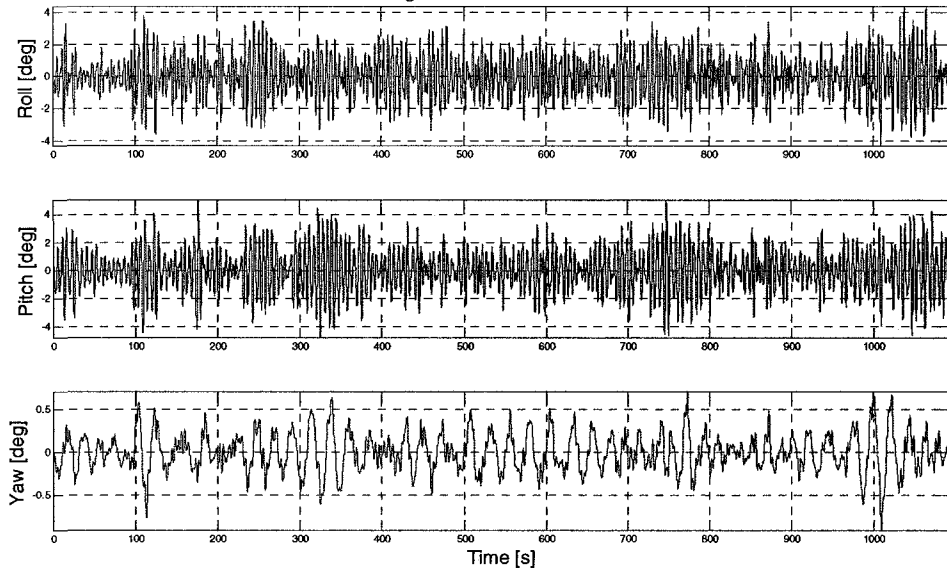
Wave Rider Translations: 03-12-2008 at 04 UTC



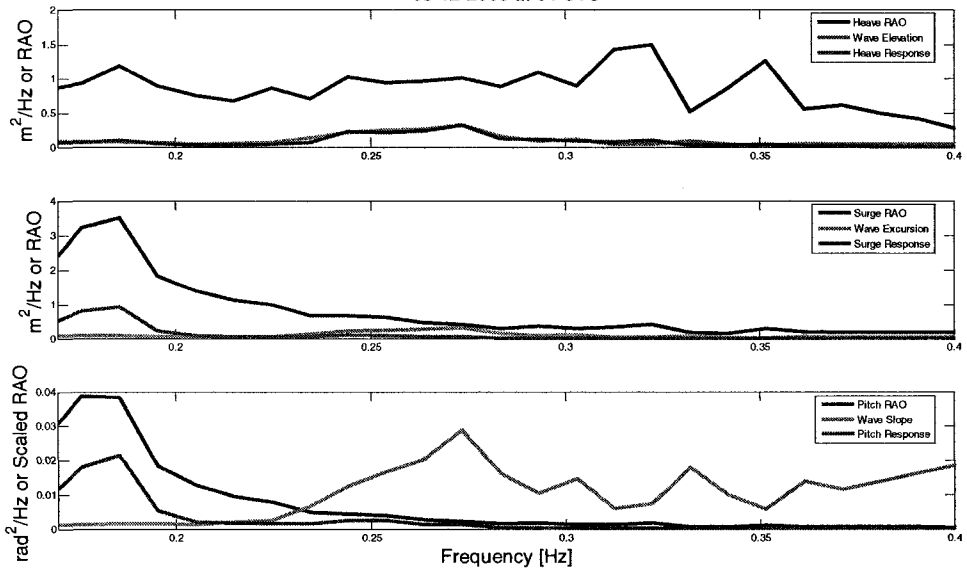
Motion Package Translations: 03-12-2008 at 04 UTC

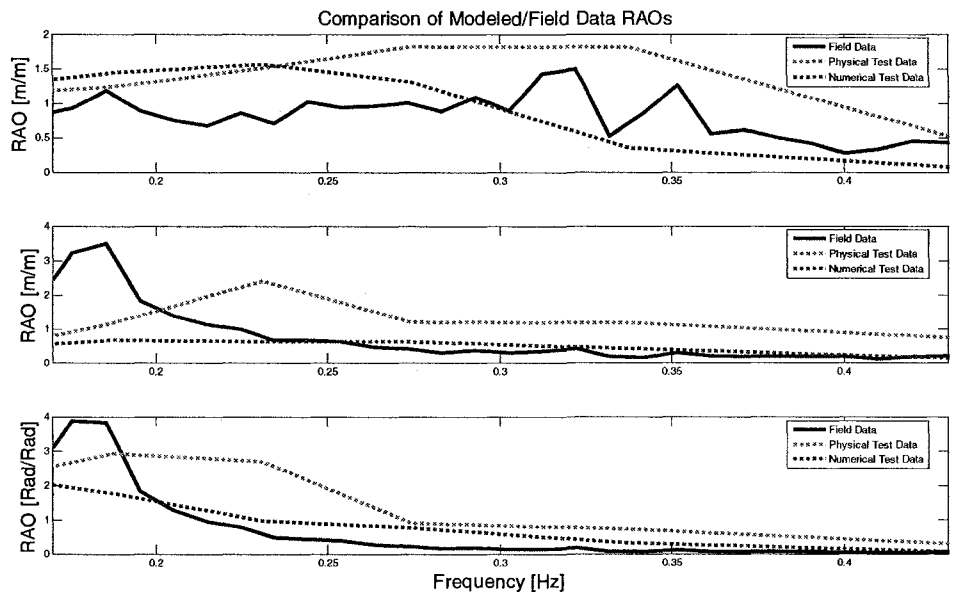
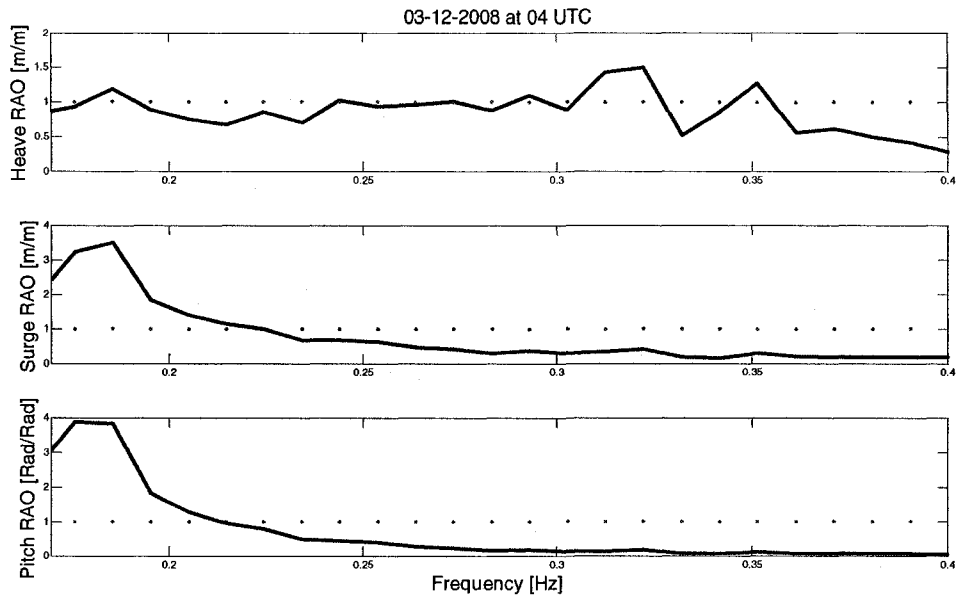


Motion Package Rotations: 03-12-2008 at 04 UTC



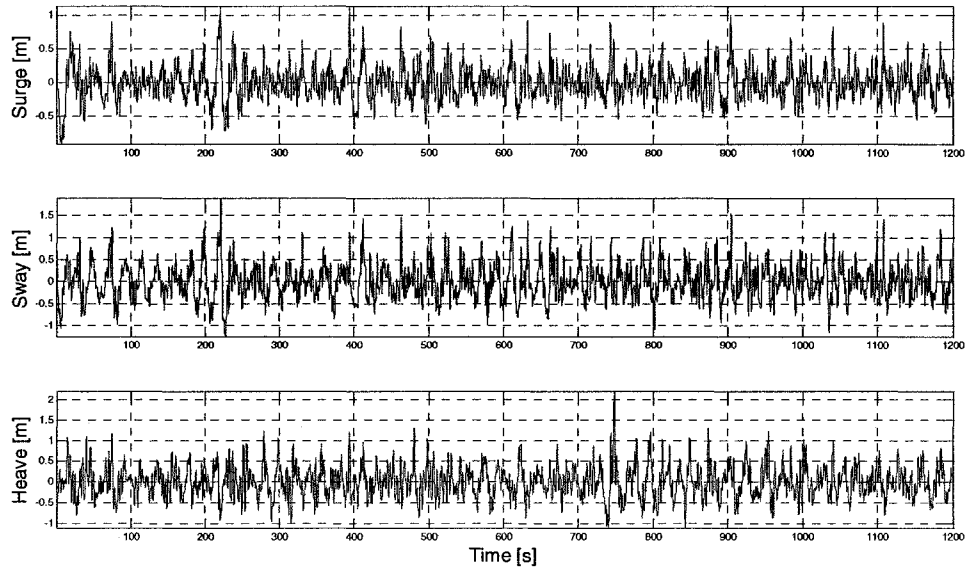
03-12-2008 at 04 UTC



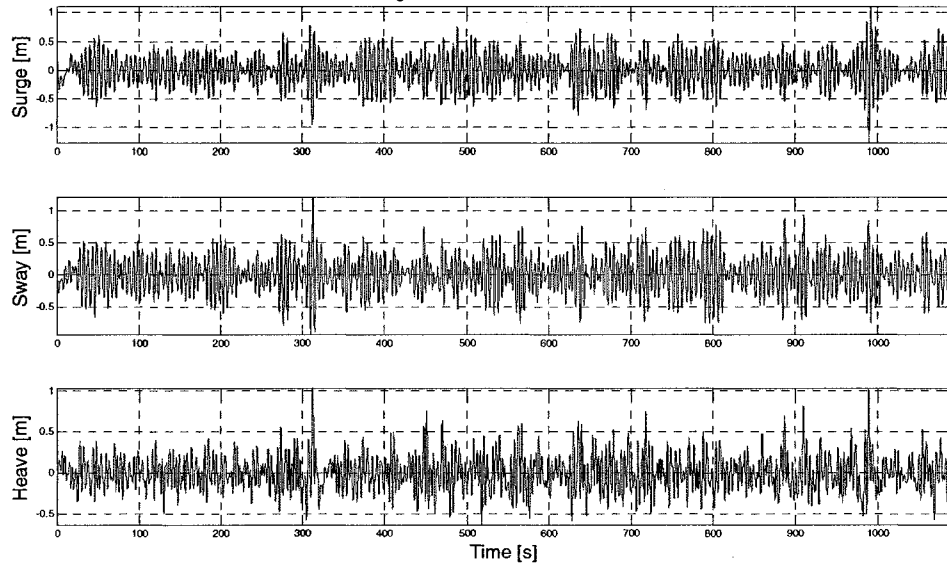


3/12/2008 at 6:00:00 UTC

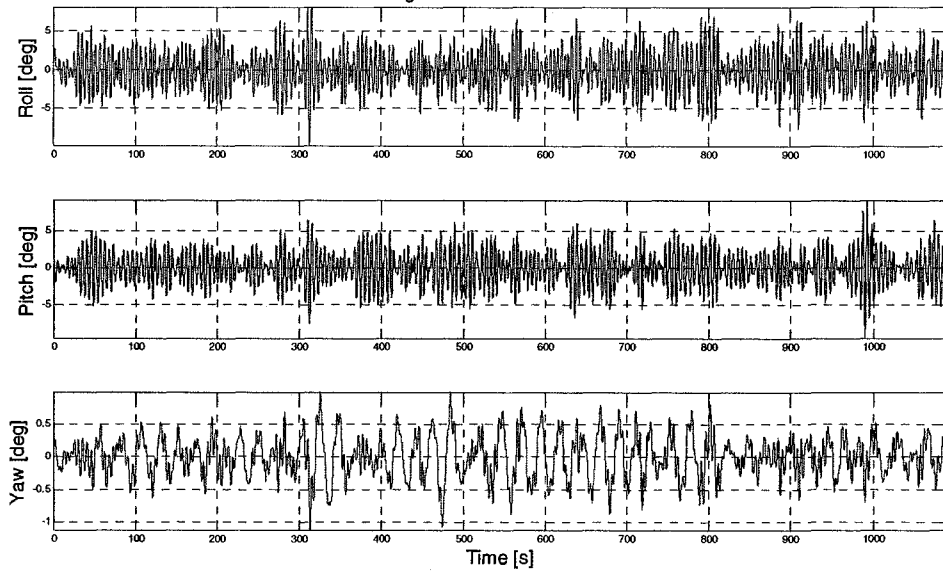
Wave Rider Translations: 03-12-2008 at 06 UTC



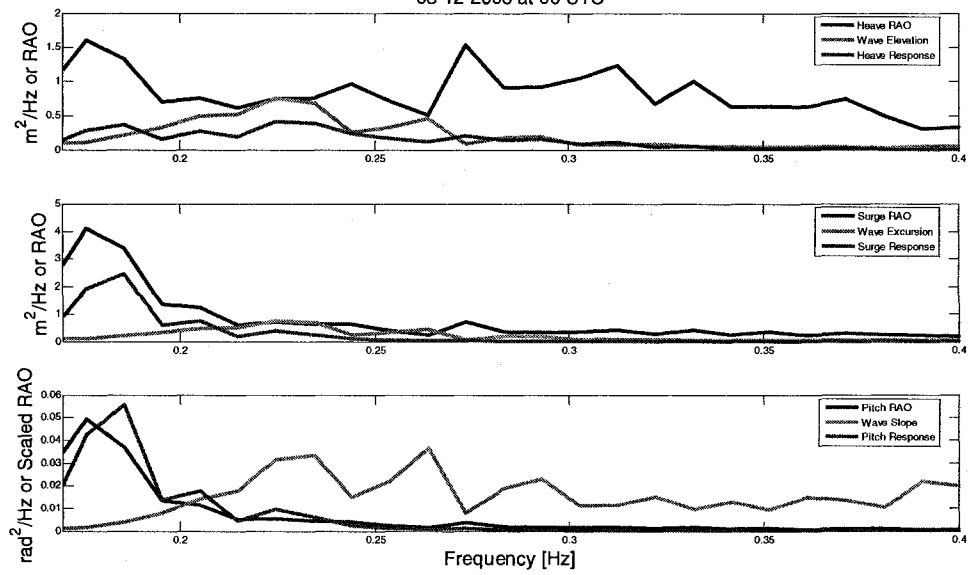
Motion Package Translations: 03-12-2008 at 06 UTC

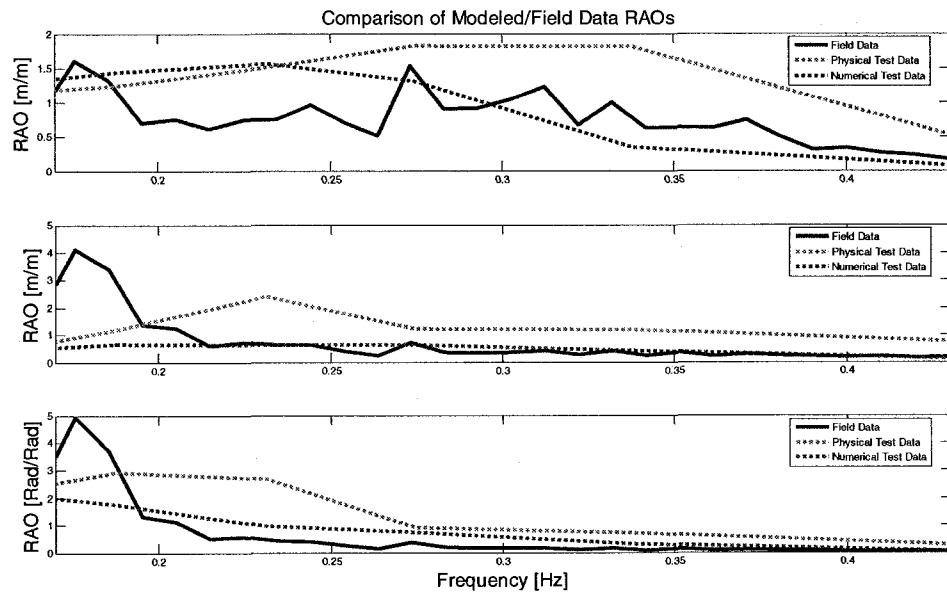
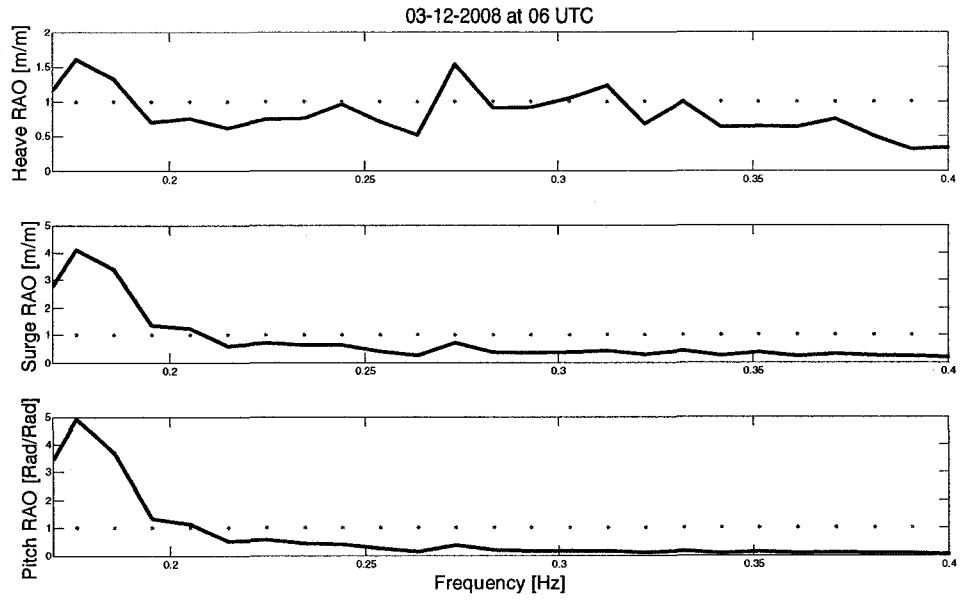


Motion Package Rotations: 03-12-2008 at 06 UTC

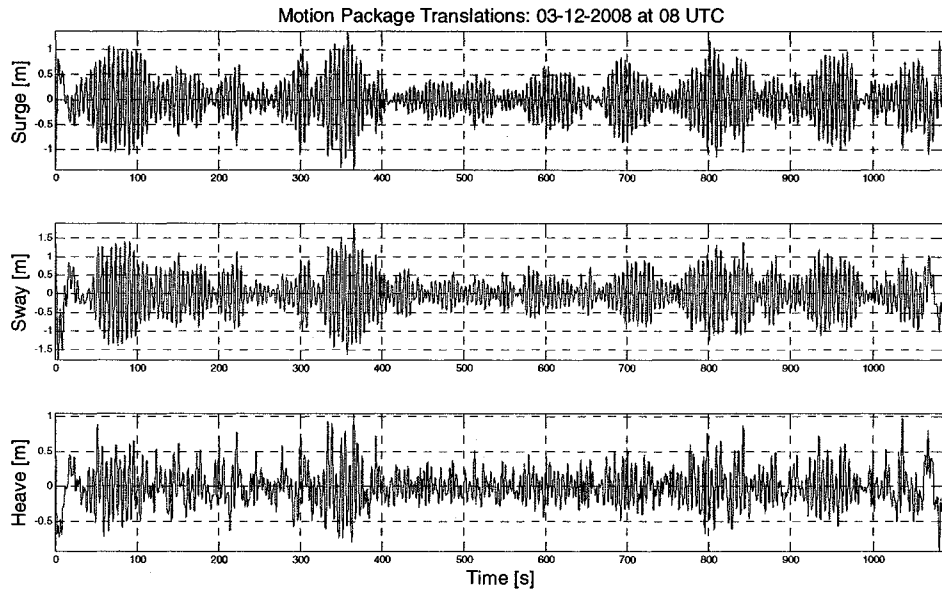
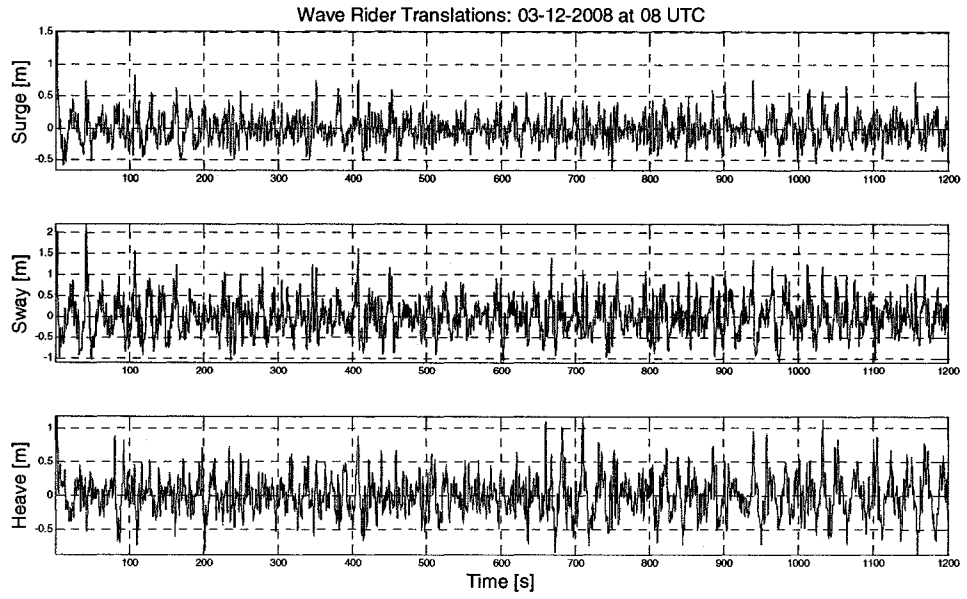


03-12-2008 at 06 UTC

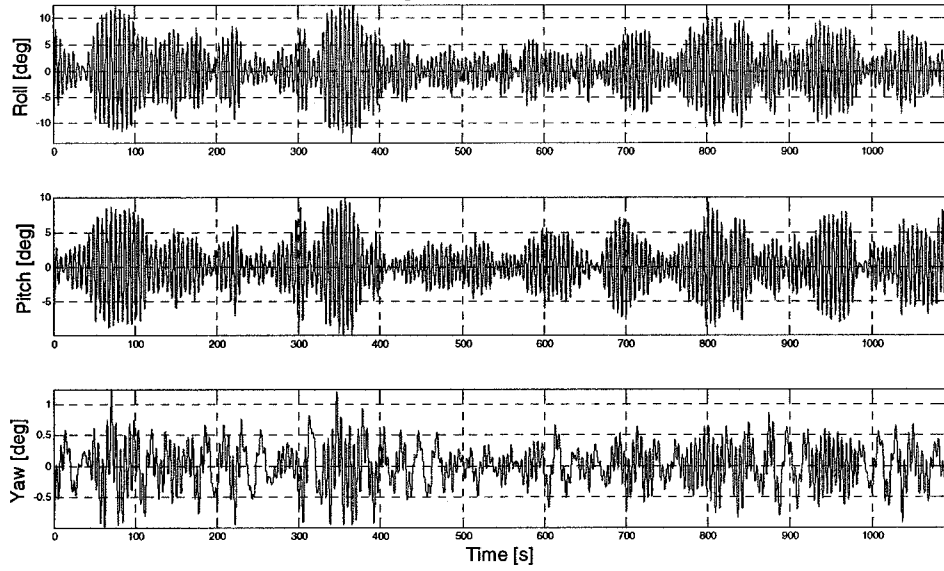




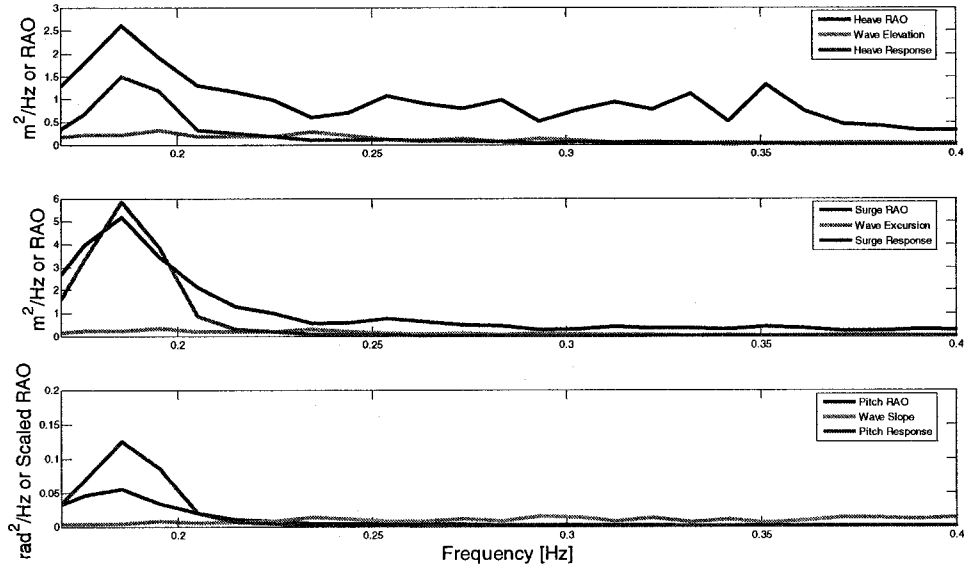
3/12/2008 at 8:00:00 UTC



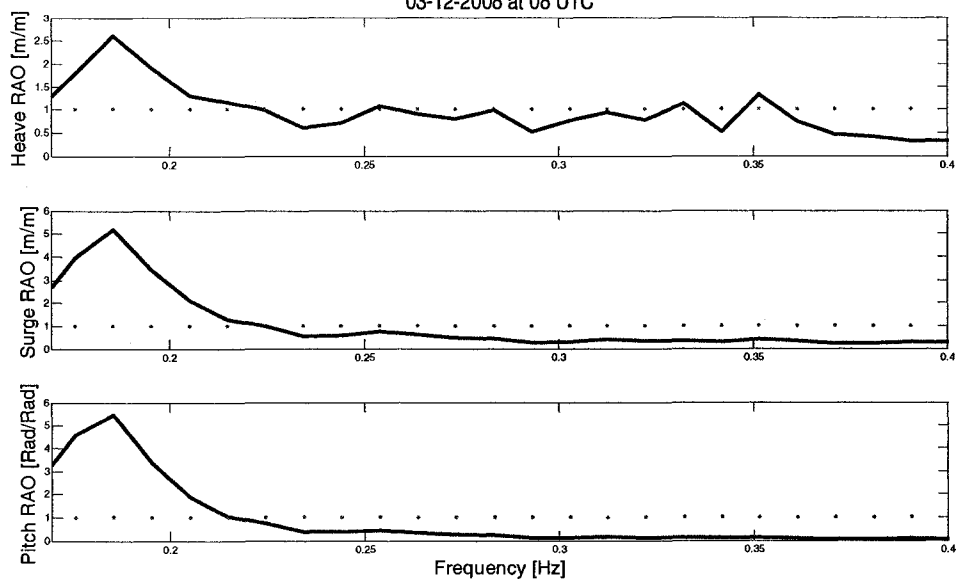
Motion Package Rotations: 03-12-2008 at 08 UTC



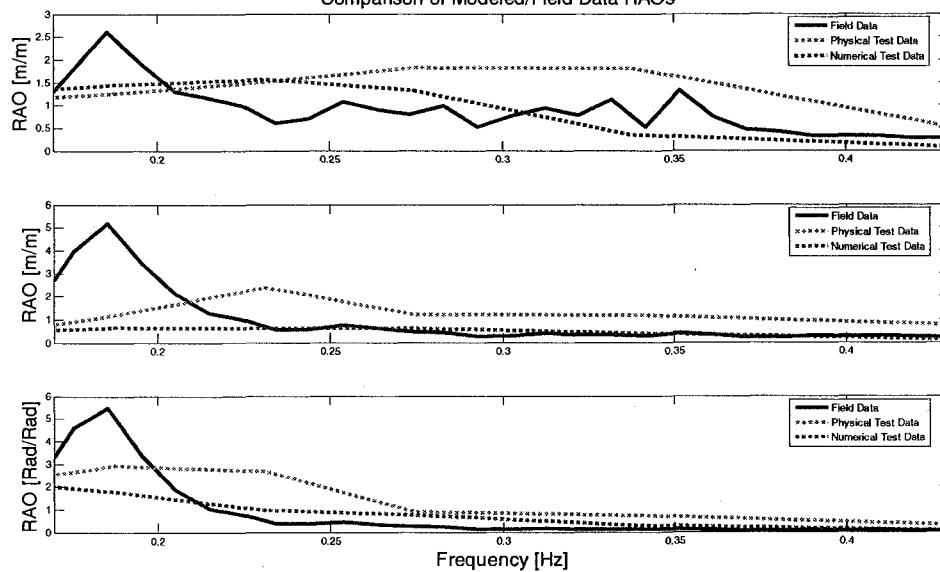
03-12-2008 at 08 UTC



03-12-2008 at 08 UTC

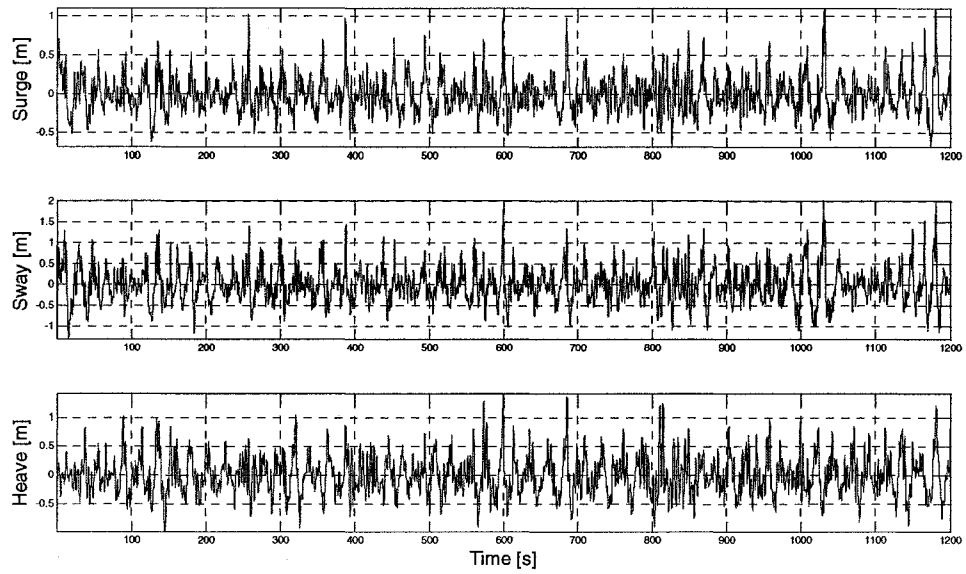


Comparison of Modeled/Field Data RAOs

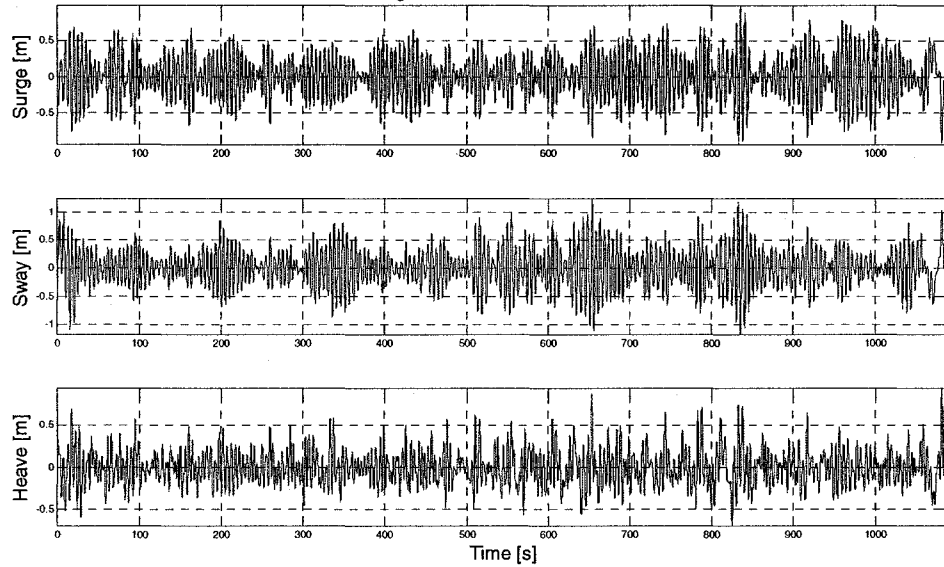


3/12/2008 at 10:00:00 UTC

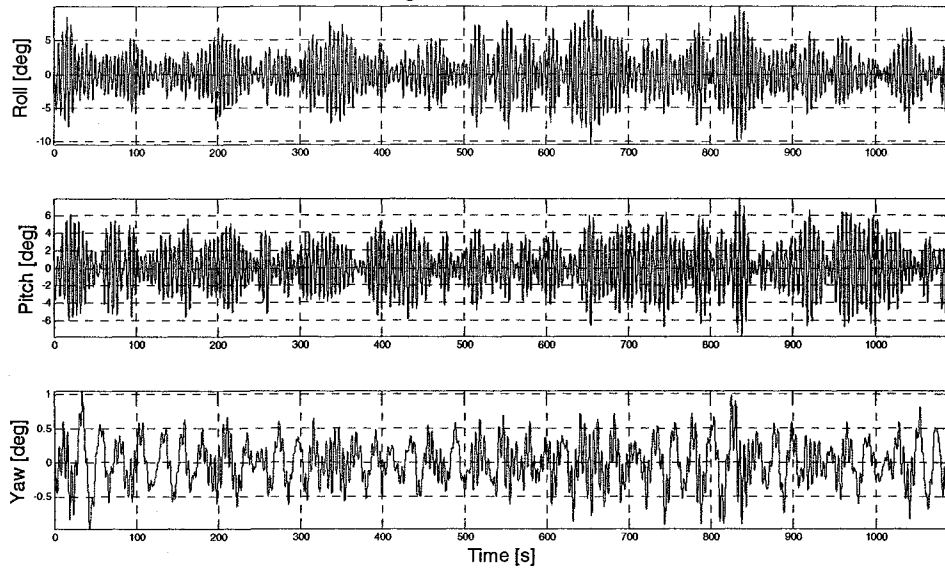
Wave Rider Translations: 03-12-2008 at 10 UTC



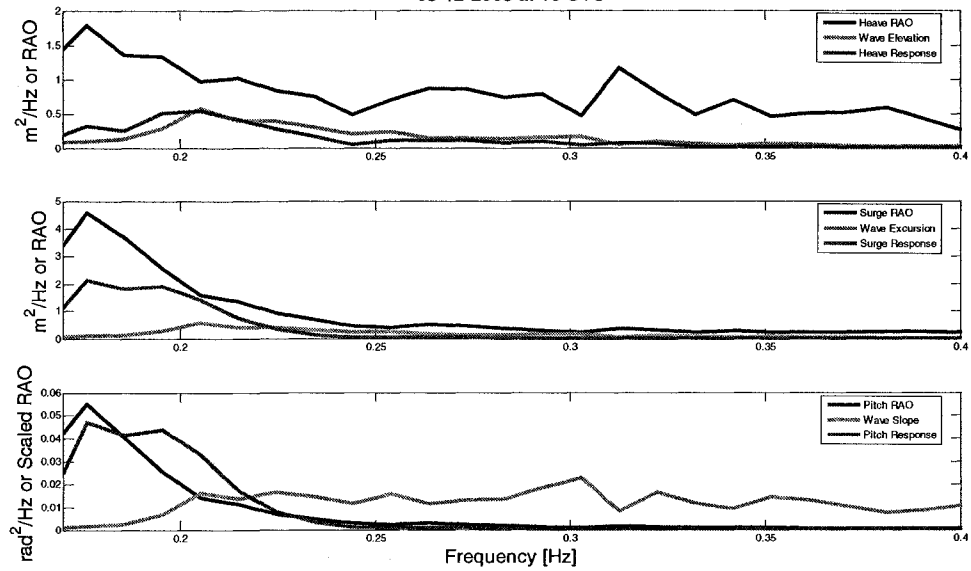
Motion Package Translations: 03-12-2008 at 10 UTC

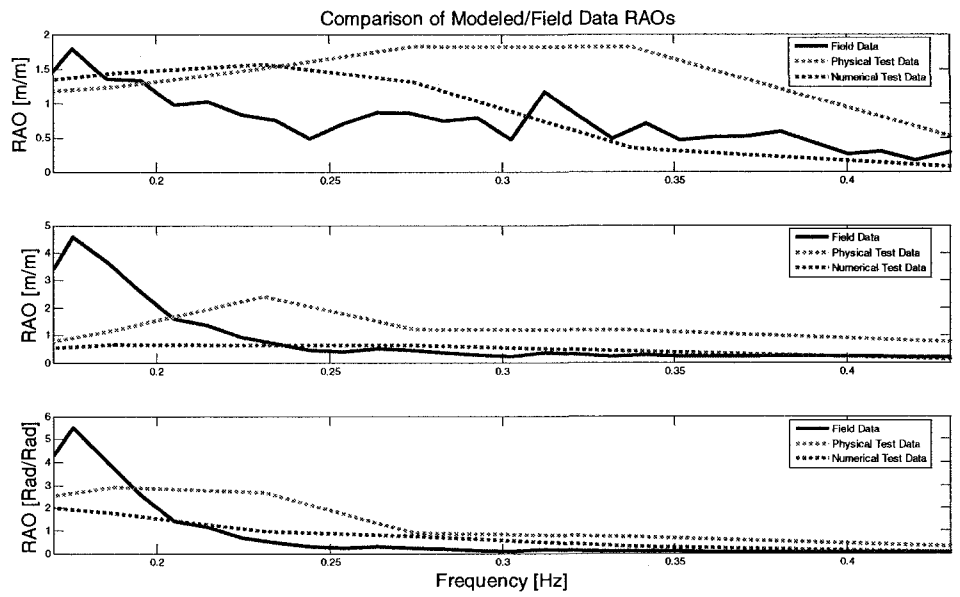
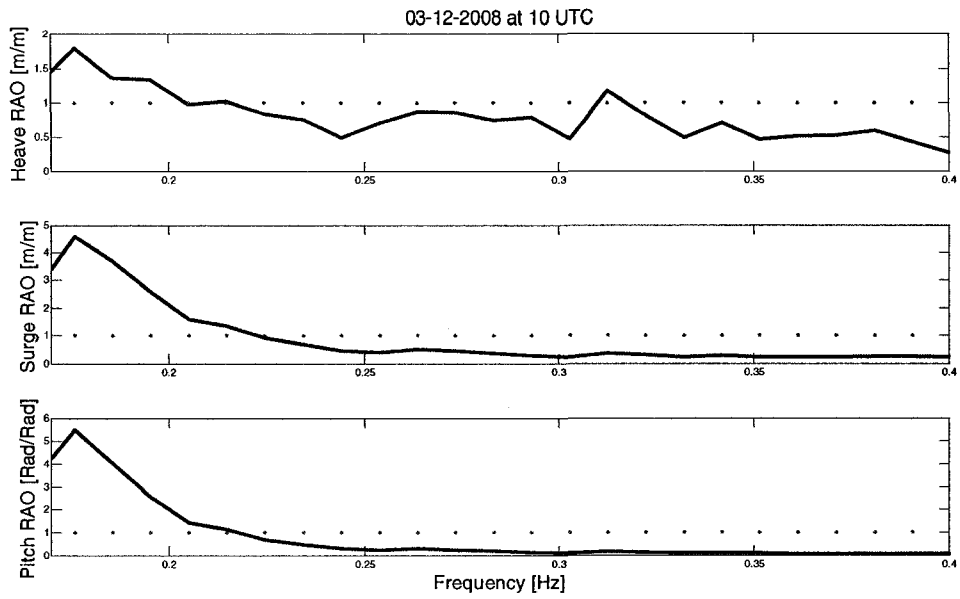


Motion Package Rotations: 03-12-2008 at 10 UTC



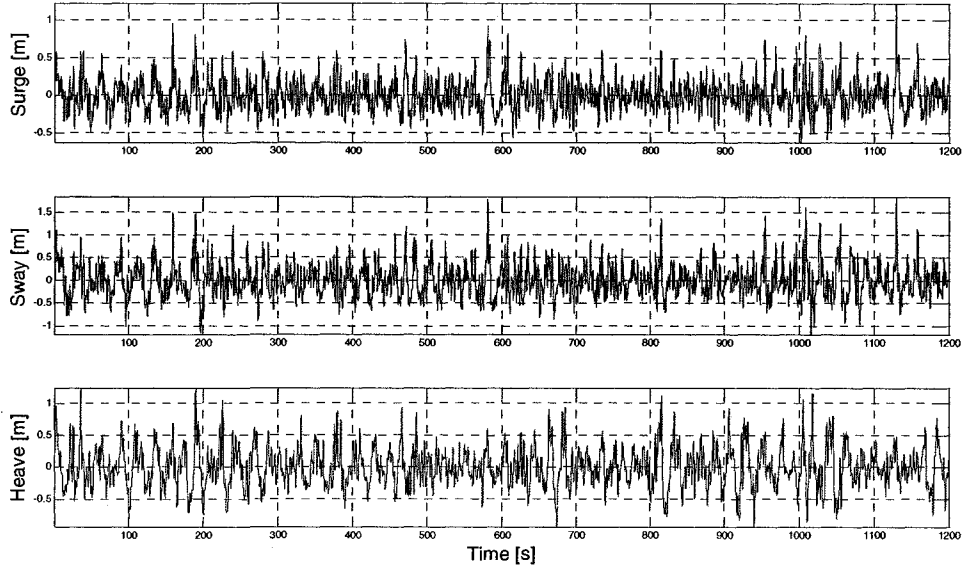
03-12-2008 at 10 UTC



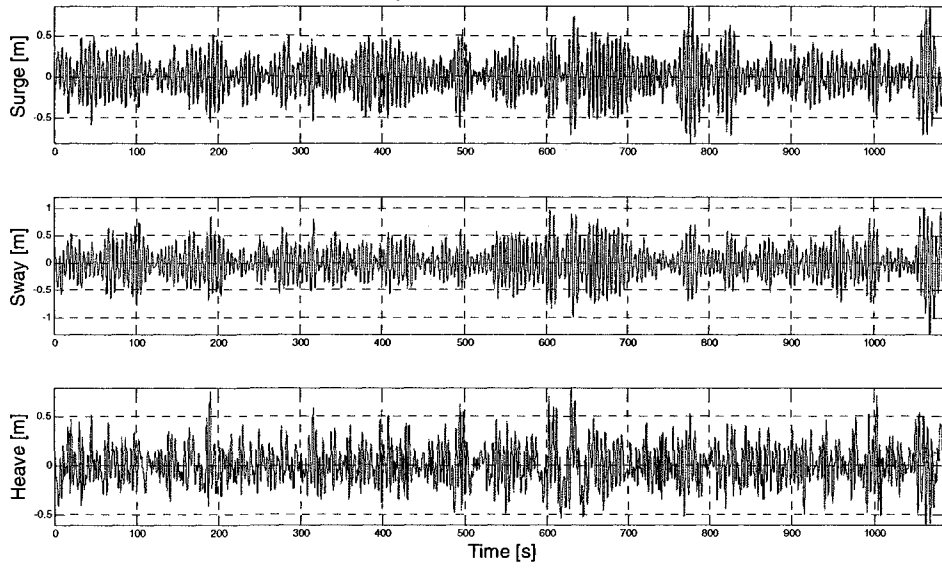


3/12/2008 at 12:00:00 UTC

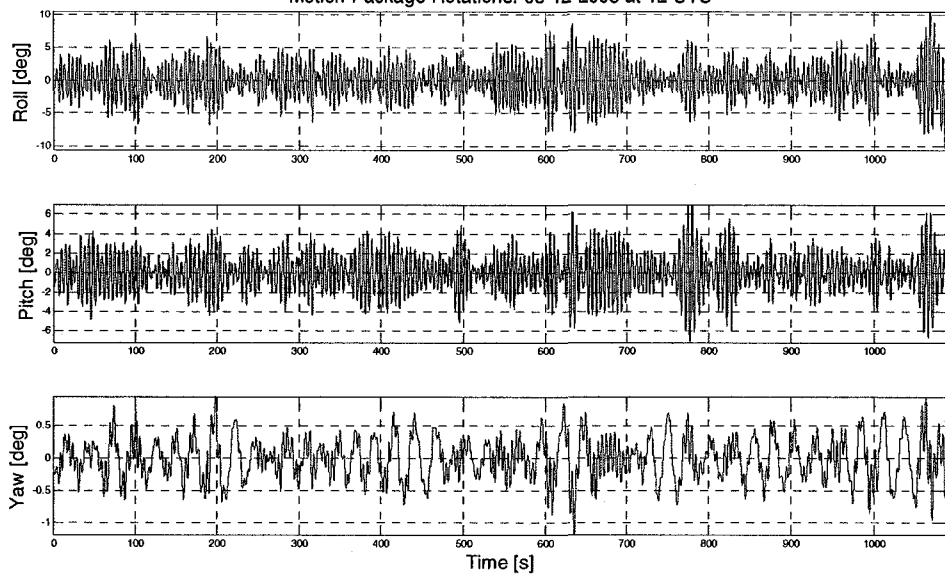
Wave Rider Translations: 03-12-2008 at 12 UTC



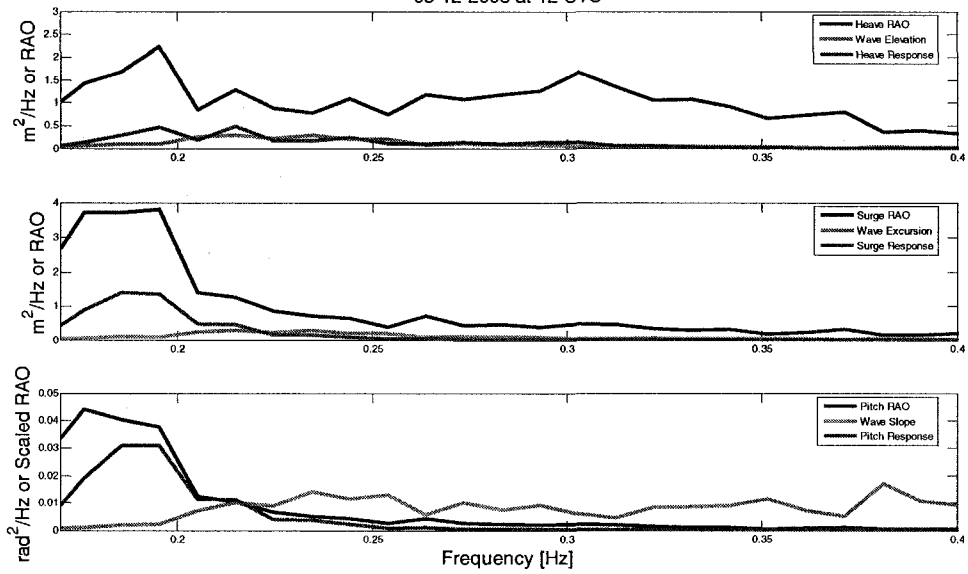
Motion Package Translations: 03-12-2008 at 12 UTC

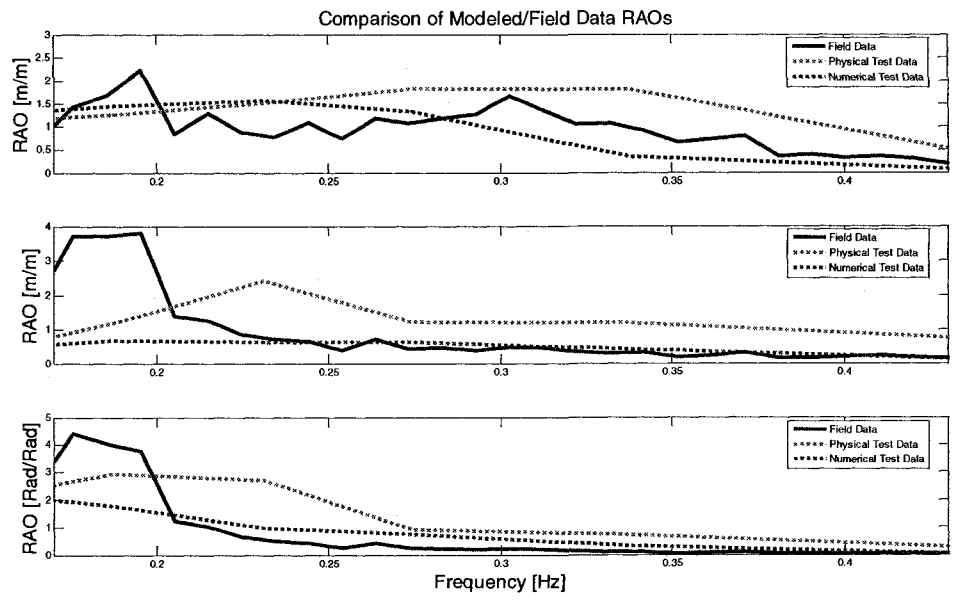
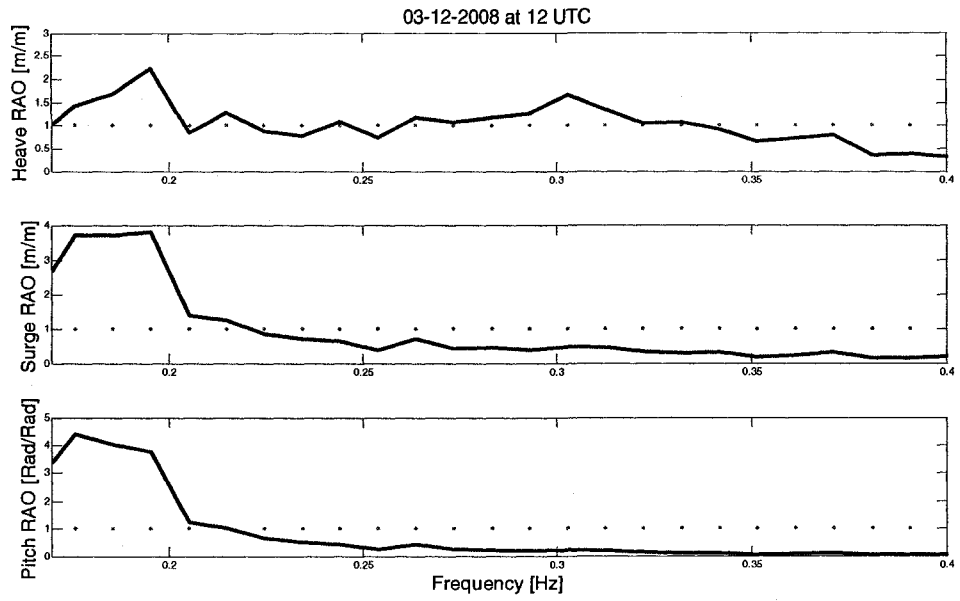


Motion Package Rotations: 03-12-2008 at 12 UTC



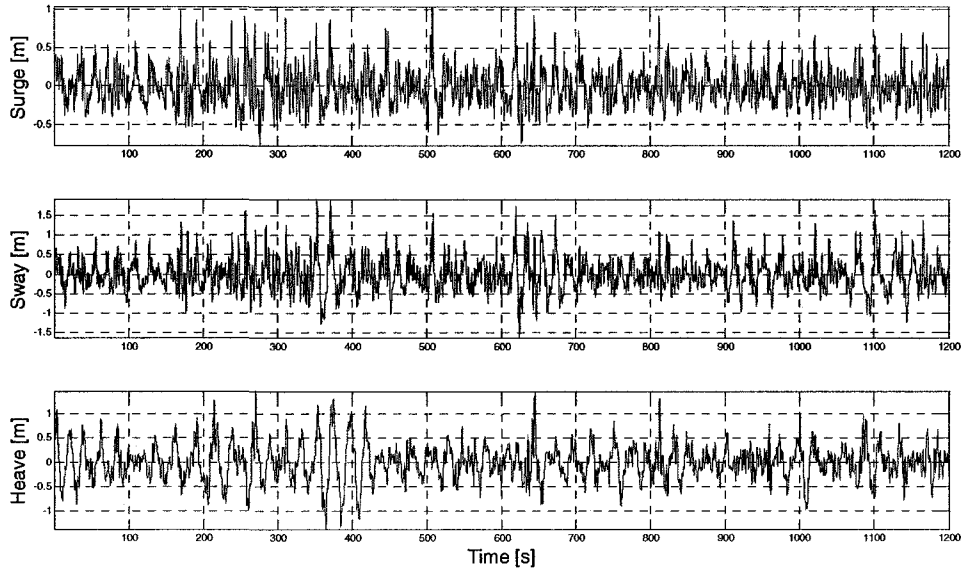
03-12-2008 at 12 UTC



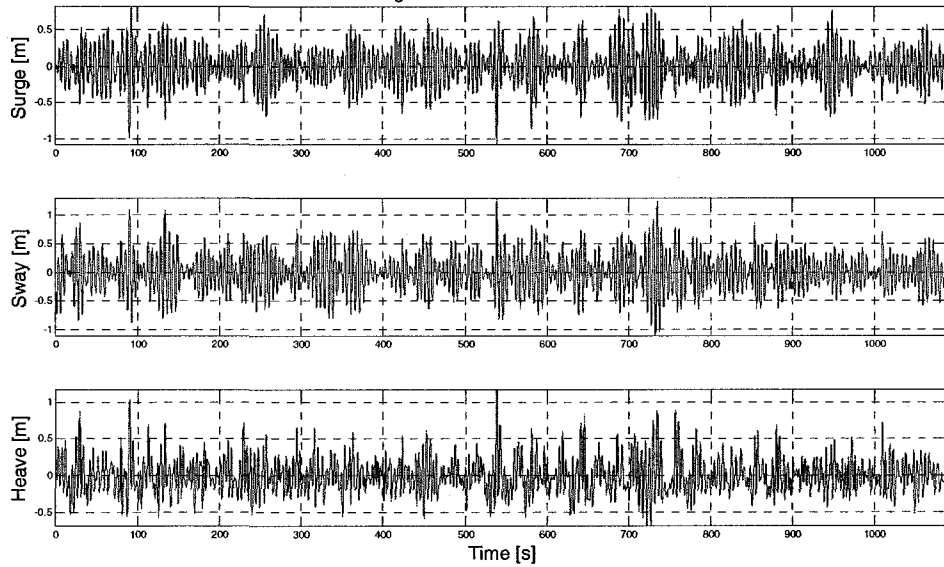


3/12/2008 at 14:00:00 UTC

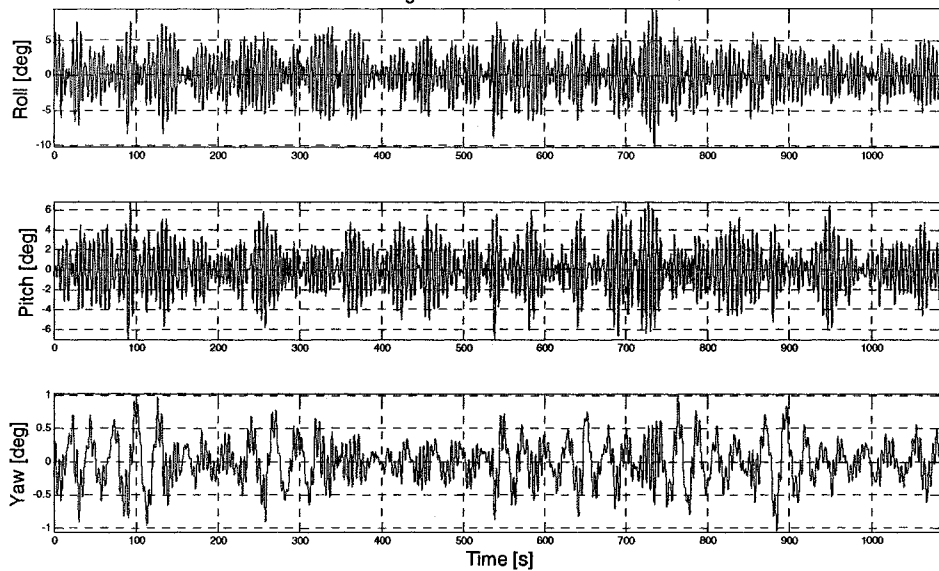
Wave Rider Translations: 03-12-2008 at 14 UTC



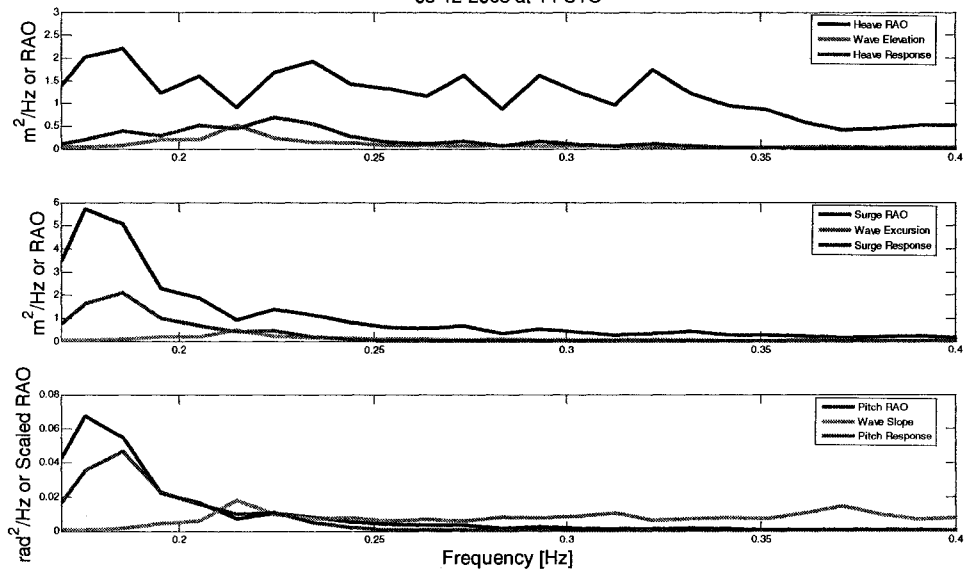
Motion Package Translations: 03-12-2008 at 14 UTC

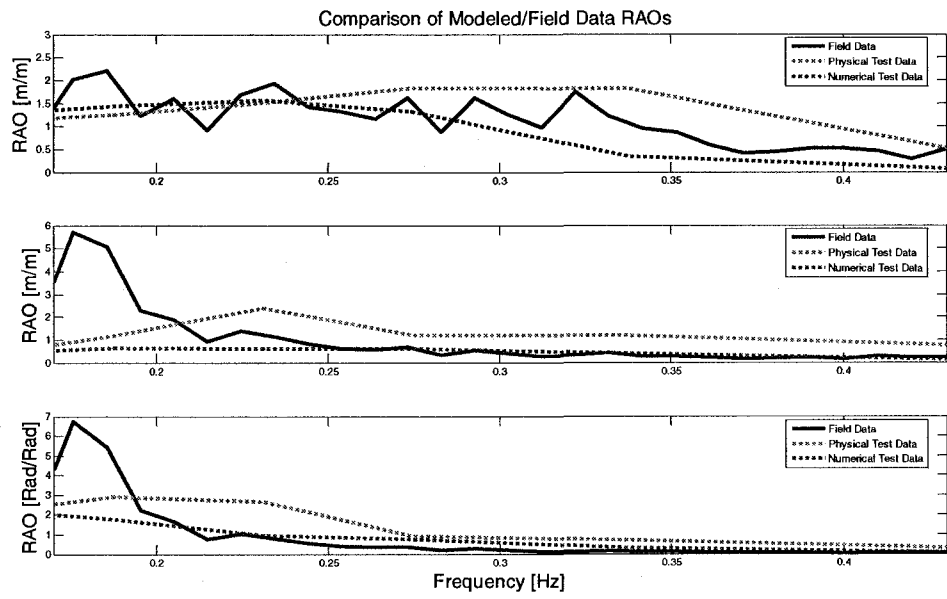
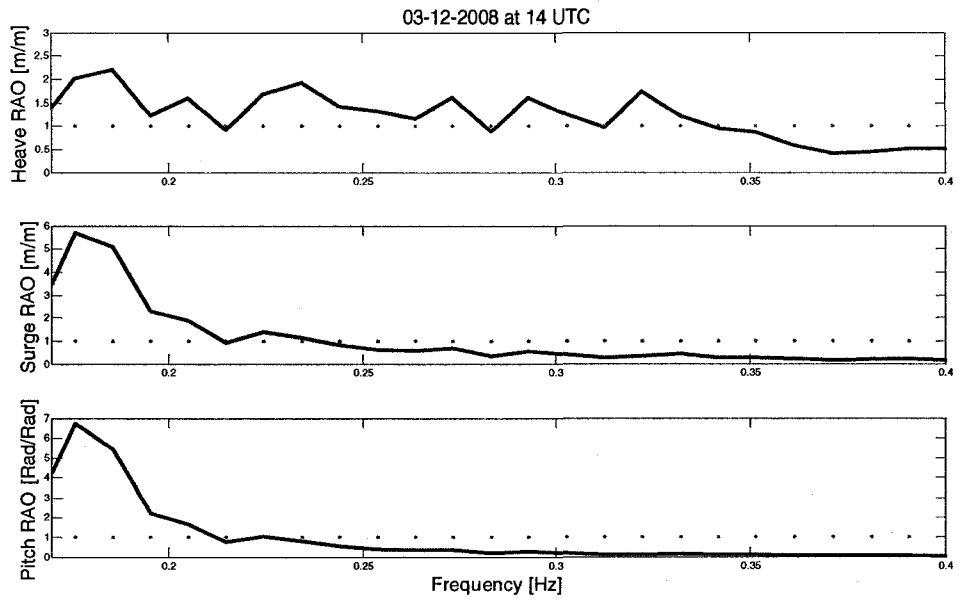


Motion Package Rotations: 03-12-2008 at 14 UTC



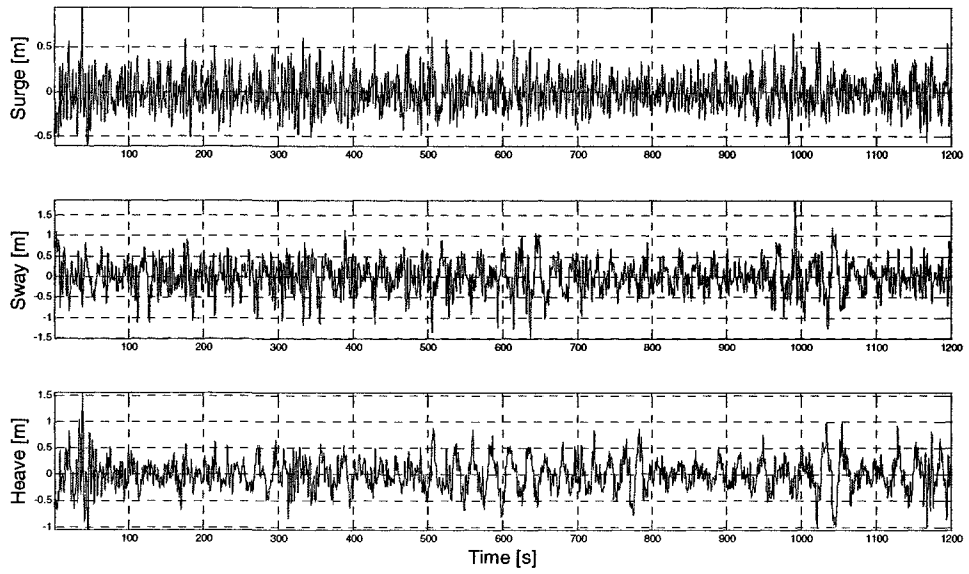
03-12-2008 at 14 UTC



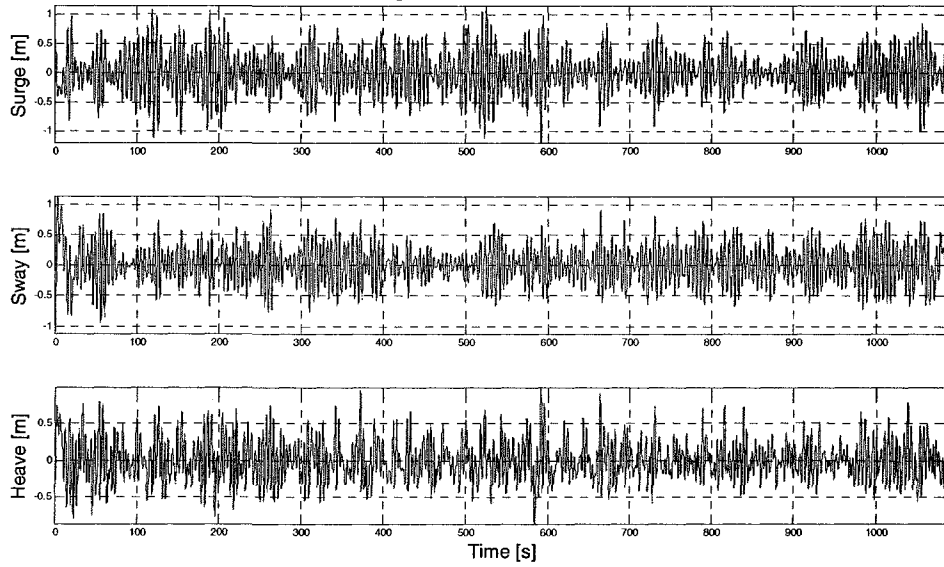


3/12/2008 at 16:00:00 UTC

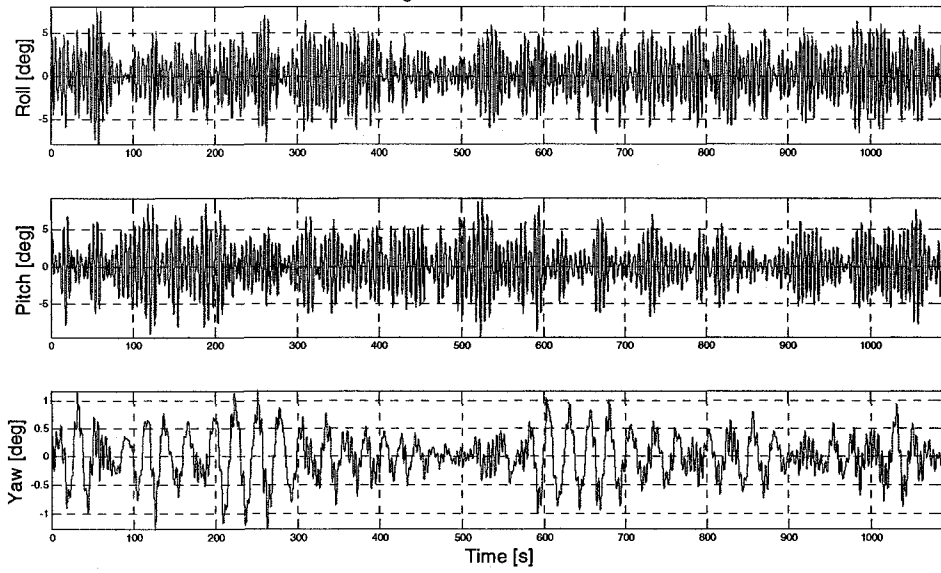
Wave Rider Translations: 03-12-2008 at 16 UTC



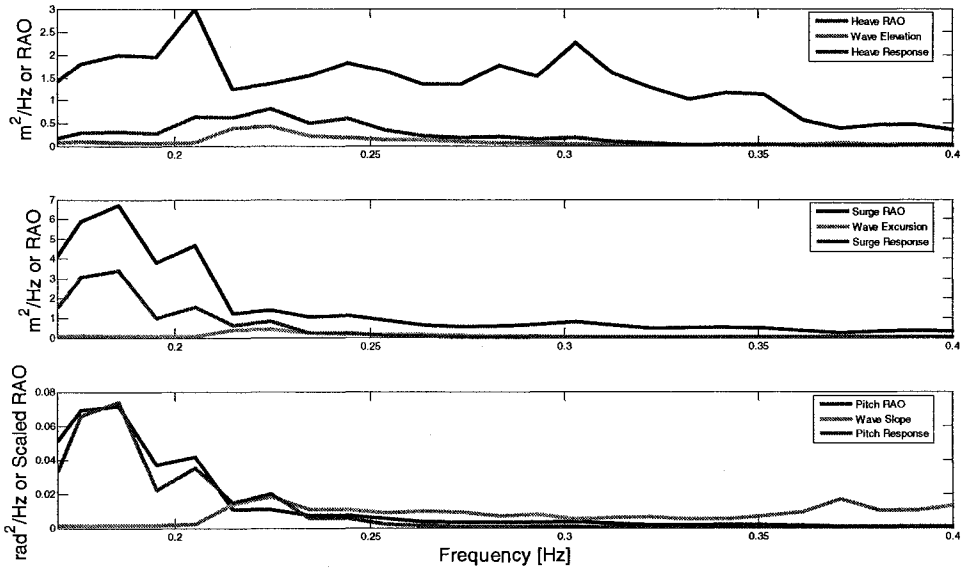
Motion Package Translations: 03-12-2008 at 16 UTC

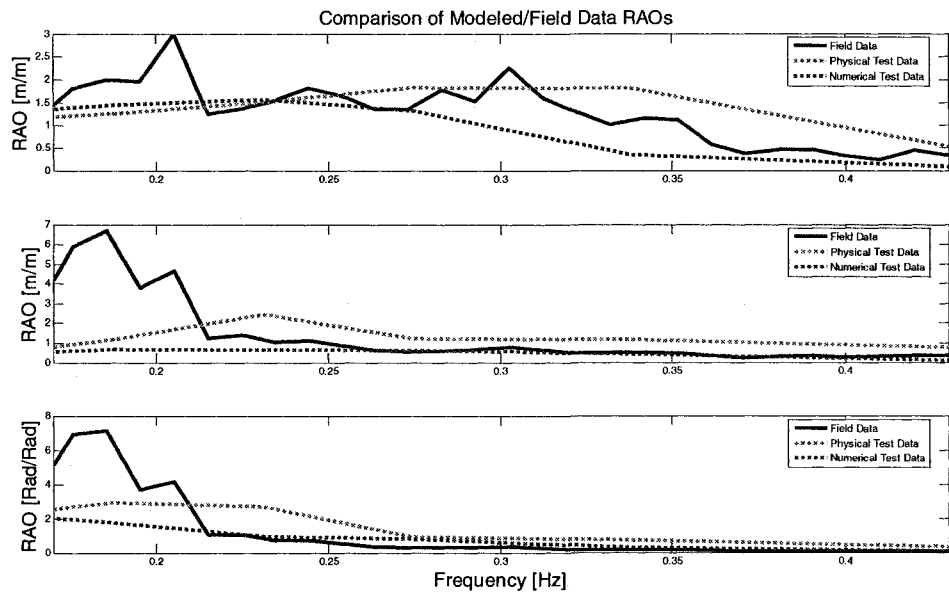
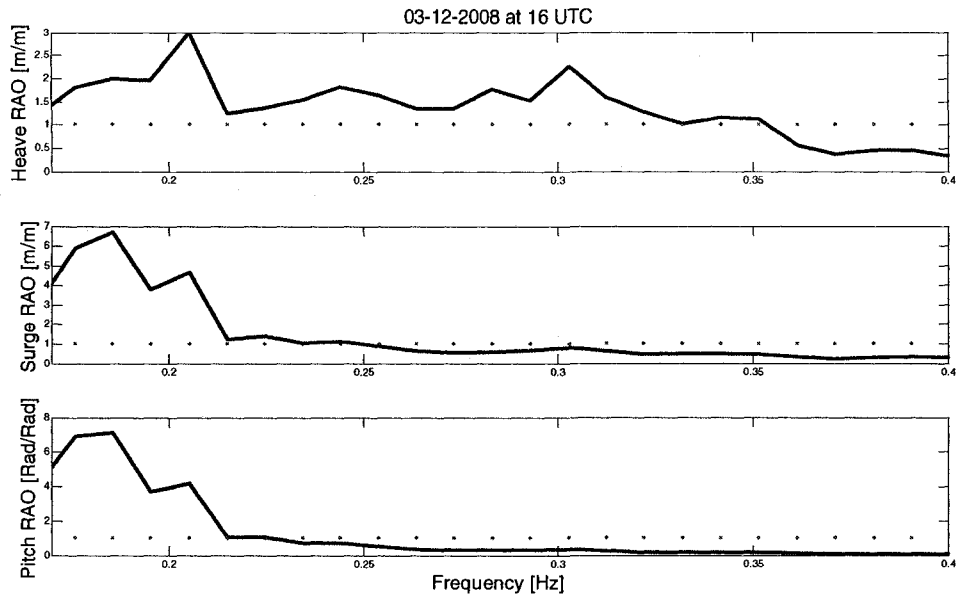


Motion Package Rotations: 03-12-2008 at 16 UTC



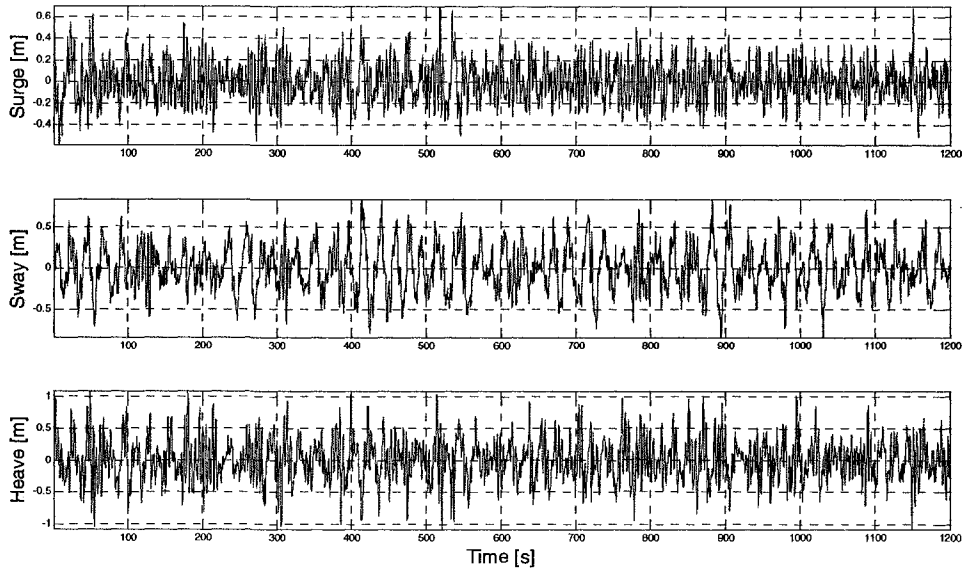
03-12-2008 at 16 UTC



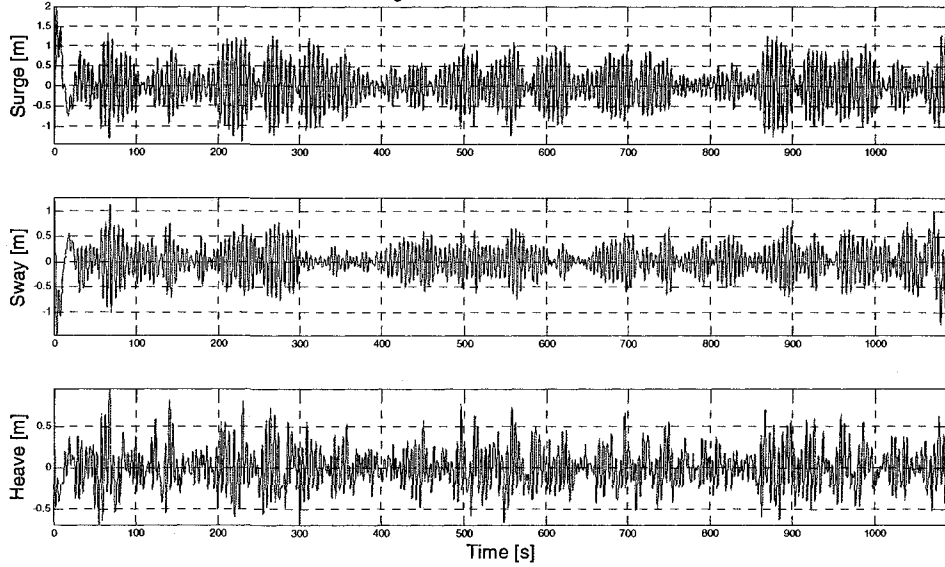


3/12/2008 at 18:00:00 UTC

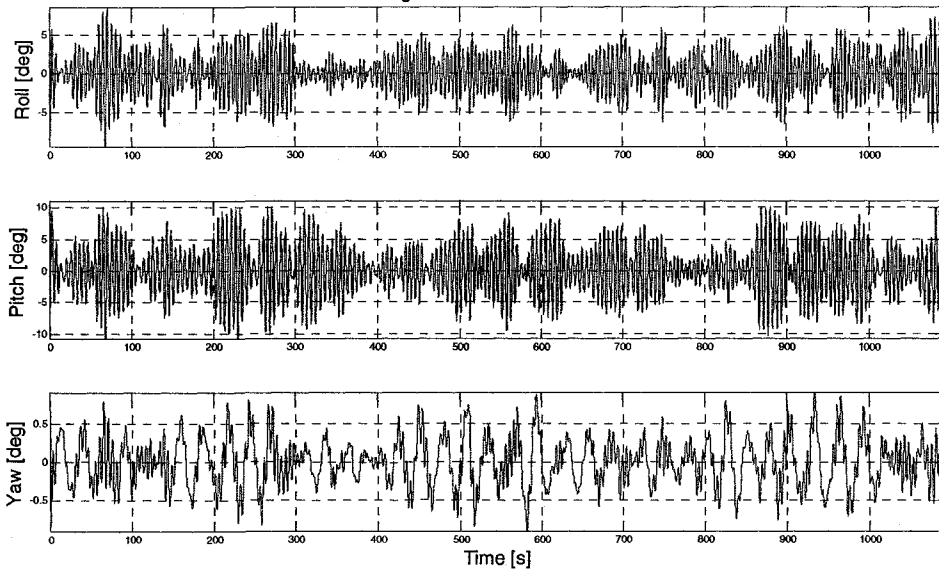
Wave Rider Translations: 03-12-2008 at 18 UTC



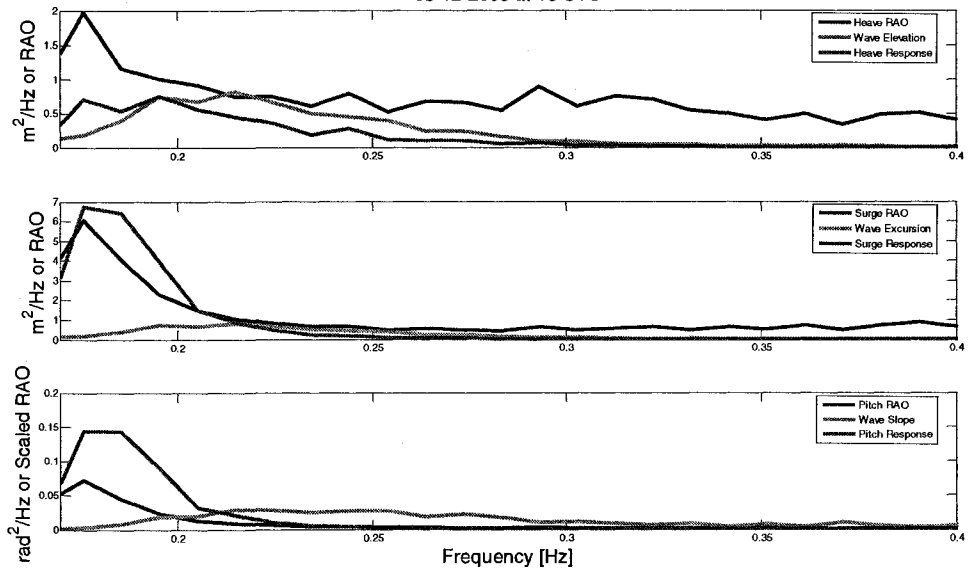
Motion Package Translations: 03-12-2008 at 18 UTC

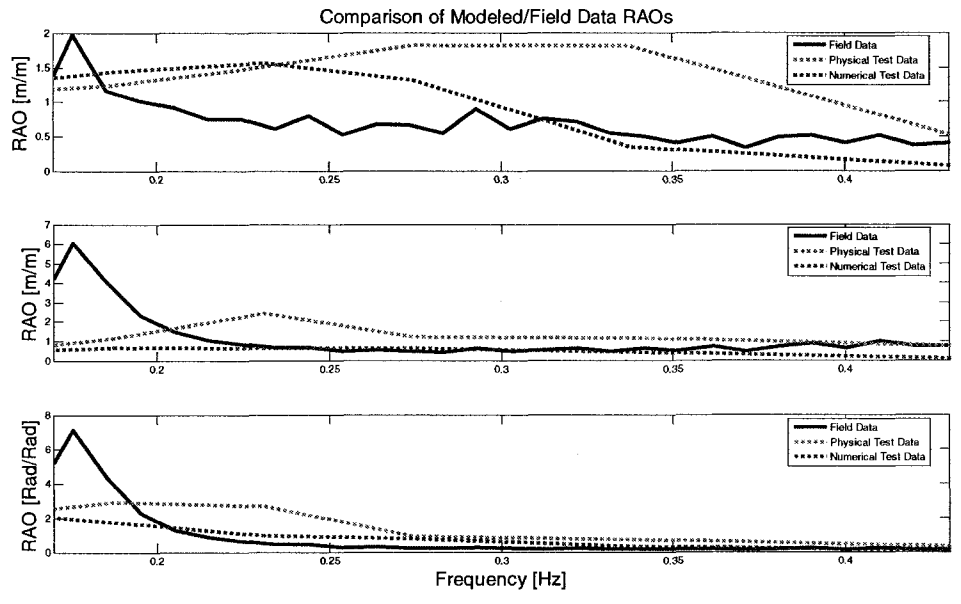
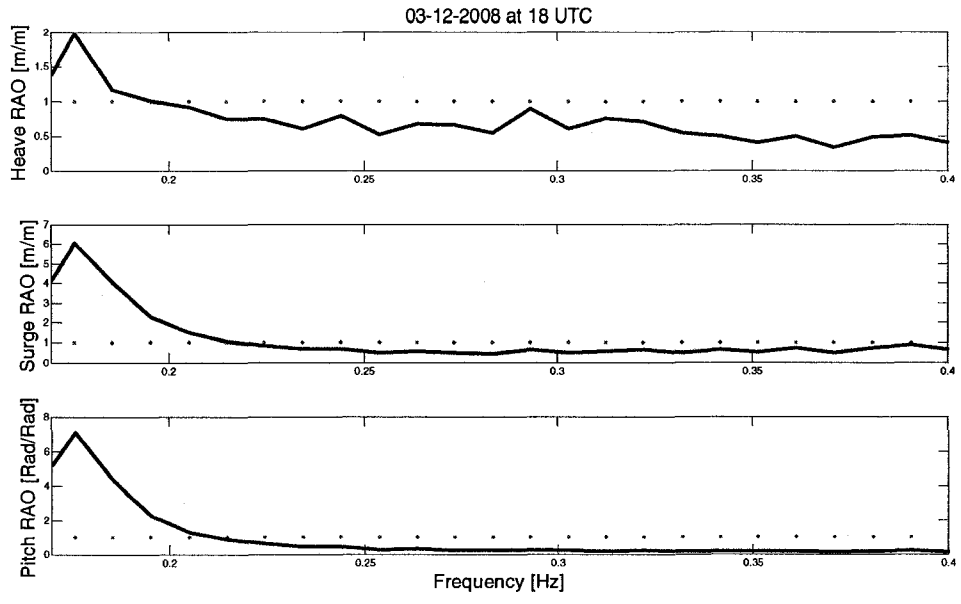


Motion Package Rotations: 03-12-2008 at 18 UTC



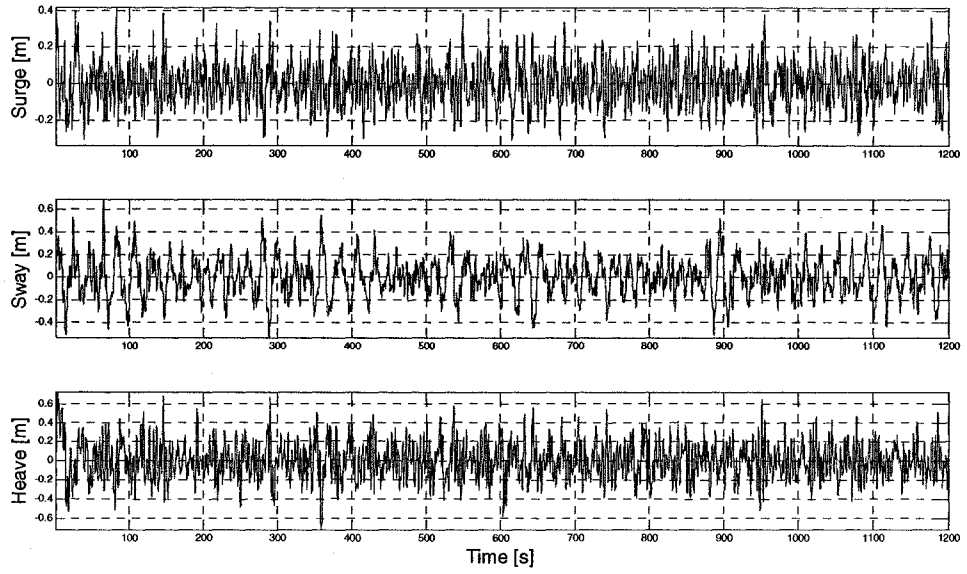
03-12-2008 at 18 UTC



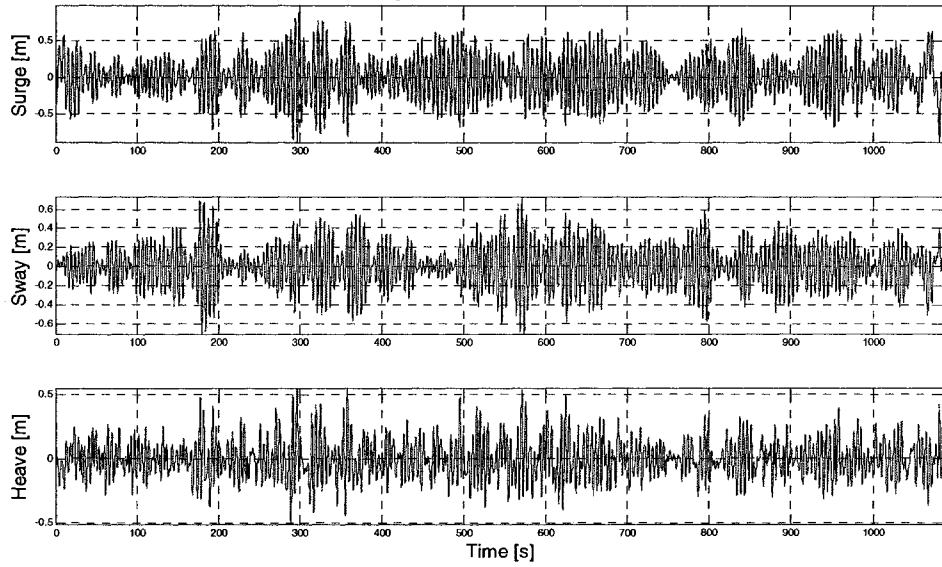


3/12/2008 at 20:00:00 UTC

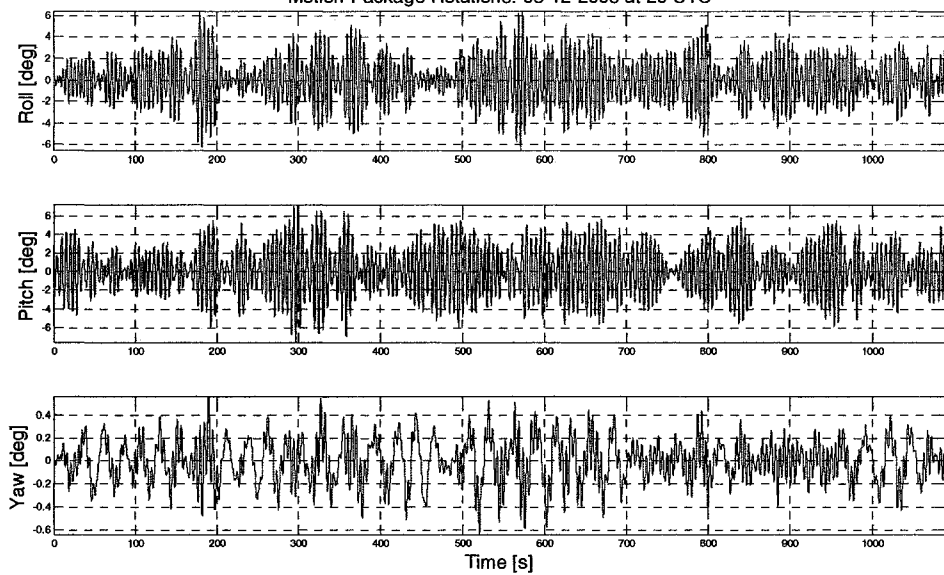
Wave Rider Translations: 03-12-2008 at 20 UTC



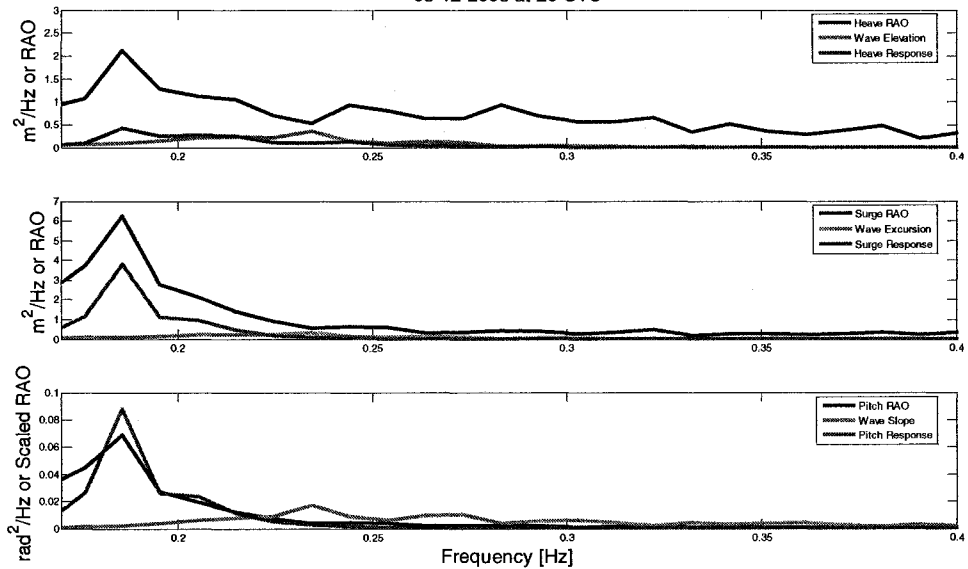
Motion Package Translations: 03-12-2008 at 20 UTC



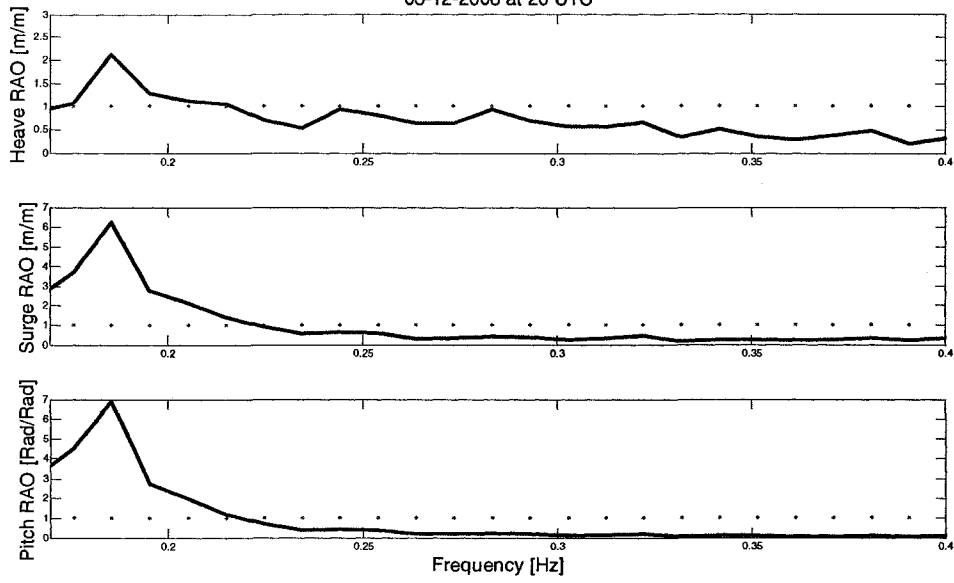
Motion Package Rotations: 03-12-2008 at 20 UTC



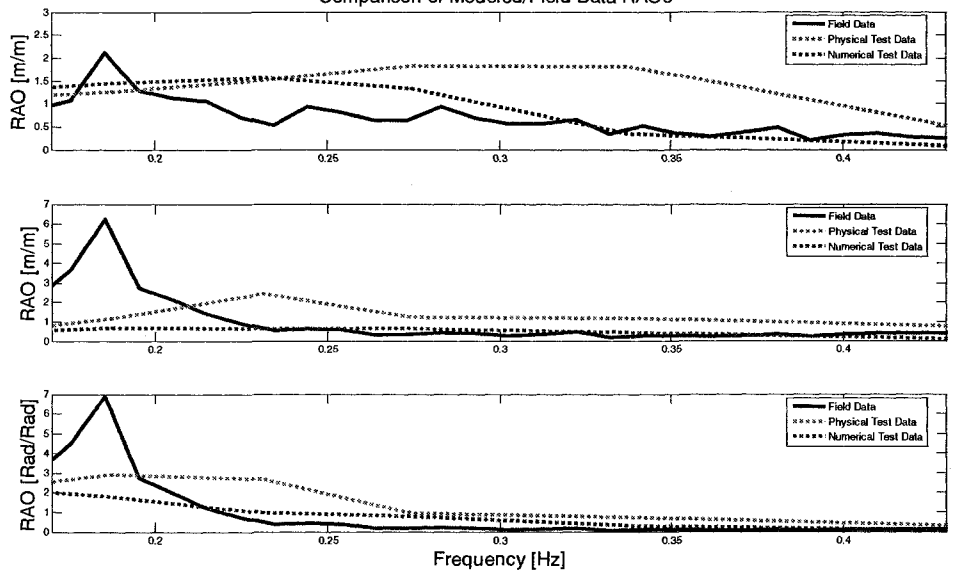
03-12-2008 at 20 UTC



03-12-2008 at 20 UTC

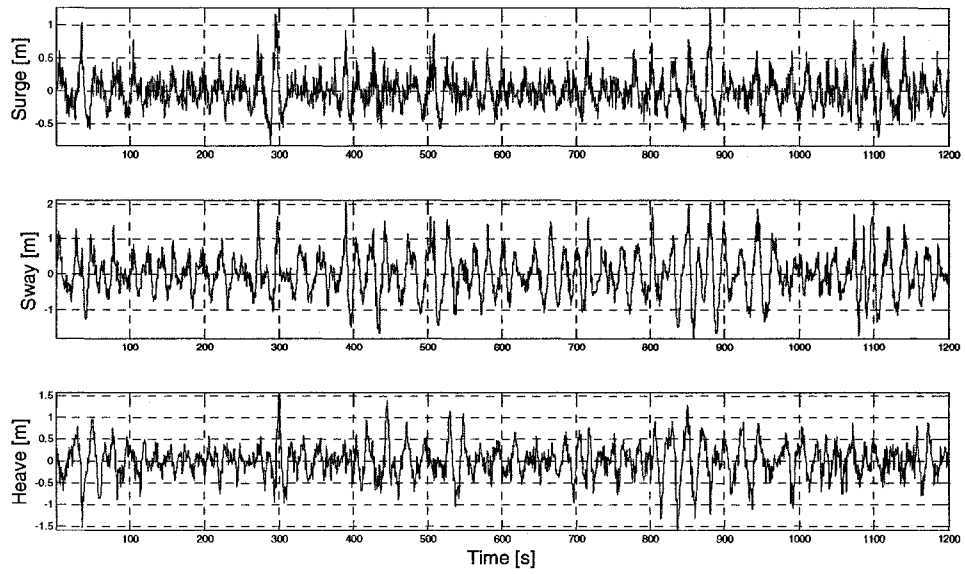


Comparison of Modeled/Field Data RAOs

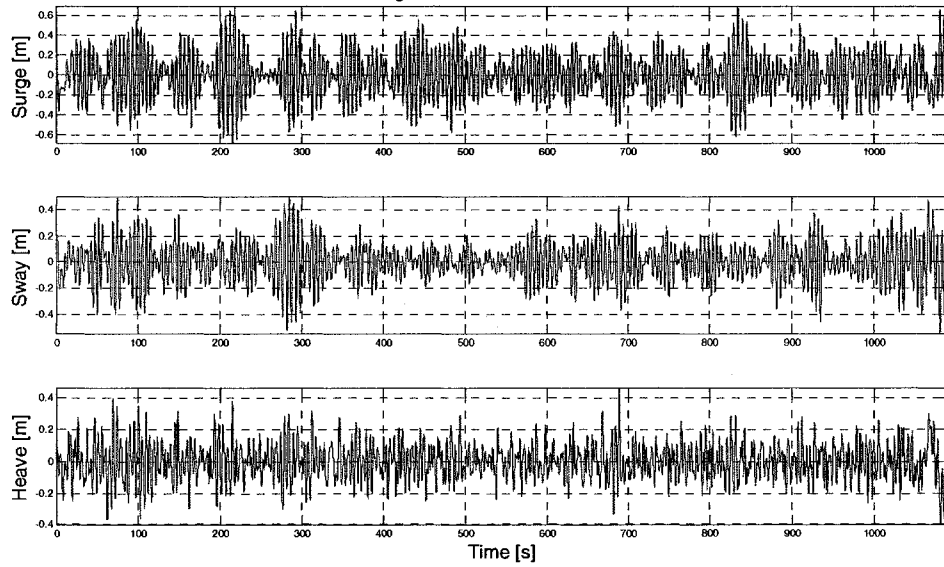


3/12/2008 at 22:00:00 UTC

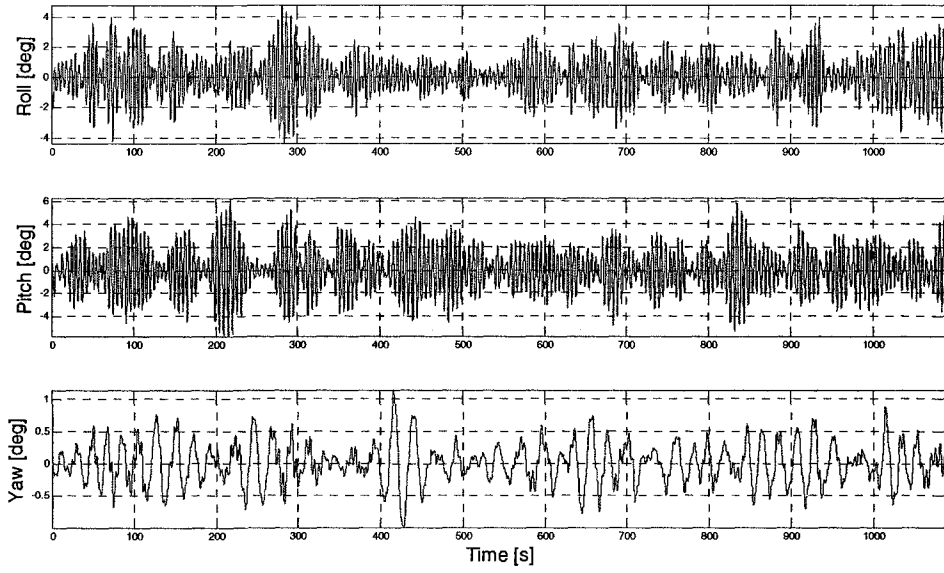
Wave Rider Translations: 03-12-2008 at 22 UTC



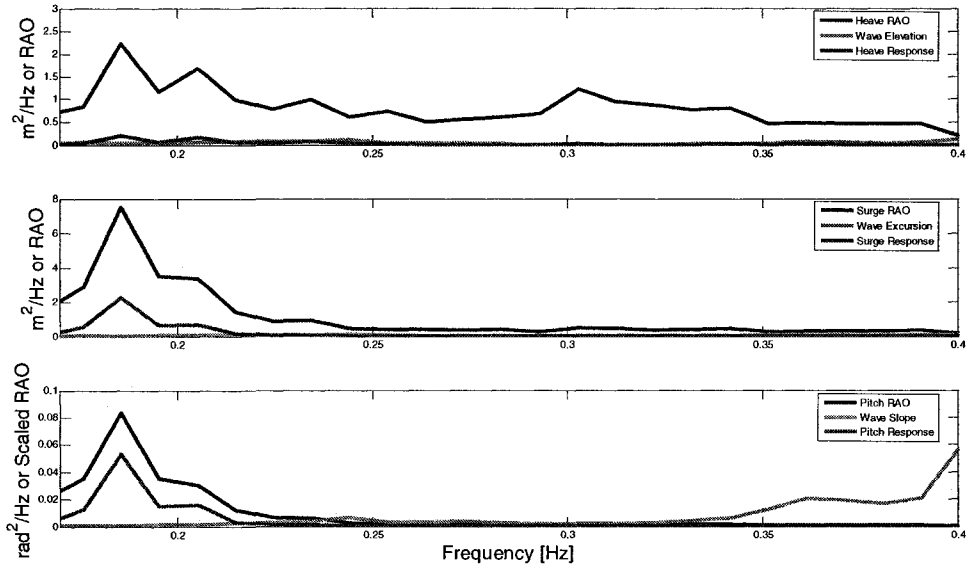
Motion Package Translations: 03-12-2008 at 22 UTC

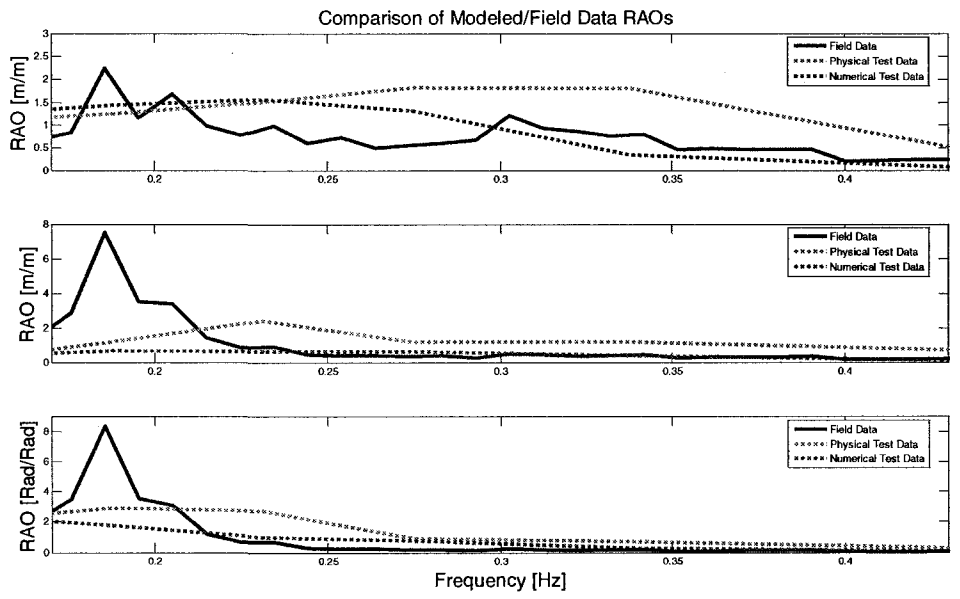
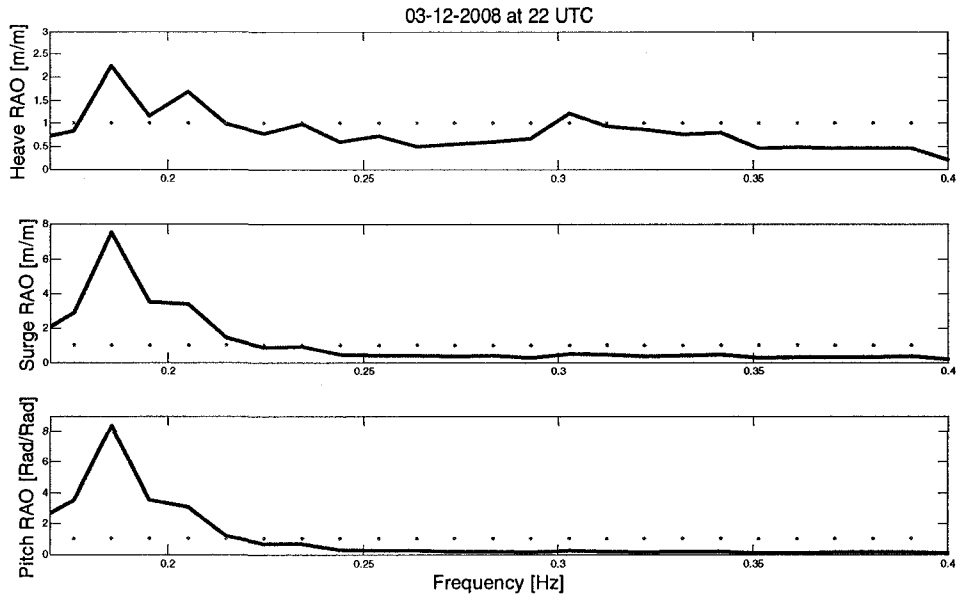


Motion Package Rotations: 03-12-2008 at 22 UTC



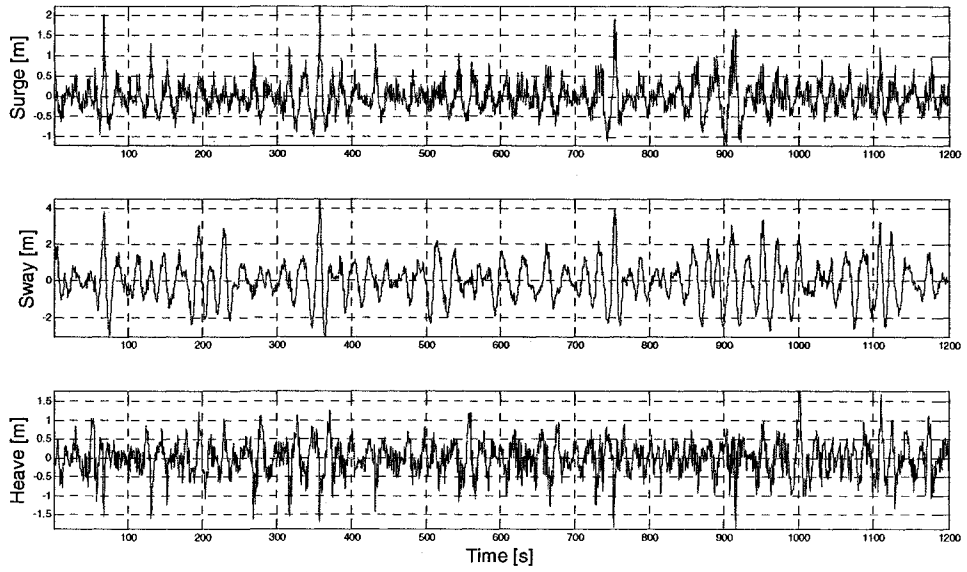
03-12-2008 at 22 UTC



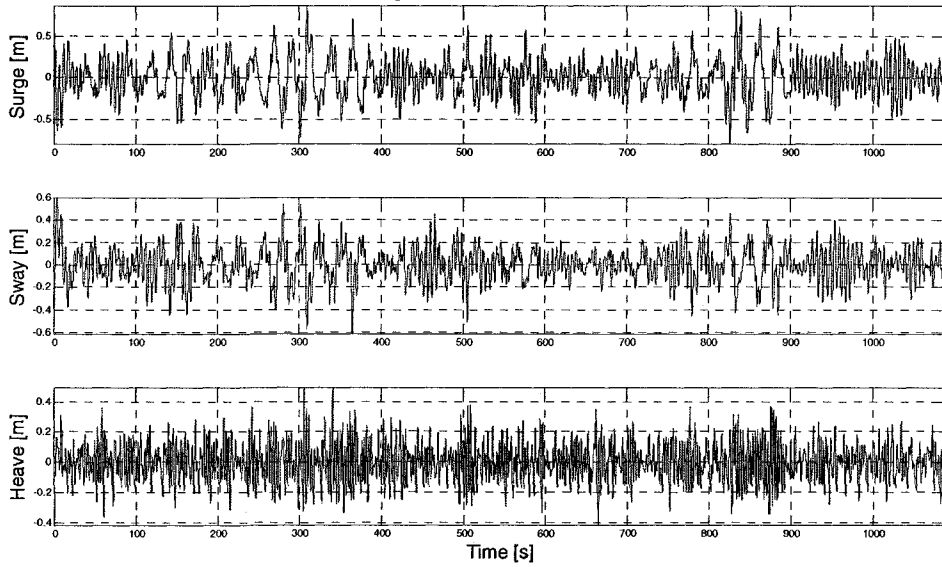


3/13/2008 at 0:00:00 UTC

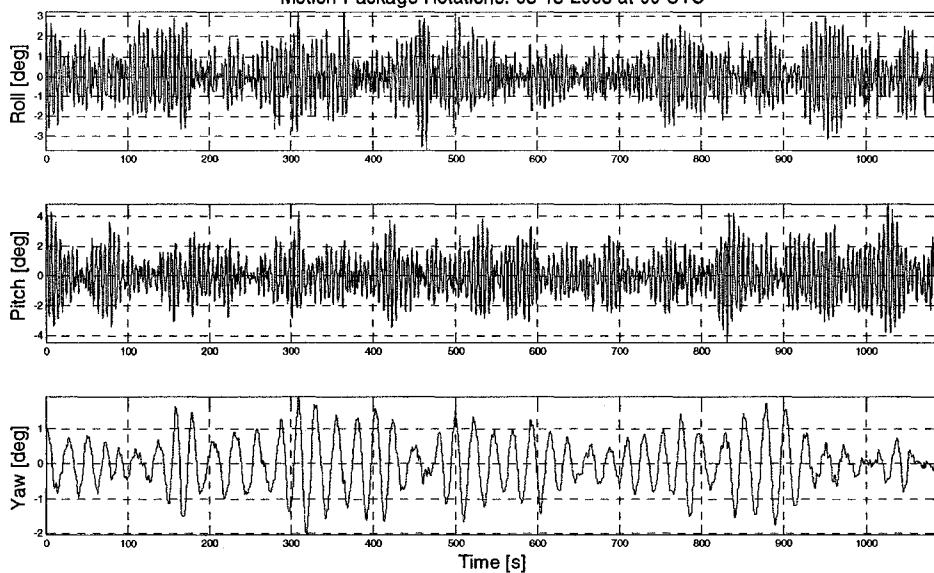
Wave Rider Translations: 03-13-2008 at 00 UTC



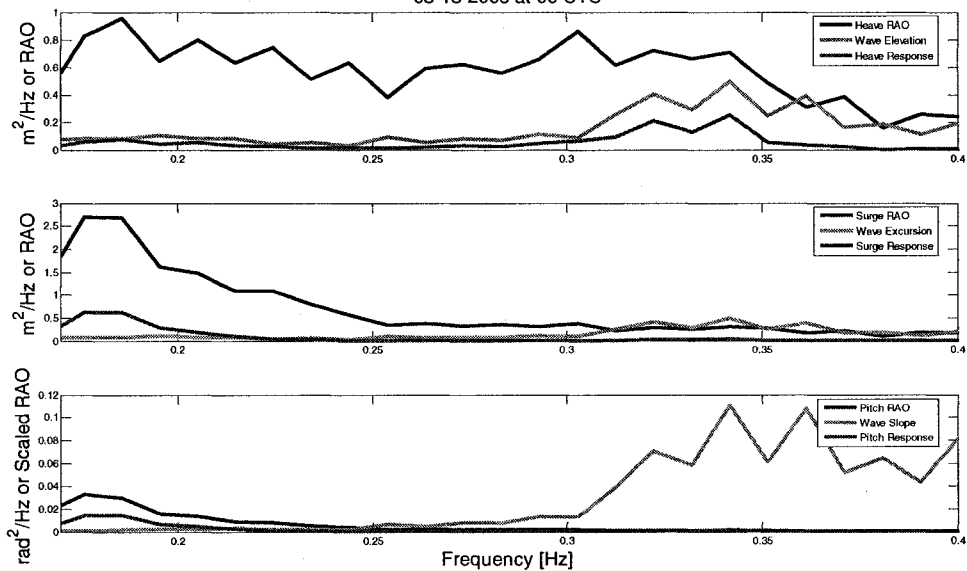
Motion Package Translations: 03-13-2008 at 00 UTC

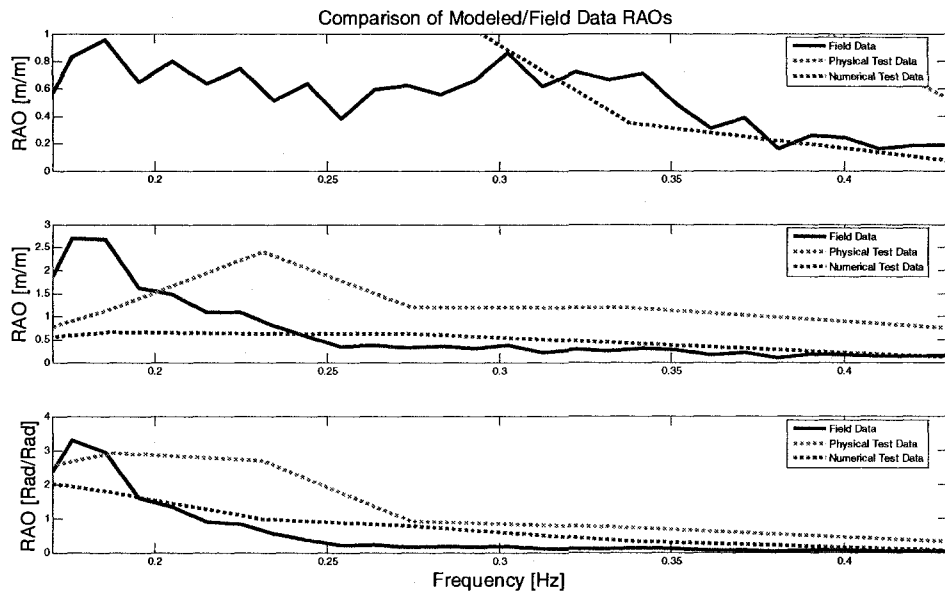
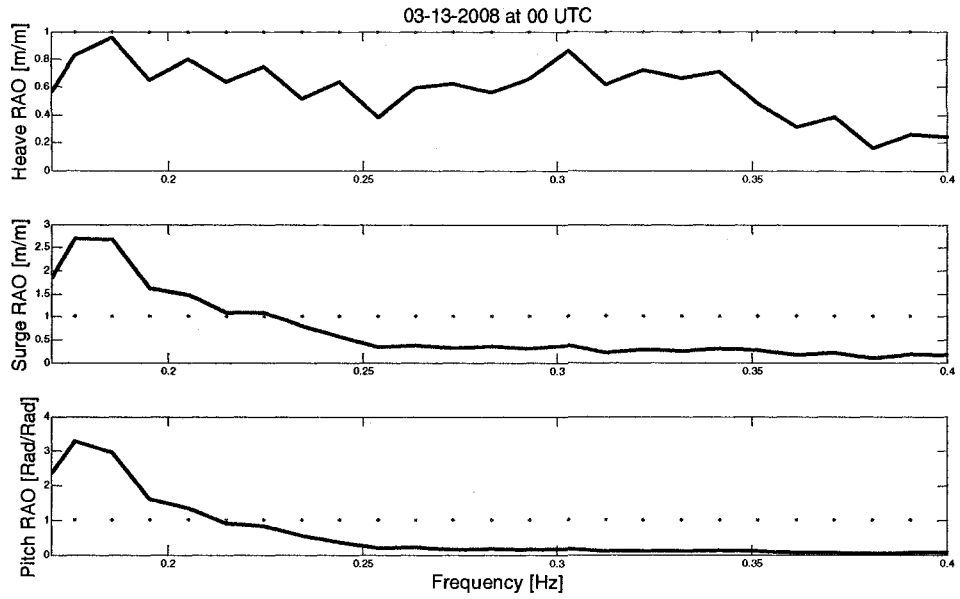


Motion Package Rotations: 03-13-2008 at 00 UTC



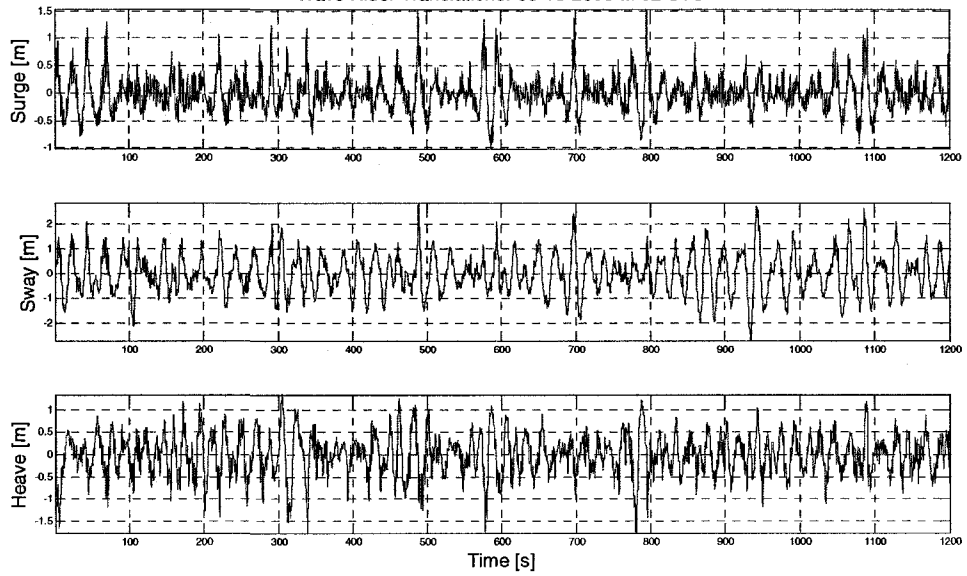
03-13-2008 at 00 UTC



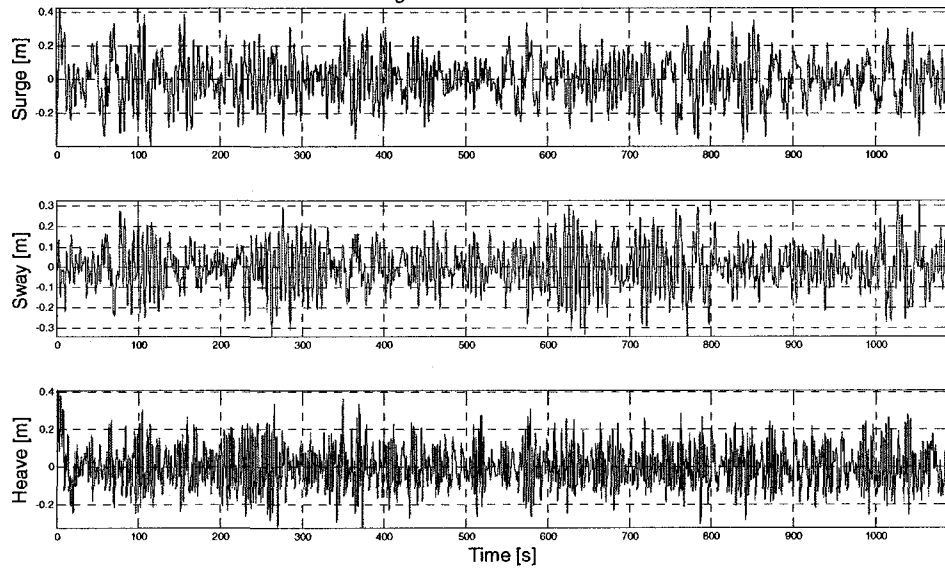


3/13/2008 at 2:00:00 UTC

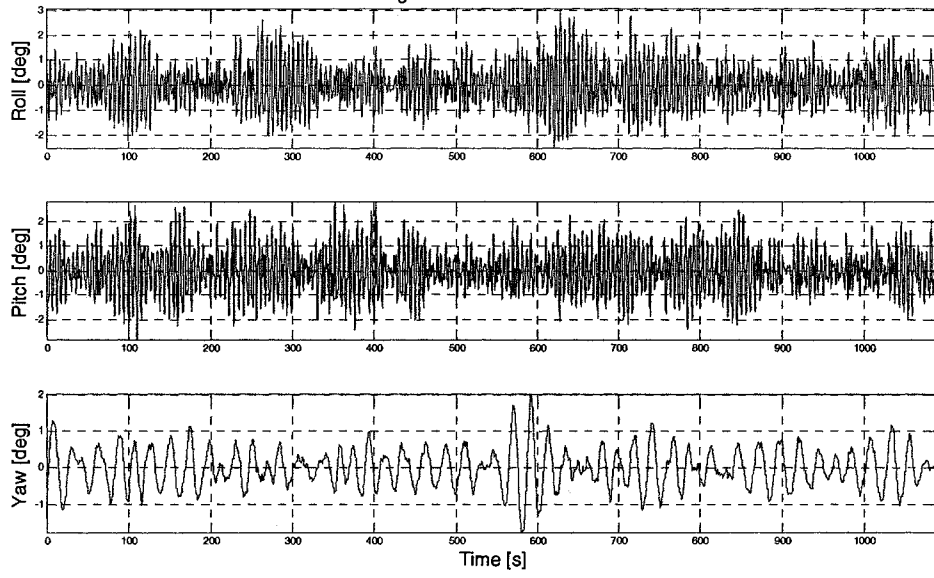
Wave Rider Translations: 03-13-2008 at 02 UTC



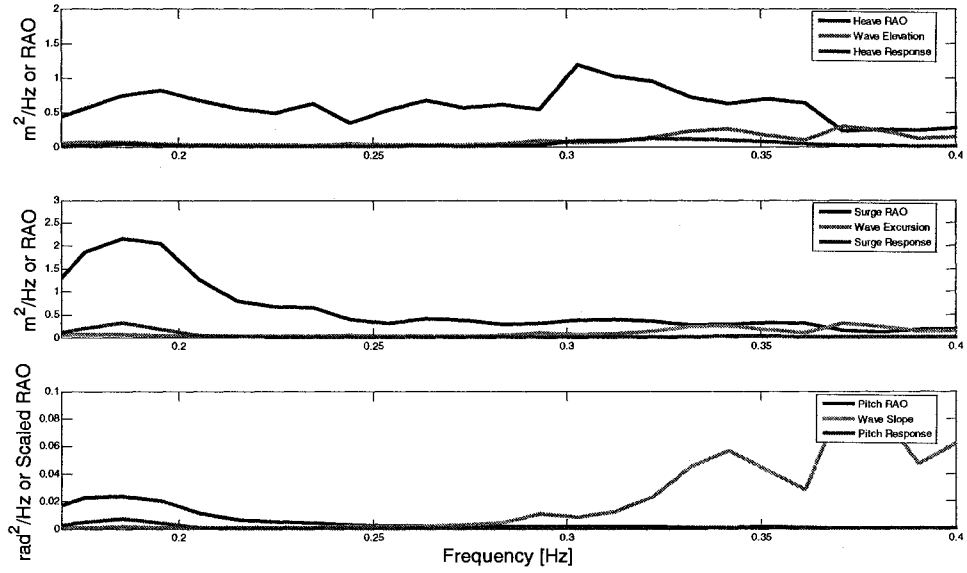
Motion Package Translations: 03-13-2008 at 02 UTC

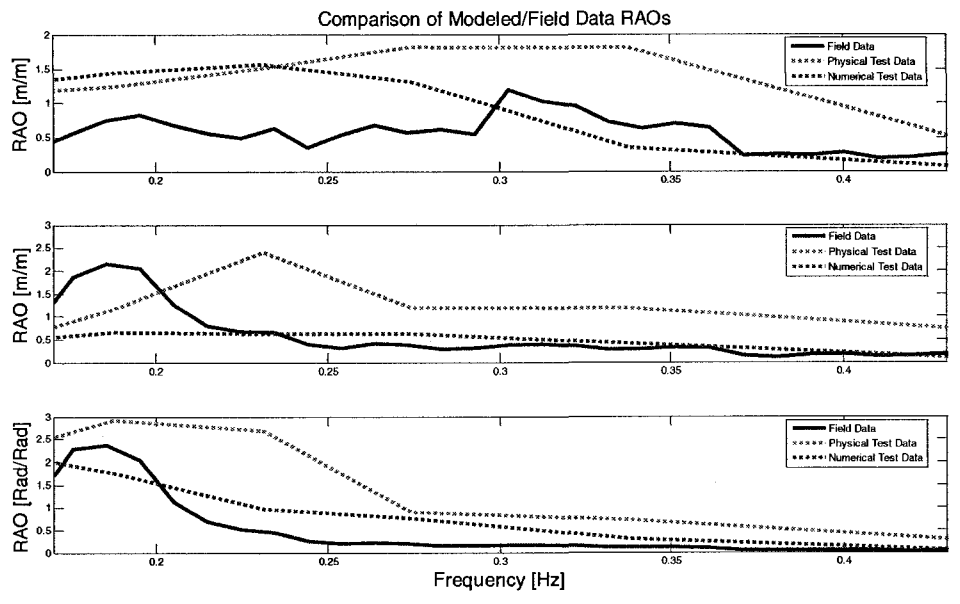
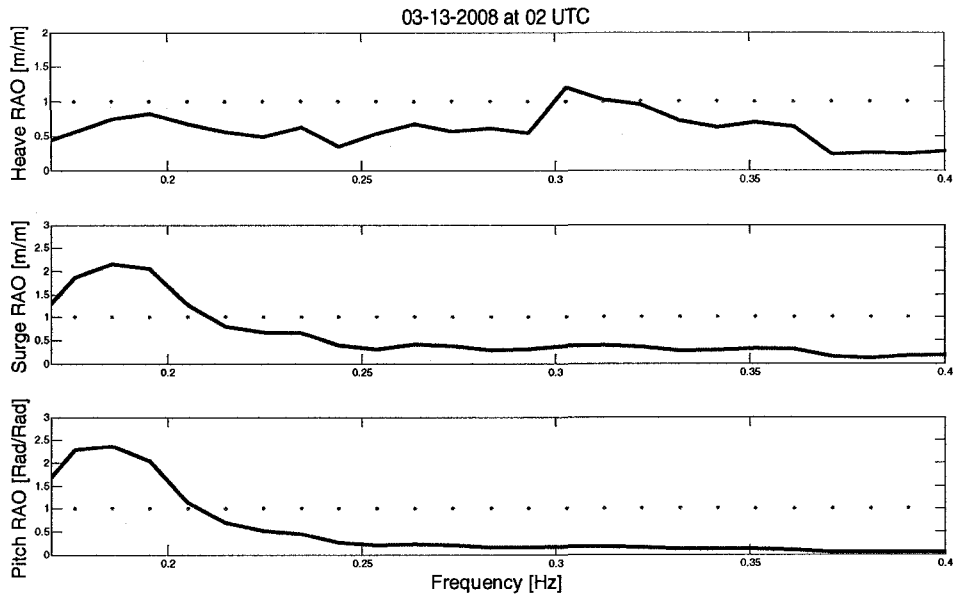


Motion Package Rotations: 03-13-2008 at 02 UTC



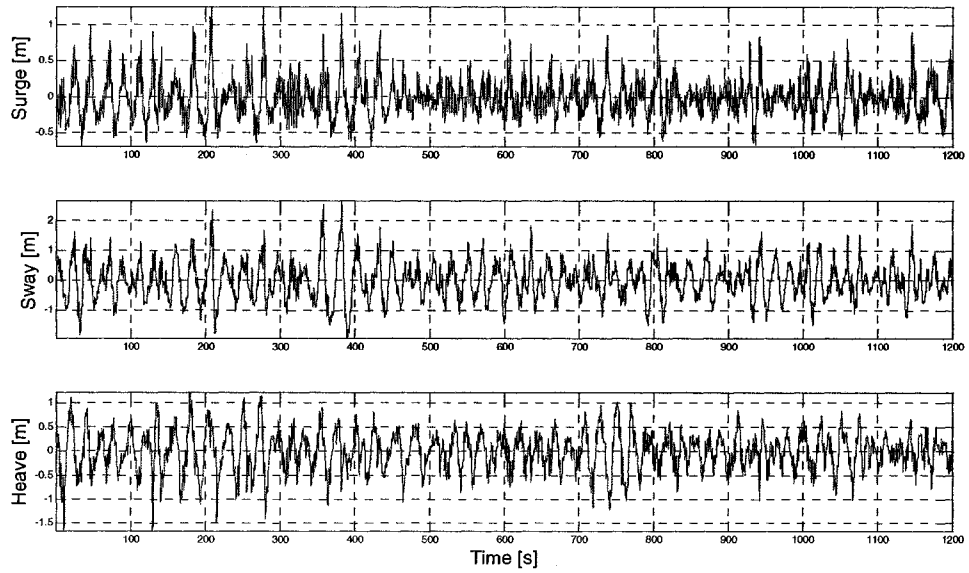
03-13-2008 at 02 UTC



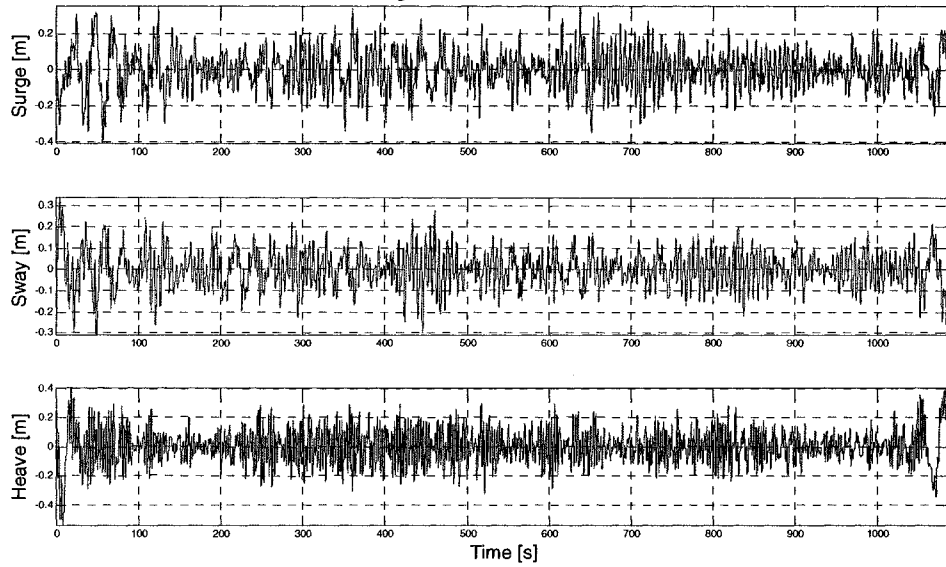


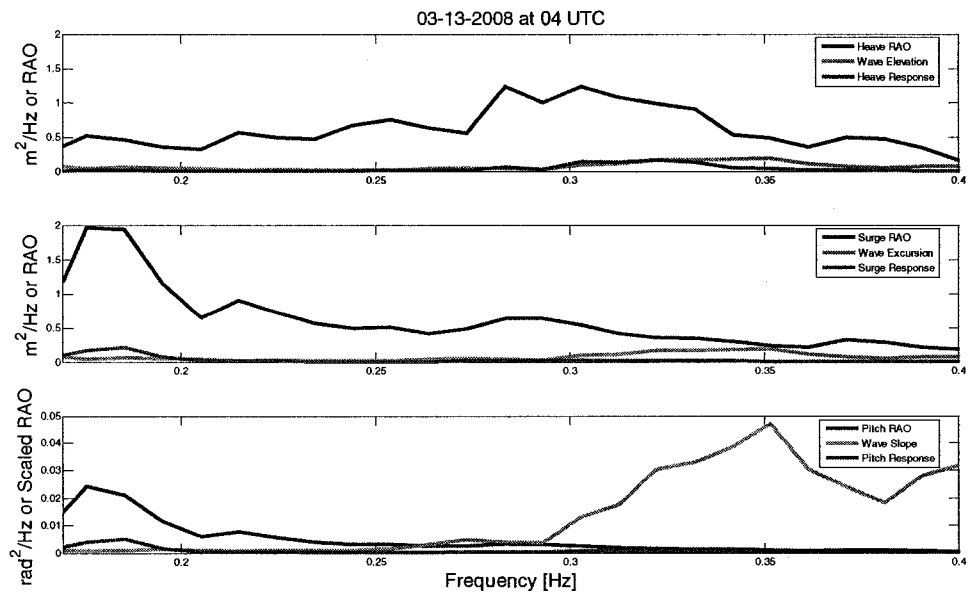
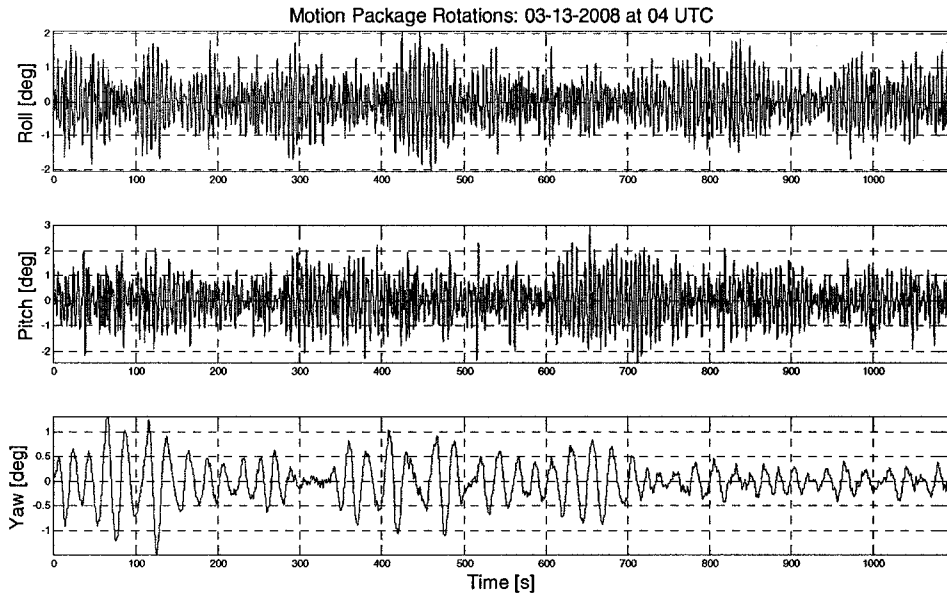
3/13/2008 at 4:00:00 UTC

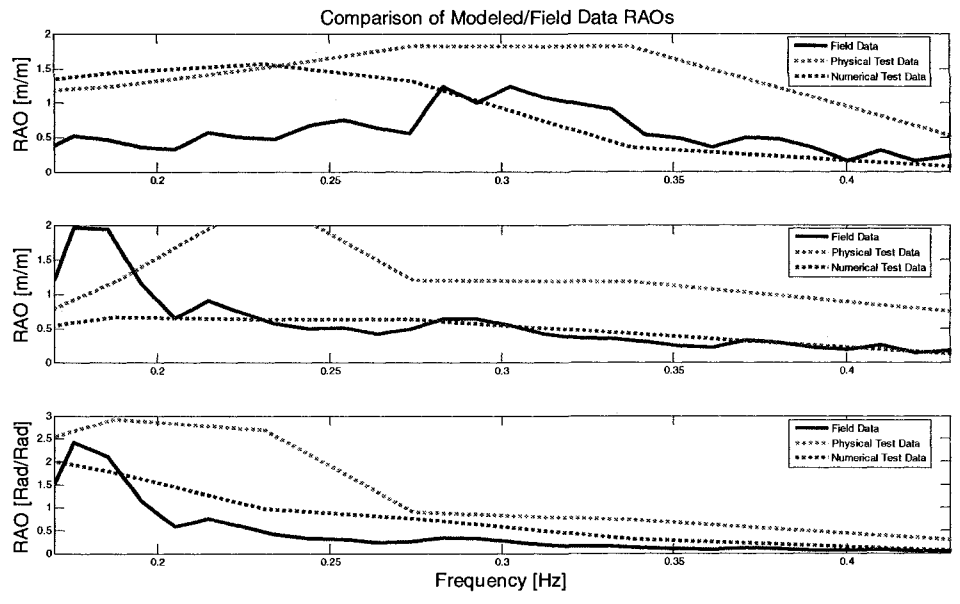
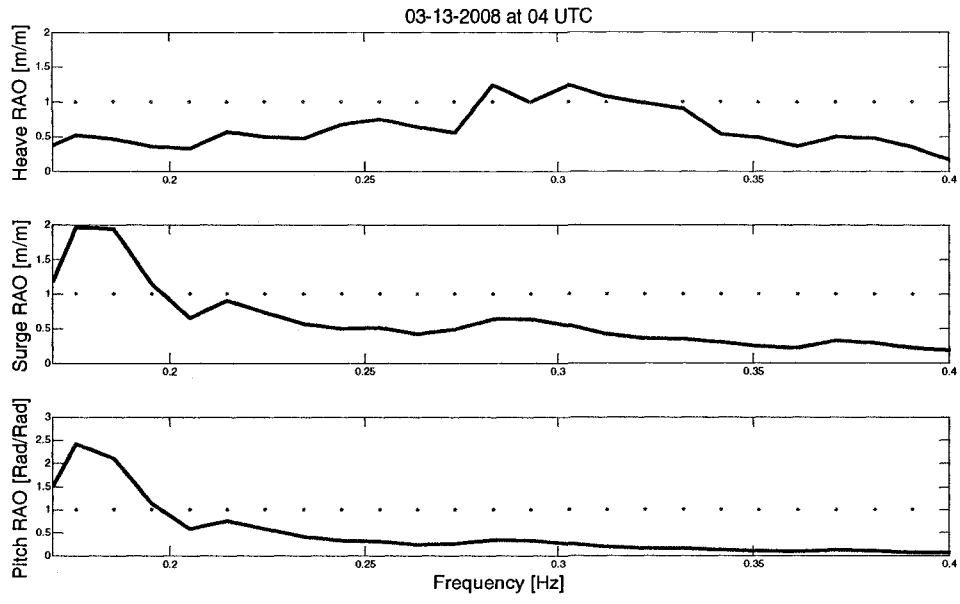
Wave Rider Translations: 03-13-2008 at 04 UTC



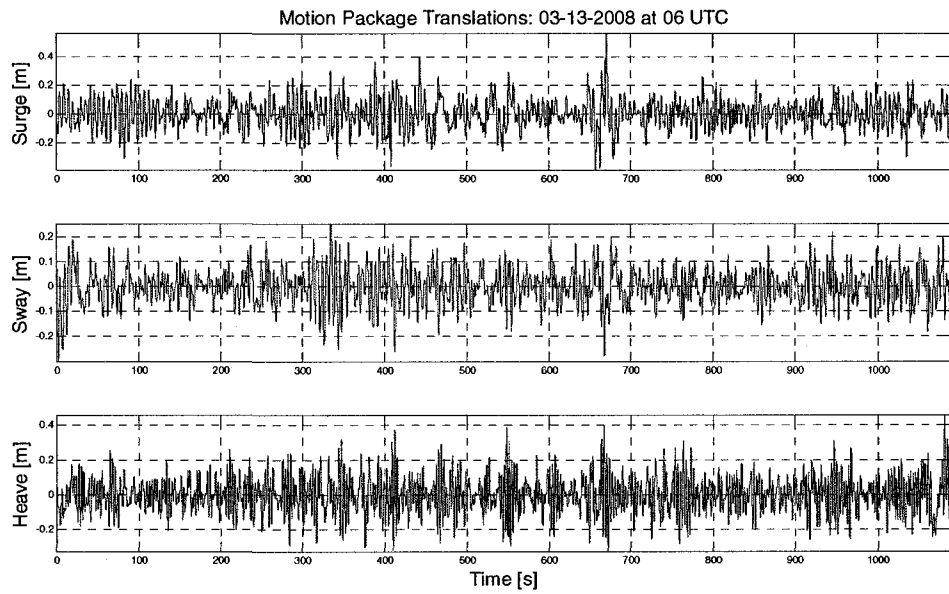
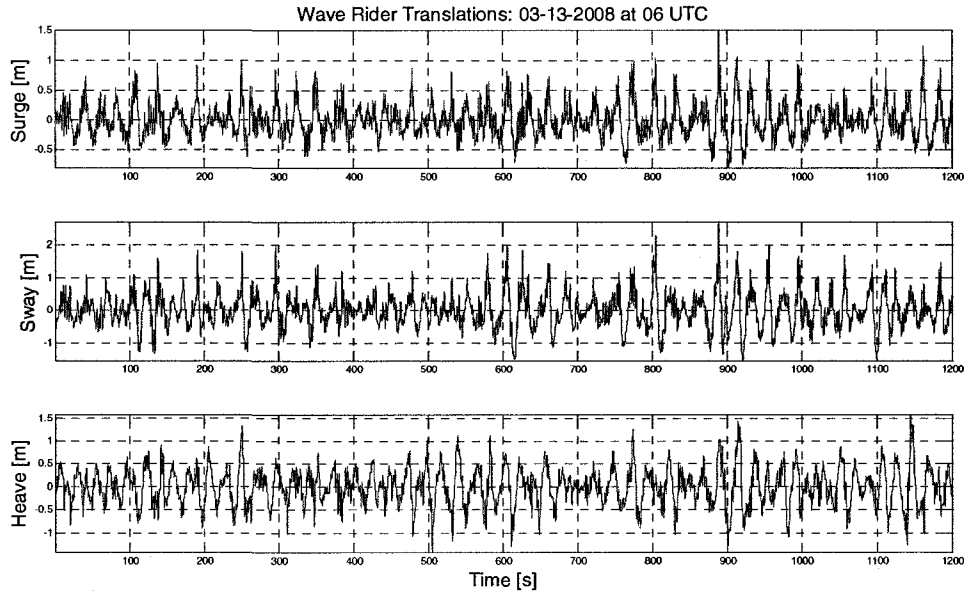
Motion Package Translations: 03-13-2008 at 04 UTC



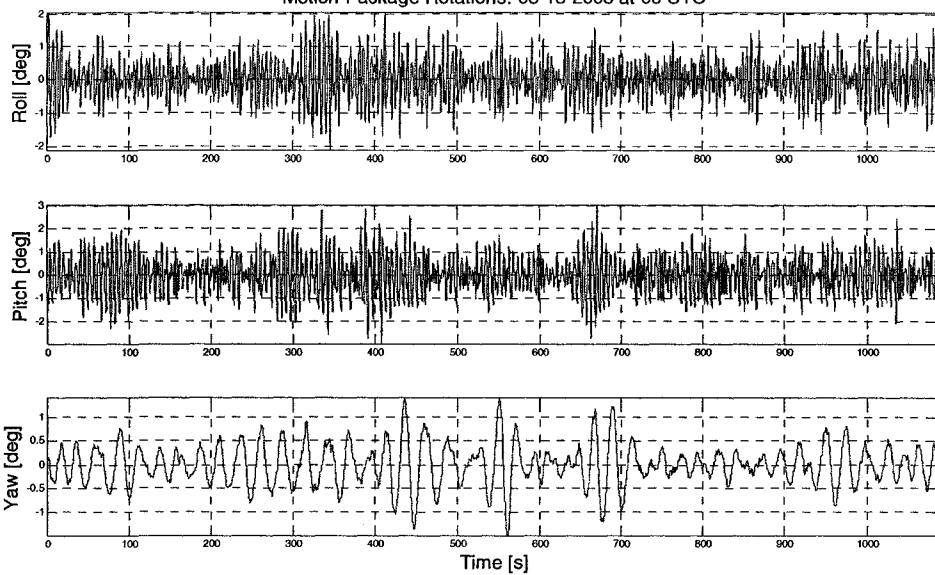




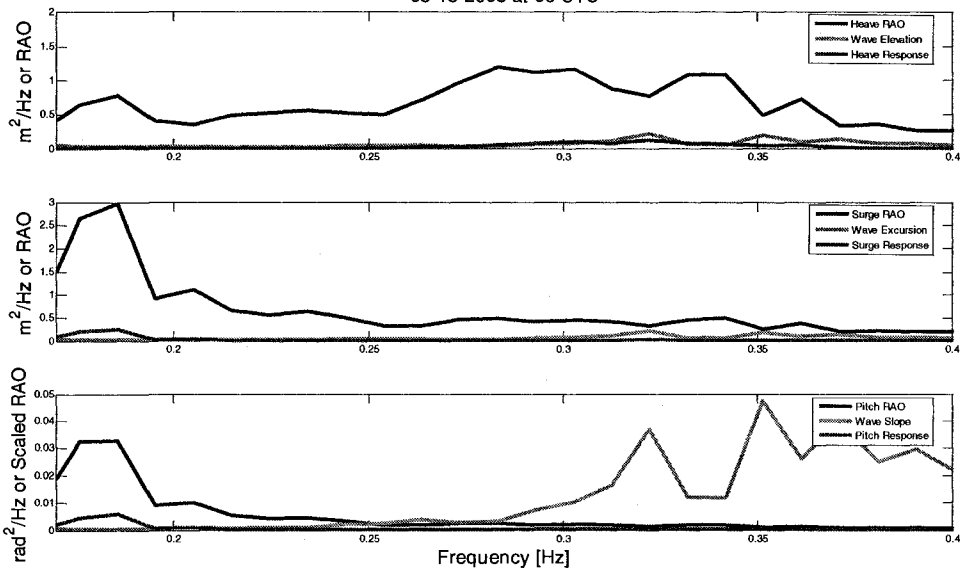
3/13/2008 at 6:00:00 UTC

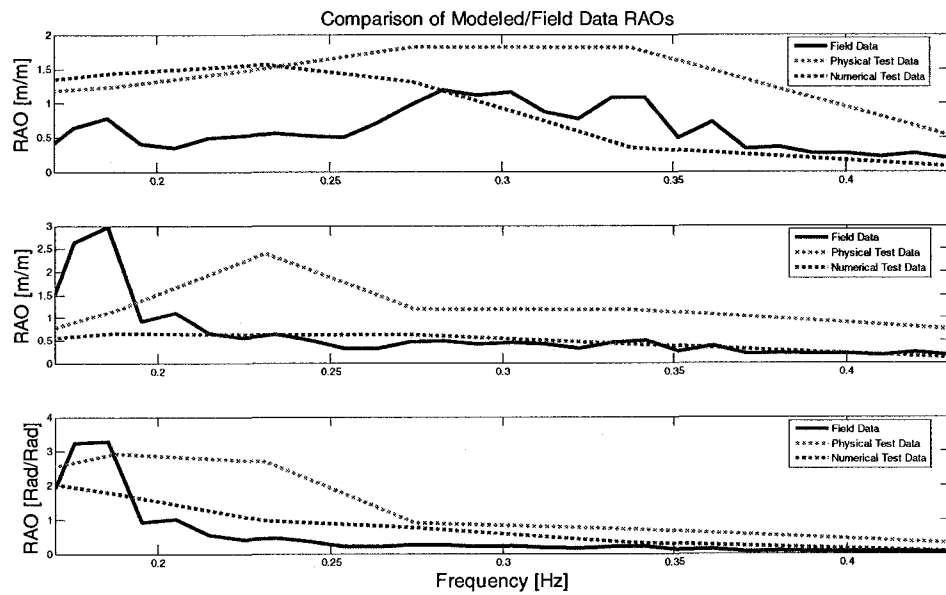
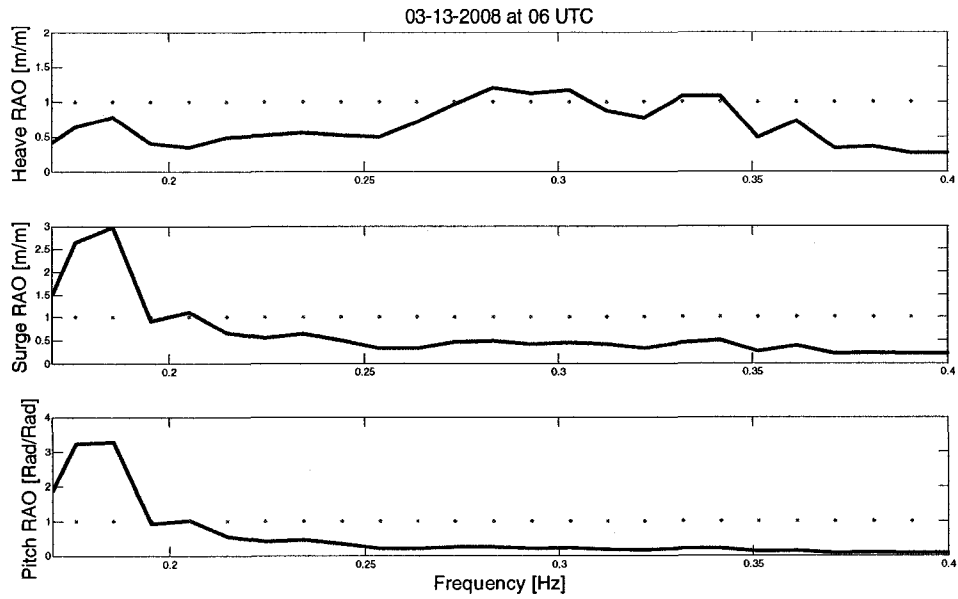


Motion Package Rotations: 03-13-2008 at 06 UTC



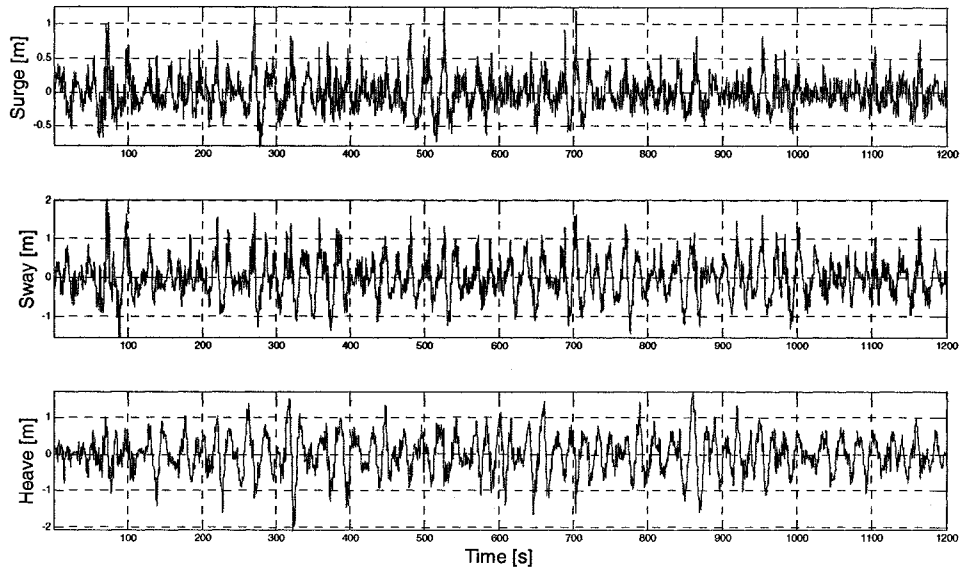
03-13-2008 at 06 UTC



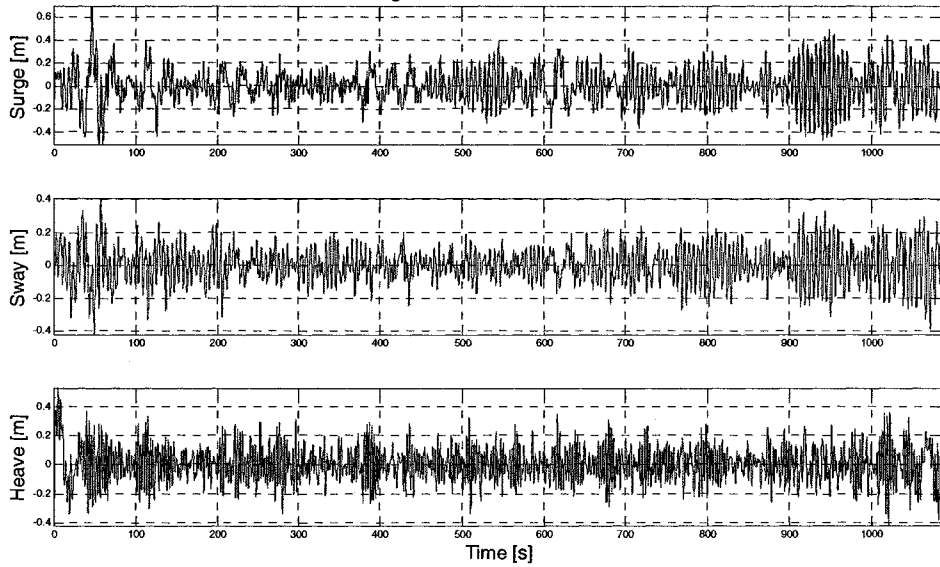


3/13/2008 at 8:00:00 UTC

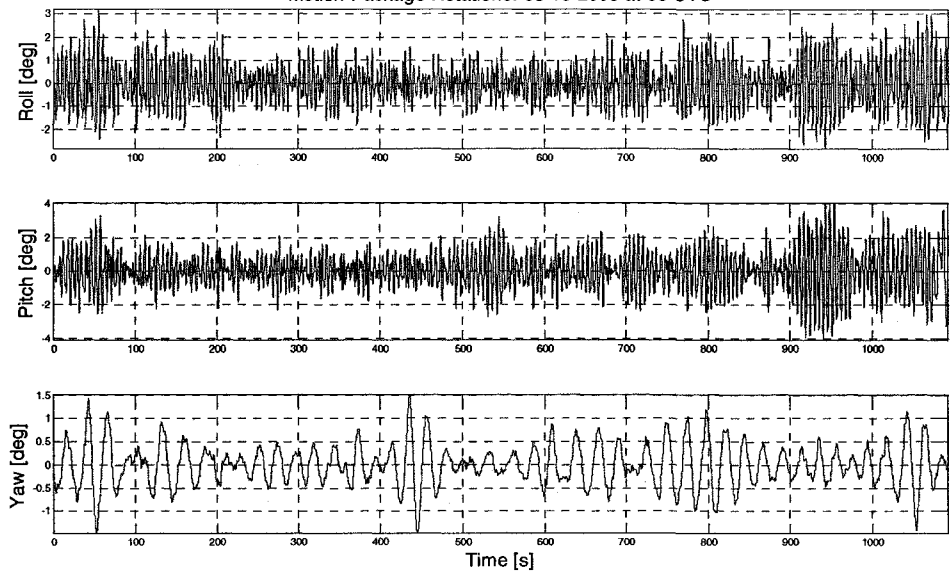
Wave Rider Translations: 03-13-2008 at 08 UTC



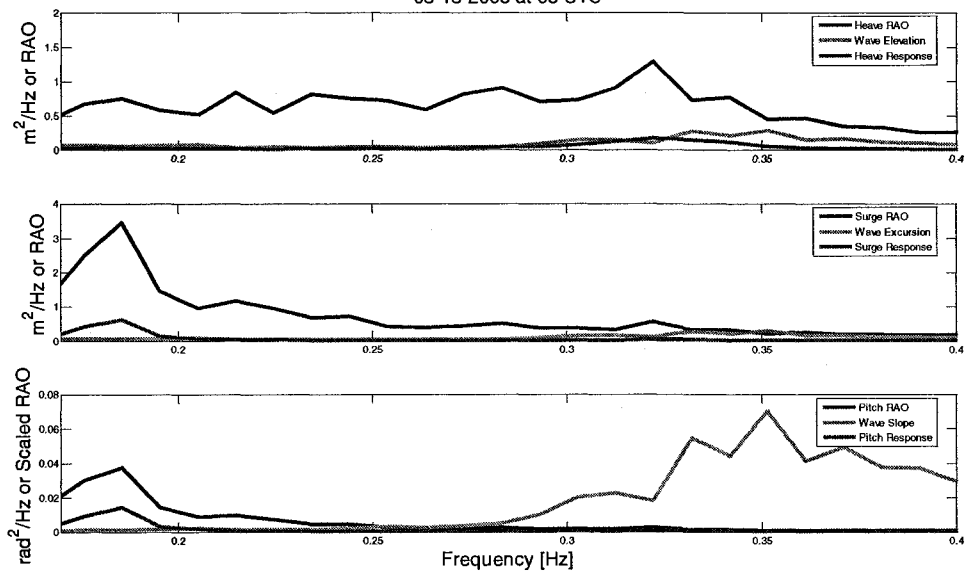
Motion Package Translations: 03-13-2008 at 08 UTC

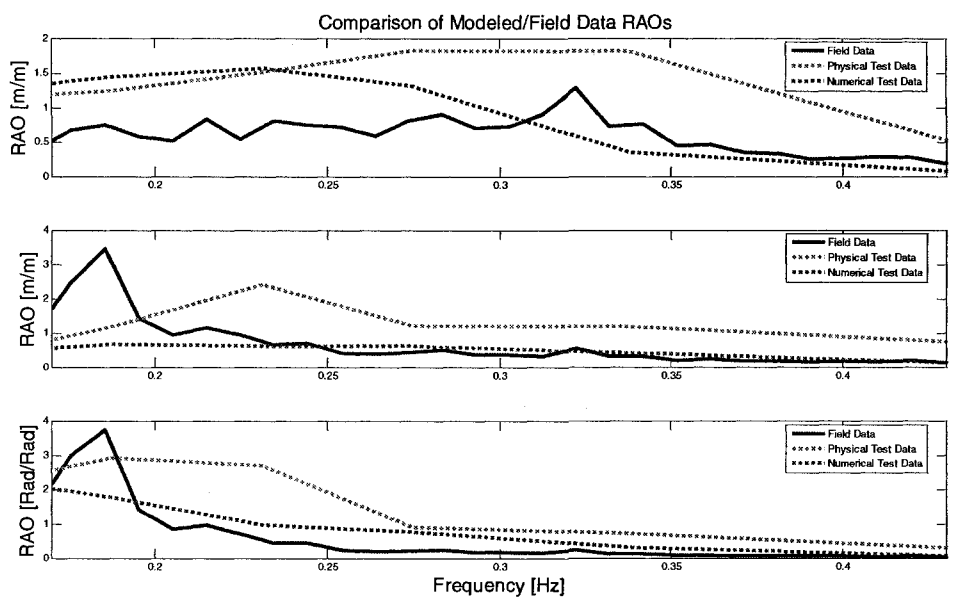
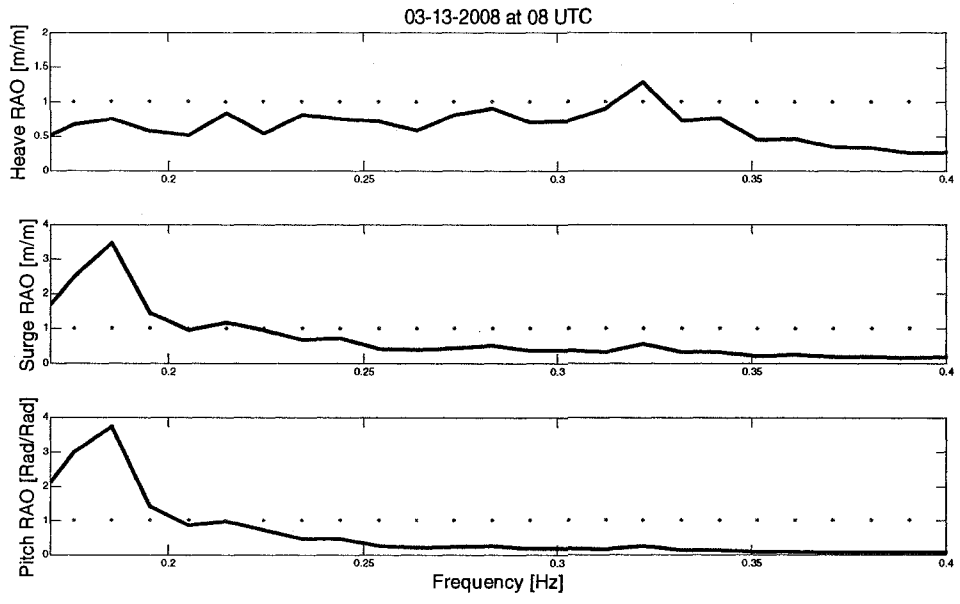


Motion Package Rotations: 03-13-2008 at 08 UTC



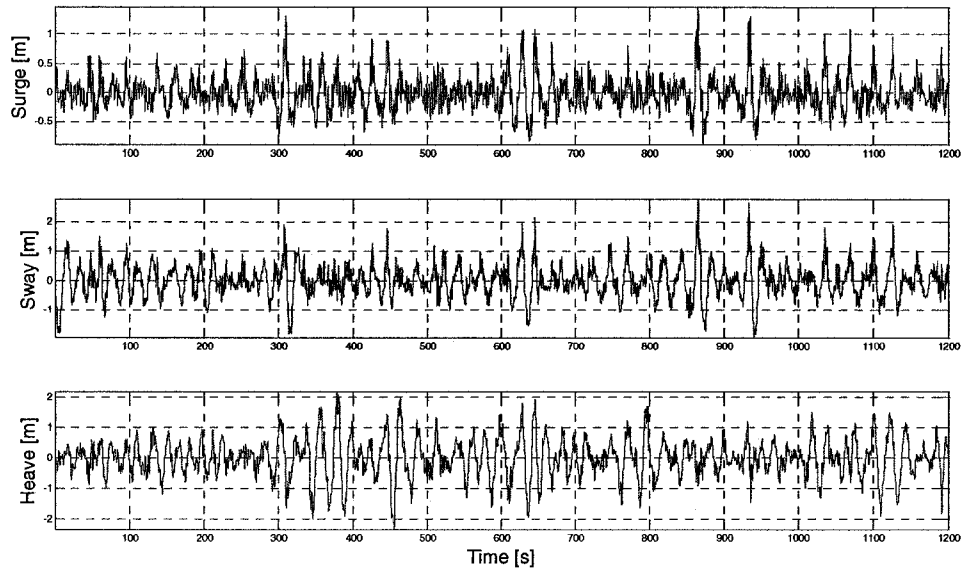
03-13-2008 at 08 UTC



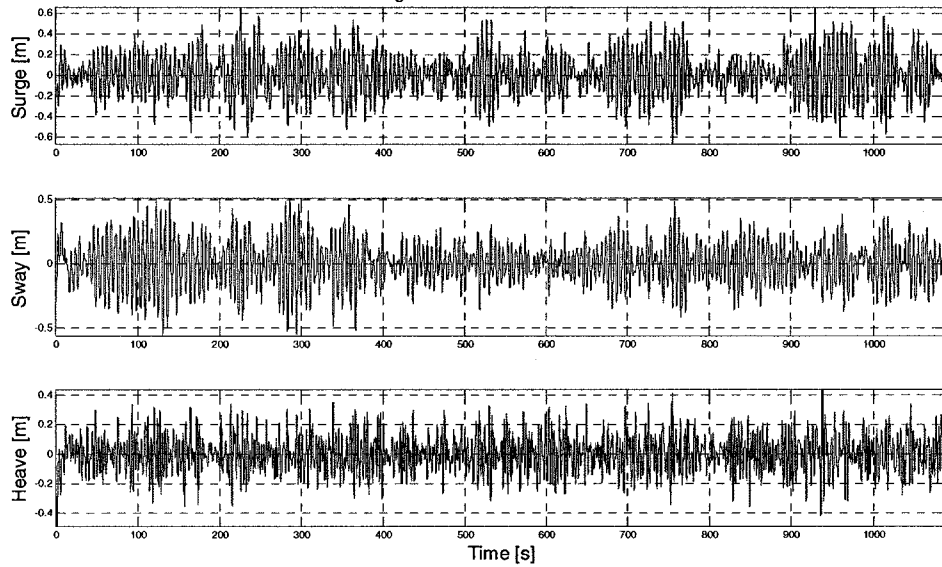


3/13/2008 at 10:00:00 UTC

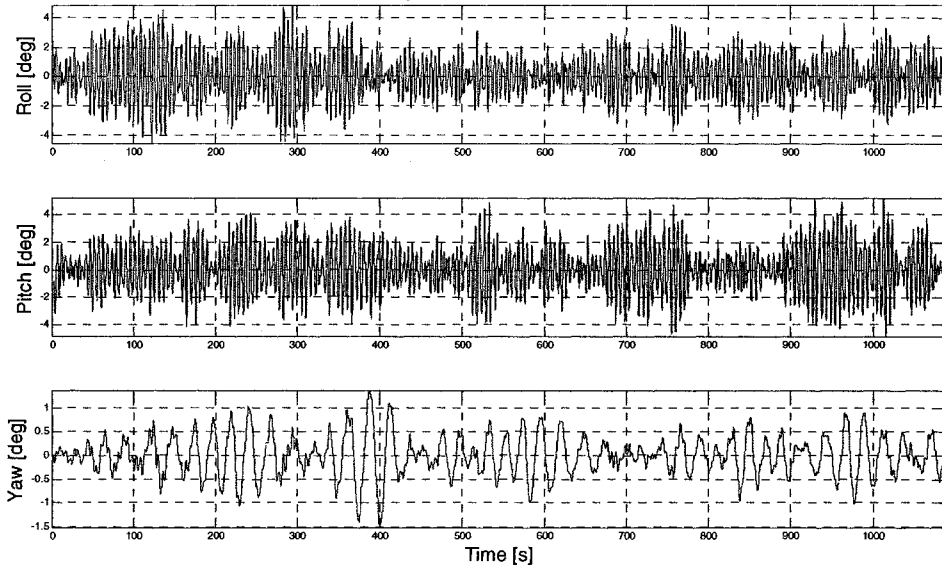
Wave Rider Translations: 03-13-2008 at 10 UTC



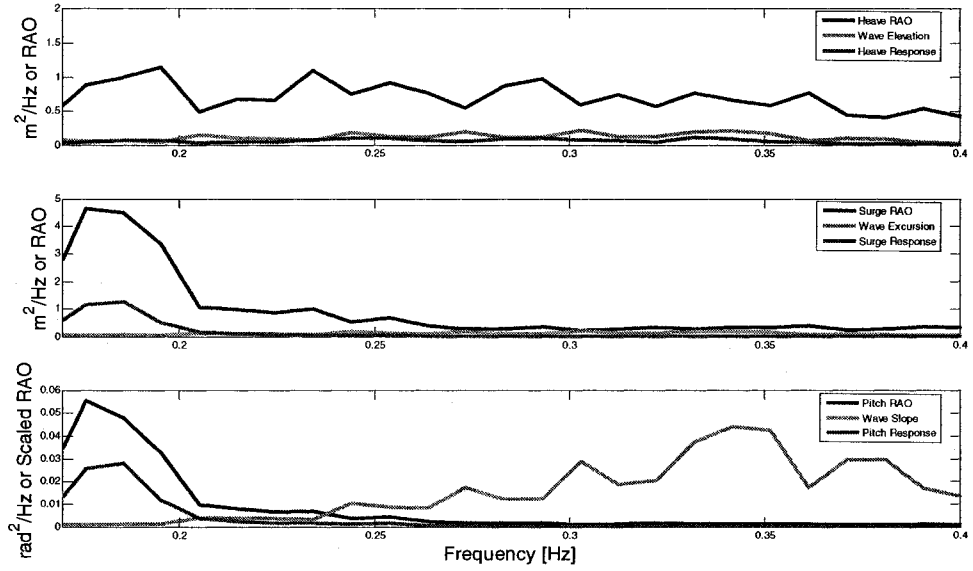
Motion Package Translations: 03-13-2008 at 10 UTC

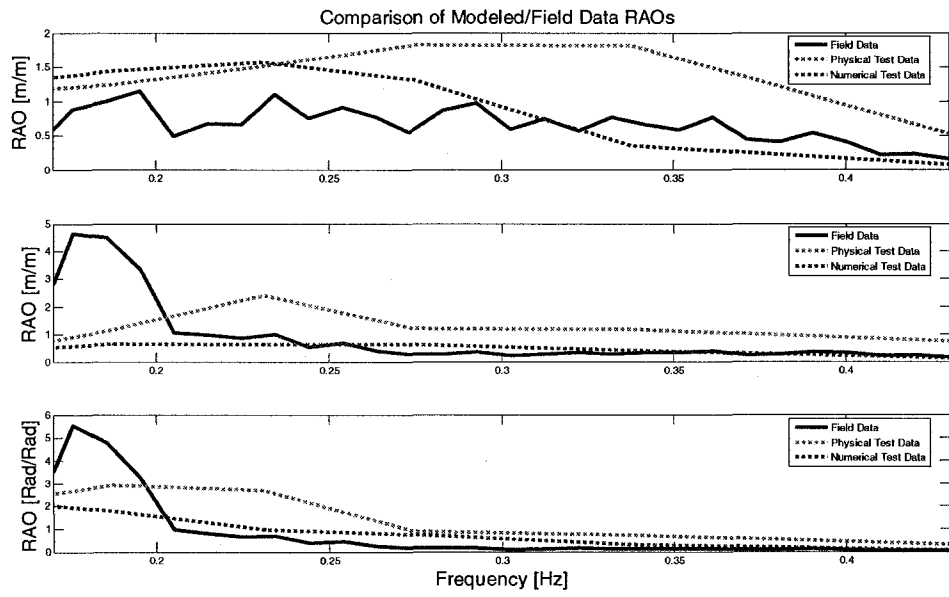
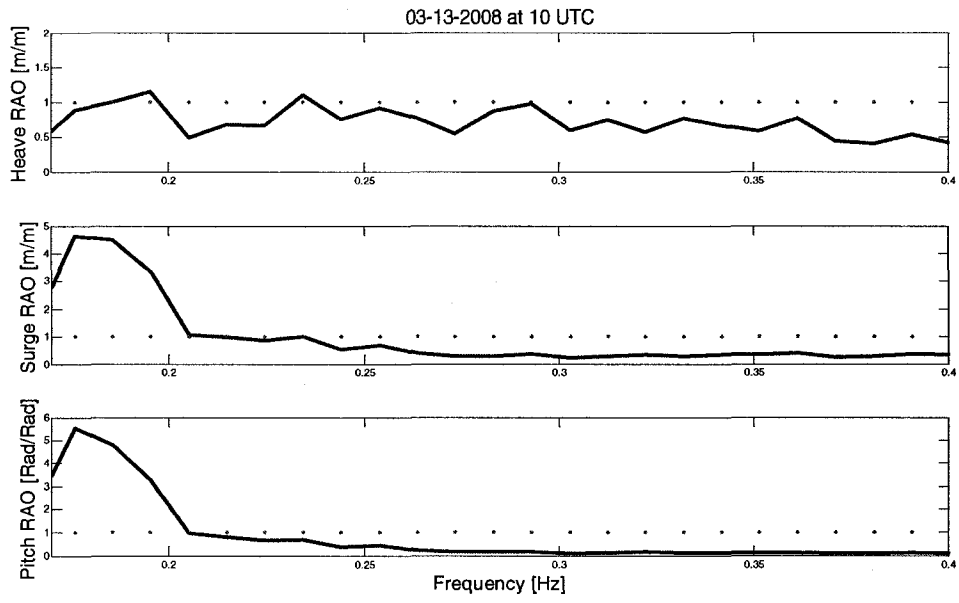


Motion Package Rotations: 03-13-2008 at 10 UTC

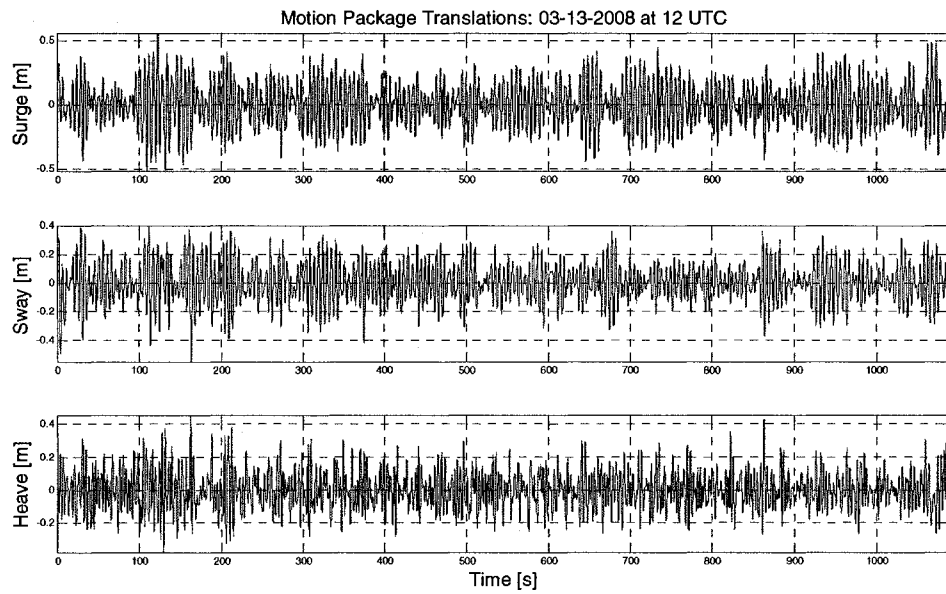
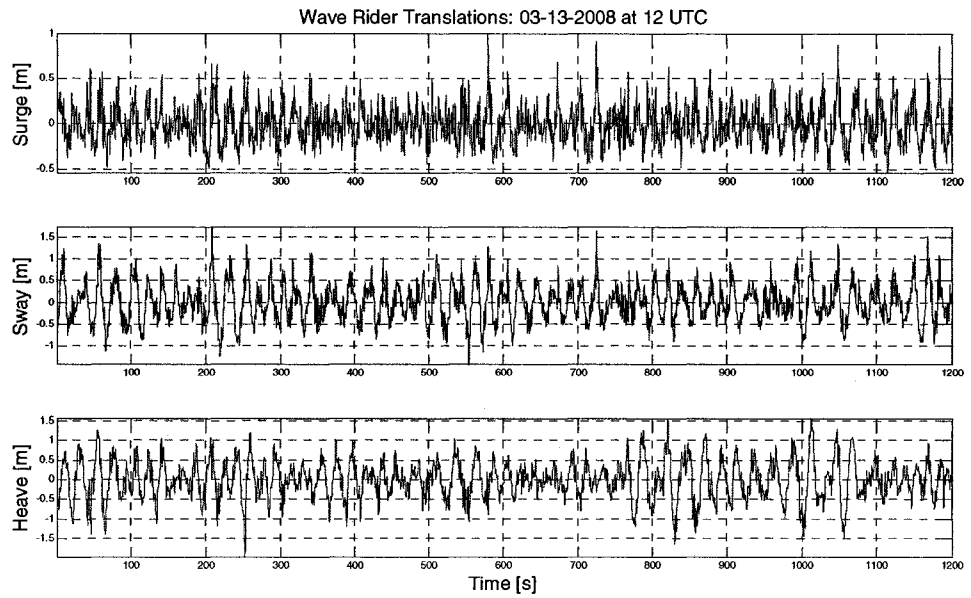


03-13-2008 at 10 UTC

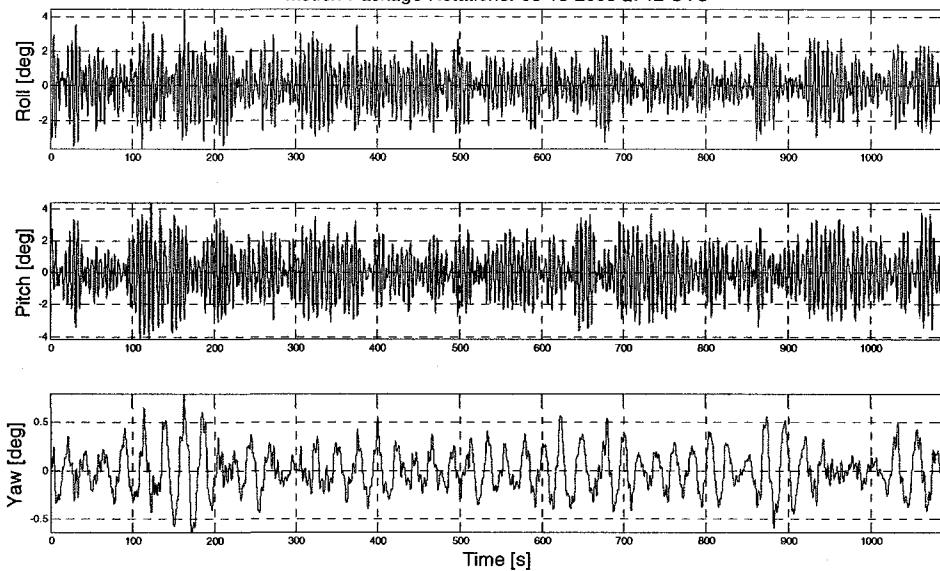




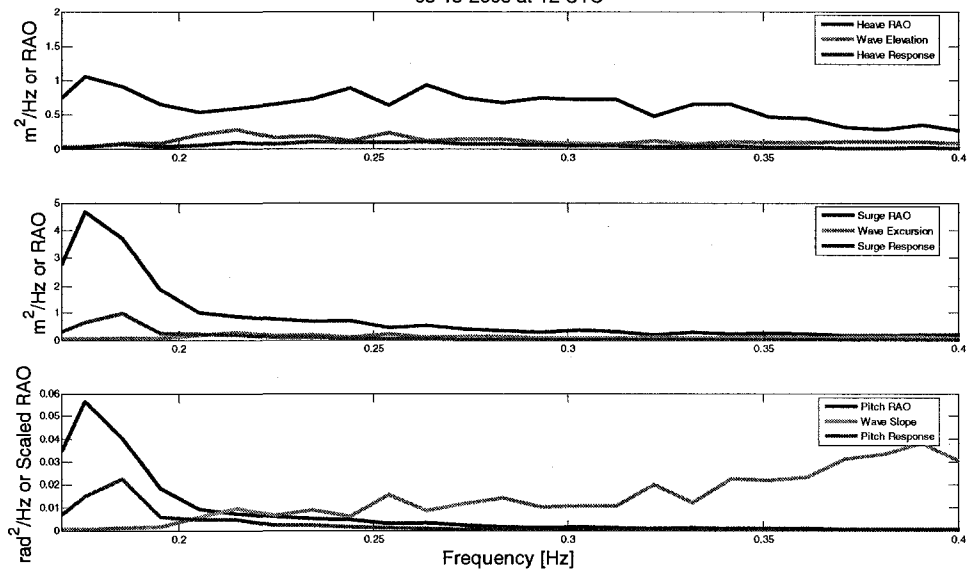
3/13/2008 at 12:00:00 UTC

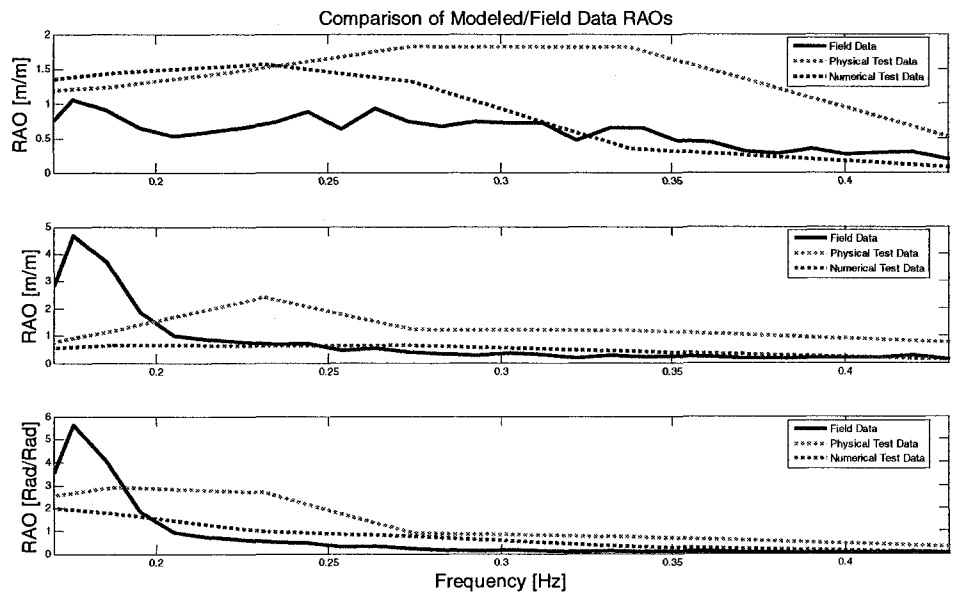
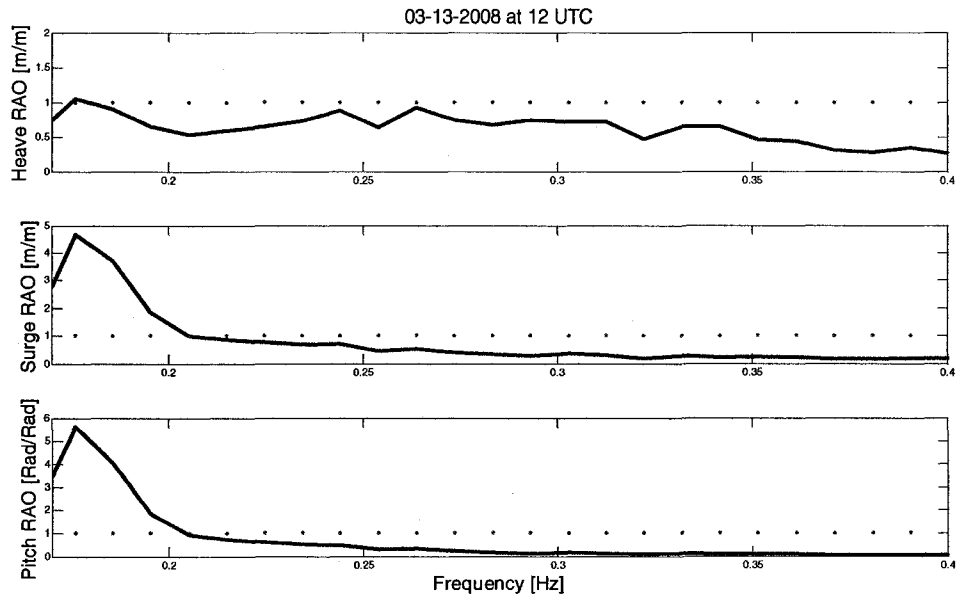


Motion Package Rotations: 03-13-2008 at 12 UTC



03-13-2008 at 12 UTC





APPENDIX B

MATLAB[®] DATA PROCESSING CODE

PROGRAM: ThesisMainProgram.m

```
%%%%%%%%%%%%%%%%%%%%%%%%%%%%%%%%%%%%%%%%%%%%%%%%%%%%%%%%%%%%%%%%%%%%%%%%%
% Title: Thesis Main Program
% Author: Jonathan Horton
%%%%%%%%%%%%%%%%%%%%%%%%%%%%%%%%%%%%%%%%%%%%%%%%%%%%%%%%%%%%%%%%%%%%%%%%%

clc
close all
clear all

MP_n = 1024; % Number of points in FFTs
WR_n = 512; % Number of points in FFTs

%%%%%%%%%%%%%%%%%%%%%%%%%%%%%%%%%%%%%%%%%%%%%%%%%%%%%%%%%%%%%%%%%%%%%%%%%
% MOTION PACK DATA
%%%%%%%%%%%%%%%%%%%%%%%%%%%%%%%%%%%%%%%%%%%%%%%%%%%%%%%%%%%%%%%%%%%%%%%%%

fname = input('What is the motion package filename? ','s');

MP_rate = 10; % Motion Pack Sampling Rate in Hertz

% Acquires Motion Pack Data
[MP_date, MP_time,t,xacc,xrate,yacc,yrate,zacc,zrate] = MotionPackData(fname);

% Processes Motion Pack Data (Displacement)
[t1,dxx,Pxx,fxx,dyy,Pyy,fyy,dzz,Pzz,fzz]=AnalyzeDataMP(fname, MP_rate, MP_n);

% Processes Motion Pack Data (Rotational)
[t1,roll,pitch,yaw,R,freq_r,P,freq_p,Y,freq_y]=AnalyzeDataMPRot(fname, MP_rate, MP_n);

%%%%%%%%%%%%%%%%%%%%%%%%%%%%%%%%%%%%%%%%%%%%%%%%%%%%%%%%%%%%%%%%%%%%%%%%%
% WAVE RIDER DATA
%%%%%%%%%%%%%%%%%%%%%%%%%%%%%%%%%%%%%%%%%%%%%%%%%%%%%%%%%%%%%%%%%%%%%%%%%

fname2 = input('What is the wave rider filename? ','s');

WR_rate = 5; % Wave Rider Sampling Rate in Hertz

% Acquires Wave Rider Data
[t2,xac,yac,zac] = WaveRiderData(fname);

% Processes Wave Rider Data (Displacement)
[t2,dx,Px,fx,dy,Py,fy,dz,Pz,fz]=AnalyzeDataWR(fname2, WR_rate, WR_n);
```



```

%% Responses and RAOs
%%
d = 52; % Depth in meters at OOA site

% Gravity
g = 9.81;

% Frequency
f = fzz(1:256);

% Wavenumber
k = ((2*pi*f).^2)/g;

wave_elevation = Pz;

heave_response = Pzz(1:256);
surge_response = Pxx(1:256);
pitch_response = P(1:256);

i = length(wave_elevation);
for j = 1:i

    k(j) = ((2*pi*f(j))^2)/g;

    wave_excursion(j) = wave_elevation(j)*(tanh(k(i)*d))^(-2);

    wave_slope(j) = wave_elevation(j)*(k(j))^2;

    heave_trans(j) = sqrt(heave_response(j)/wave_elevation(j));
    surge_trans(j) = sqrt(surge_response(j)/wave_excursion(j));
    pitch_trans(j) = sqrt(pitch_response(j)/wave_slope(j));

end

```

FUNCTION: AnalyzeDataMP.m

```
function [t,dxx,Pxx,fxx,dyy,Py,y,dyz,Pzz,fzz]=AnalyzeDataMP(fname, rate, n)
```

```
%%%%%%%%%%%%%%%%%%%%%%%%%%%%%%%%%%%%%%%%%%%%%%%%%%%%%%%%%%  
% Title: Analyze Motion Pack Data  
% Author: Jonathan Horton  
% Based on code by: James D. Irish  
%%%%%%%%%%%%%%%%%%%%%%%%%%%%%%%%%%%%%%%%%%%%%%%%%%%%%%%%%%  
%  
% Function Inputs:  
%     fname = Name of the time series motion pack data file.  
%           The file name should be in string format.  
%           Typically the file name is in the form  
%           "filename.00".  
%  
%     rate = Sampling rate of the data  
%  
%     n = Number of points in FFT  
%%%%%%%%%%%%%%%%%%%%%%%%%%%%%%%%%%%%%%%%%%%%%%%%%%%%%%%%%%  
[MP_date, MP_time,t,xacc,xrate,yacc,yrate,zacc,zrate] = MotionPackData(fname);  
  
%+-----+  
% Remove linear trend and mean of data, Filter, and convert g's to  
% displacement data  
  
[dxx, vxx] = Accel2Dsp(xacc, rate, 0, 0);  
[dyy, vyy] = Accel2Dsp(yacc, rate, 0, 0);  
[dzz, vzz] = Accel2Dsp(zacc, rate, 0, 0);  
  
% Compute raw power spectrum from displacement data  
  
[Pxx, fxx] = RawSpectrum(dxx,n,0.1);  
[Pyy, fyy] = RawSpectrum(dyy,n,0.1);  
[Pzz, fzz] = RawSpectrum(dzz,n,0.1);  
  
%+-----+
```

FUNCTION: AnalyzeDataMPRot.m

```
function [t,roll,pitch,yaw,R,freq_r,P,freq_p,Y,freq_y]=AnalyzeDataMPRot(fname, rate, n)
```

```
%%%%%%%%%%%%%%%%%%%%%%%%%%%%%%%%%%%%%%%%%%%%%%%%%%%%%%%%%%%%%%%%%%%%%%%%%
```

```
% Title: Analyze Motion Pack Rotational Data
```

```
% Author: Jonathan Horton
```

```
% Based on code by: Jim Irish
```

```
%%%%%%%%%%%%%%%%%%%%%%%%%%%%%%%%%%%%%%%%%%%%%%%%%%%%%%%%%%%%%%%%%%%%%%%%%
```

```
% Function Inputs:
```

```
%     fname = Name of the time series motion pack data file.
```

```
%     The file name should be in string format.
```

```
%     Typically the file name is in the form
```

```
%     "filename.00".
```

```
%
```

```
%     rate = Sampling rate of the data
```

```
%
```

```
%     n = Number of points in FFT
```

```
%%%%%%%%%%%%%%%%%%%%%%%%%%%%%%%%%%%%%%%%%%%%%%%%%%%%%%%%%%%%%%%%%%%%%%%%%
```

```
[MP_date, MP_time,t,xacc,xrate,yacc,yrate,zacc,zrate] = MotionPackData(fname);
```

```
%+-----+
```

```
% Remove linear trend and mean of data, Filter, and convert to
```

```
% degree data
```

```
roll = Rot2Deg(xrate, rate, 0);
```

```
pitch = Rot2Deg(yrate, rate, 0);
```

```
yaw = Rot2Deg(zrate, rate, 0);
```

```
% Convert to radians
```

```
roll = roll*(pi/180);
```

```
pitch = pitch*(pi/180);
```

```
yaw = yaw*(pi/180);
```

```
% Compute raw power spectrum from displacement data
```

```
[R,freq_r] = RawSpectrum(roll,n,0.1);
```

```
[P,freq_p] = RawSpectrum(pitch,n,0.1);
```

```
[Y,freq_y] = RawSpectrum(yaw,n,0.1);
```

```
%+-----+
```

FUNCTION: AnalyzeDataWR.m

```
function [t,dx,Px,fx,dy,Py,fy,dz,Pz,fz]=AnalyzeDataWR(fname, rate, n)
```

```
%%%%%%%%%%%%%%%%%%%%%%%%%%%%%%%%%%%%%%%%%%%%%%%%%%%%%%%%%%%%%%%%%%%%%%%%%
```

```
% Title: Analyze Wave Rider Data
```

```
% Author: Jonathan Horton
```

```
% Based on code by: James D. Irish
```

```
%%%%%%%%%%%%%%%%%%%%%%%%%%%%%%%%%%%%%%%%%%%%%%%%%%%%%%%%%%%%%%%%%%%%%%%%%
```

```
%
```

```
%
```

```
% Function Inputs:
```

```
%     fname = Name of the time series wave rider data file.
```

```
%     The file name should be in string format.
```

```
%     Typically the file name is in the form
```

```
%     "filename.dat".
```

```
%
```

```
%     rate = Sampling rate of the data
```

```
%
```

```
%     n = Number of points in FFT
```

```
%%%%%%%%%%%%%%%%%%%%%%%%%%%%%%%%%%%%%%%%%%%%%%%%%%%%%%%%%%%%%%%%%%%%%%%%%
```

```
[t,xac,yac,zac] = WaveRiderData(fname);
```

```
%+-----+
```

```
% Remove linear trend and mean of data, Filter, and convert g's to  
% displacement data
```

```
[dx, vx] = Accel2Dsp(xac, rate, 0, 0);
```

```
[dy, vy] = Accel2Dsp(yac, rate, 0, 0);
```

```
[dz, vz] = Accel2Dsp(zac, rate, 0, 0);
```

```
% Compute raw power spectrum from displacement data
```

```
[Px, fx] = RawSpectrum(dx,n,0.2);
```

```
[Py, fy] = RawSpectrum(dy,n,0.2);
```

```
[Pz, fz] = RawSpectrum(dz,n,0.2);
```

```
%+-----+
```

FUNCTION: MotionPackData.m

```
function [MP_date, MP_time,t,xacc,xrate,yacc,yrate,zacc,zrate] = MotionPackData(fname)
```

```
%%%%%%%%%%%%%%%%%%%%%%%%%%%%%%%%%%%%%%%%%%%%%%%%%%%%%%%%%%%%%%%%%%%%%%%%%%  
% Thesis Code: Motion Pack Function  
%%%%%%%%%%%%%%%%%%%%%%%%%%%%%%%%%%%%%%%%%%%%%%%%%%%%%%%%%%%%%%%%%%%%%%%%%  
% Author: Jonathan Horton  
% Code Adapted from: James D. Irish  
% Last Updated: May 18, 2008  
%%%%%%%%%%%%%%%%%%%%%%%%%%%%%%%%%%%%%%%%%%%%%%%%%%%%%%%%%%%%%%%%%%%%%%%%%  
% The purpose of this function is to read in a data file from the UNH Open  
% Ocean Aquaculture motion package and return appropriate acceleration and  
% rotation data. The function is in the form:  
%  
% [MP_date, MP_time,t,xacc,xrate,yacc,yrate,zacc,zrate] =  
% MotionPackData(fname);  
%  
% Inputs:  
%     fname = the file name in string format. Typically  
%           the file name is in the form "filename.00".  
% Outputs:  
%     t     = Time (x-axis time base) in seconds  
%     xacc  = Acceleration in the x-direction  
%     xrate = Rotation rate in the x-direction  
%     yacc  = Acceleration in the y-direction  
%     yrate = Rotation rate in the y-direction  
%     zacc  = Acceleration in the z-direction  
%     zrate = Rotation rate in the z-direction  
%  
% The motion package data is organized as such on the file:  
%  
% 112 bytes of header:  
%  
%                               48 bytes of title  
%                               9 bytes of date  
%                               9 bytes of time  
%                               7 bytes of battery voltage  
%                               38 bytes of free space filled with zeros  
%                               1 byte of fixed end "1A" hex  
%  
% 12 A/D channels sampled at 10 hz:  
% 1. Motion Pack Acceleration - z axis  
% 2. Motion Pack Acceleration - y axis  
% 3. Motion Pack Acceleration - x axis  
% 4. Motion Pack Rotation - z axis
```



```

% Digitizer is set to plus and minus 10 volts, or 20 volts over 12 bits...
% therefore, volts output is 0.00488 volts/bit * counts. The reshape command
% returns the channel-by-np matrix whose elements are taken column-wise from
% rdat.

```

```

ndat = 0.00488 .* reshape(rdat, channels, np);

```

```

% +-----+
% Calculates x-axis time base
[n,tim]=size(ndat);
if n~=channels, disp('error in size'), end
t = 0:(tim-1);
t = t./10;
% +-----+

```

```

% +-----+
% convert accelerations to g's

% factory calibration is 3.742 volts/g in z axis with 0.00083 g bias
zacc = ndat(1,:)/3.742 - 0.00083;

% factory calibration is 7.458 volts/g in y axis with -0.00176 g bias
yacc = ndat(2,:)/7.485 + 0.00176;

% factory calibration is 7.504 volts/g in x axis with 0.00033 g bias
xacc = ndat(3,:)/7.504 - 0.00033;
% +-----+

```

```

% +-----+
% convert rates to deg/sec

% factory calibration is 0.050304 volts per deg/sec rate with 0.06 deg/s bias
% lab tests show offset of 0.1523 deg/s
zrate = ndat(4,:)/0.050304-0.06-0.1523;

% factory calibration is 0.049933 volts per deg/sec rate with 0.14 deg/s bias
% lab tests show offset of 0.1508 deg/s
yrate = ndat(5,:)/0.049933-0.14-0.1508;

% factory calibration is 0.050101 volts per deg/sec rate with 0.06 deg/s bias
% lab tests show offset of 0.1348 deg/s
xrate = ndat(6,:)/0.050101-0.06-0.1348 ;
% +-----+

```

```

% Load cell data:

```

```
load_cell_1 = ndat(7,:);
load_cell_2 = ndat(8,:);

% Optical backscattering sensor data:
opt_bk_scatter = ndat(9,:);
%
% battery or bus voltage after diodes
bus_voltage = 1.565 .* ndat(10,:);

MP_time = file_header(58:59);

dat1=file_header(52:53)
dat2=file_header(55:56)
dat3=file_header(49:50)

MP_date = [dat1,'-',dat2,'-20',dat3];
```


FUNCTION: WaveRiderData.m

```
function [t,xac,yac,zac] = WaveRiderData(fname)
```

```
%%%%%%%%%%%%%%%%%%%%%%%%%%%%%%%%%%%%%%%%%%%%%%%%%%%%%%%%%%%%%%%%%%%%%%%%%%  
% Thesis Code: Wave Rider Function  
%%%%%%%%%%%%%%%%%%%%%%%%%%%%%%%%%%%%%%%%%%%%%%%%%%%%%%%%%%%%%%%%%%%%%%%%%%  
% Author: Jonathan Horton  
% Code Adapted from: James D. Irish  
%%%%%%%%%%%%%%%%%%%%%%%%%%%%%%%%%%%%%%%%%%%%%%%%%%%%%%%%%%%%%%%%%%%%%%%%%%  
% The purpose of this function is to read in a data file from the UNH Open  
% Ocean Aquaculture wave rider buoy and return appropriate acceleration and  
% rotation data. The function is in the form:  
%  
% [t,xac,yac,zac, battery] = WaveRiderData(fname)  
%  
% Inputs:  
%     fname = the file name in string format. Typically  
%           the file name is in the form "filename.00".  
% Outputs:  
%     t = Time (x-axis time base) in minutes  
%     xac = Acceleration in the x-direction  
%     yac = Acceleration in the y-direction  
%     zac = Acceleration in the z-direction  
%  
% The motion package data is organized as such on the file:  
%  
% 46 bytes of header  
% 12,000 samples of 2 bytes each of 4 channels  
%  
%                               1. Z-direction acceleration  
%                               2. Y-direction acceleration  
%                               3. X-direction acceleration  
%  
%%%%%%%%%%%%%%%%%%%%%%%%%%%%%%%%%%%%%%%%%%%%%%%%%%%%%%%%%%%%%%%%%%%%%%%%%%
```

```
% +-----+
```

```
fid = fopen(fname,'r'); % Opens the file for reading
```

```
% Reads in the first 36000 bytes of data (Unsigned integer; 8 bits)
```

```
[dat,count] = fread(fid,36000,'uint8');
```

```
% Reads in the z-directional data
```

```
zv=2.5.*[256*dat(1:6:36000) + dat(2:6:36000)]./32768;
```

```
% Reads in the x-directional data
```

```

xv=2.5.*[256*dat(3:6:36000) + dat(4:6:36000)]./32768;

% Reads in the y-directional data
yv=2.5.*[256*dat(5:6:36000) + dat(6:6:36000)]./32768;

fclose(fid); % Closes file
% +-----+
% Converts data into acceleration data
xac=2.0726*(xv-1.2332);
yac = 2.*(yv-1.25);
zac = 2.*(zv-1.25);

% +-----+

% +-----+
% Takes the means of the acceleration data
zac_mean=mean(zac);
xac_mean=mean(xac);
yac_mean=mean(yac);
% +-----+

% +-----+
% Takes the standard deviations of the acceleration data
zac_std=std(zac);
xac_std=std(xac);
yac_std=std(yac);
% +-----+

% Calculates the time (x-axis)
t=(1:6000)./60./5;

```



```

norm = 2*dt/k/m;          % Normalization

% Drop mean (frequency = 0) and go only to the Nyquist frequency
PXX = Pxx(2:(m/2+1))*norm;
freq = freq(2:(m/2+1));

% Create output as two dimensional array of frequencies and spectral densities
spectrum=[freq PXX];

% %plot output
% figure
% loglog(spectrum(:,1),spectrum(:,2))
% title('Raw Spectral Densities')
% xlabel('Frequency')
% ylabel('Spectral Density')
% return

```

FUNCTION: Accel2Dsp.m

function [u, v] = Accel2Dsp(a, f, v0, u0)

```
%%%%%%%%%%%%%%%%%%%%%%%%%%%%%%%%%%%%%%%%%%%%%%%%%%%%%%%%%%%%%%%%%%%%%%%%%
% Thesis Code: Acceleraton (g's) to Displacement Function
%%%%%%%%%%%%%%%%%%%%%%%%%%%%%%%%%%%%%%%%%%%%%%%%%%%%%%%%%%%%%%%%%%%%%%%%
% Author: Jonathan Horton
% Code Adapted from: James D. Irish and Jason Gobat
%%%%%%%%%%%%%%%%%%%%%%%%%%%%%%%%%%%%%%%%%%%%%%%%%%%%%%%%%%%%%%%%%%%%%%%%
% The purpose of this function is to read in acceleration data and ouput
% displacement and velocity data. The program was originally written by
% Jason Gobat and altered by Jim Irish in January 2001 to look at UNH wave
% data: The function is in the form:
%
%       function [u, v] = accel2dsp(a, f, v0, u0)
%
% Inputs:
%   a = acceleration time series input (in g's)
%   f = sample frequency (usually 10 Hz for waverider and motion
%       package)
%   v0 = integration constant in velocity, usually zero
%   u0 = integration constant in displacement, usually zero
%
% Outputs:
%   u = displacement
%   v = velocity
%
%%%%%%%%%%%%%%%%%%%%%%%%%%%%%%%%%%%%%%%%%%%%%%%%%%%%%%%%%%%%%%%%%%%%%%%%
% Convert from g's to m/s^2

a=9.8.*a;

% +-----+
% Remove mean and trend from data

ma=mean(a);
a=a-ma;
clear ma
a = detrend(a);
% +-----+

% +-----+
% Creates high pass filter
dt = 1.0/f;
[bf,af] = butter(4,0.033333/(f/2),'high');
```

```

%[bf,af] = butter(4,0.05/(f/2),'high');
n = length(a);
v = zeros(n,1);
u = zeros(n,1);
% +-----+

% +-----+
% Starting velocity = v0
v(1) = v0;
% +-----+

% +-----+
% Trapezoidal integration of acceleration to velocity

for i = 2:n
    v(i) = dt*(a(i) + a(i-1))/2 + v(i-1);
end
% +-----+

% +-----+
% Detrend and filter to remove low frequencies

v = filtfilt(bf,af,detrend(v));
v = filtfilt(bf,af,v);
% +-----+

% +-----+
% Starting position - u0

u(1) = u0;
% +-----+

% +-----+
% Trapezoidal integration of velocity to position

for i = 2:n
    u(i) = dt*(v(i) + v(i-1))/2 + u(i-1);
end
% +-----+

% +-----+
% Apply Butterworth filter again

u = filtfilt(bf,af,detrend(u));
u = filtfilt(bf,af,u);

```

FUNCTION: Rot2Deg.m

```
function [deg] = Rot2Deg(rot, f, a0)

%%%%%%%%%%%%%%%%%%%%%%%%%%%%%%%%%%%%%%%%%%%%%%%%%%%%%%%%%%%%%%%%%%%%%%%%
% Thesis Code: Rotation to Degrees Function
%%%%%%%%%%%%%%%%%%%%%%%%%%%%%%%%%%%%%%%%%%%%%%%%%%%%%%%%%%%%%%%%%%%%%%%%
% Author: Jonathan Horton
% Code Adapted from: James D. Irish and Jason Gobat
%%%%%%%%%%%%%%%%%%%%%%%%%%%%%%%%%%%%%%%%%%%%%%%%%%%%%%%%%%%%%%%%%%%%%%%%
% The purpose of this function is to read in rotation data and ouput
% degree data.
%
% Inputs:
%   rot = Rotation data
%   f   = sample frequency (usually 5 Hz for waverider and 10 Hz motion
%         package)
%   a0  = Starting angle, usually zero
%
% Outputs:
%   deg = Degree data
%
%%%%%%%%%%%%%%%%%%%%%%%%%%%%%%%%%%%%%%%%%%%%%%%%%%%%%%%%%%%%%%%%%%%%%%%%

% +-----+
% Remove mean and trend from data

ma = mean(rot);
rot = rot-ma;
clear ma
a = detrend(rot);
% +-----+

% +-----+
dt = 1.0/f;
[bf,af] = butter(4,0.033333/(f/2),'high');
%[bf,af] = butter(4,0.05/(f/2),'high');
n = length(a);
deg = zeros(n,1);

% +-----+

% +-----+
% Starting angle = a0
deg(1) = a0;
% +-----+
```

```

% +-----+
% Trapezoidal integration of acceleration to velocity
for i = 2:n
    deg(i) = dt*(a(i) + a(i-1))/2 + deg(i-1);
end
% +-----+

% +-----+
% Trapezoidal integration of velocity to position

for i = 2:n
    deg(i) = dt*(a(i) + a(i-1))/2 + deg(i-1);
end

% +-----+

% +-----+
% detrend and filter to remove low frequencies

% v = filtfilt(bf,af,detrend(v));
deg = filtfilt(bf,af,deg);

% +-----+

```